Report No.
UCB/SEMM-2002/02

STRUCTURAL ENGINEERING,
MECHANICS AND MATERIALS

Decision Methodology in Seismic Risk Management of a Single Building Based on Minimum Expected Life-Cycle Cost

by
Yuji Takahashi
Armen Der Kiureghian
and
Alfredo H-S. Ang

March 2002

DEPARTMENT OF CIVIL & ENVIRONMENTAL ENGINEERING,
UNIVERSITY OF CALIFORNIA, BERKELEY

Decision Methodology in Seismic Risk Management of a Single Building Based on Minimum Expected Life-Cycle Cost

By

Yuji Takahashi

Armen Der Kiureghian

Alfredo H-S. Ang

Report No. UCB/SEMM-2002/02

Structural Engineering, Mechanics & Materials

Department of Civil & Environmental Engineering

University of California, Berkeley

March 2002

Decision Methodology in Seismic Risk Management of a Single Building Based on Minimum Expected Life-Cycle Cost

Yuji Takahashi[1]

Armen Der Kiureghian[2]

Alfredo H-S. Ang[3]

Abstract

We present a decision methodology in seismic risk management of a single building aiming to provide the client with a rational decision making among multiple alternatives. An alternative with a minimum expected life-cycle cost is chosen as the optimum selection. The expected life-cycle cost of each alternative is formulated utilizing renewal theory for the occurrence of earthquakes in time. The formulated equation can directly utilize newly acquired information as well as existing data on activities of surrounding seismic sources using arbitrary renewal models, and can make use of up-to-date simulation techniques developed in seismology, geotechnical engineering, structural engineering and economics. As an example, the methodology is applied to an actual office building in Tokyo. A simple decision problem between two design alternatives is set: a bare steel moment frame and the same frame equipped with oil dampers. Through this case study, the installation of the oil dampers is demonstrated to be effective in reducing the life-cycle cost of the building under consideration. The proposed methodology is applicable to a variety of decision problems in seismic risk management for existing buildings as well as new ones.

Key words: seismic risk management; buildings; decision making; life-cycle cost; renewal model; seismology; geotechnical engineering; structural engineering; Monte Carlo simulation; oil dampers

[1] Corresponding author, Postdoctoral Research Fellow, University of California, Berkeley from Waseda University, Tokyo, Japan, March 2000 - March 2002 (email: taka@slws1.arch.waseda.ac.jp)

[2] Taisei Professor of Civil Engineering, University of California, Berkeley

[3] Research Professor, Department of Civil & Environmental Engineering, University of California, Irvine

ACKNOWLEDGMENT

This study was supported by Kozo Keikaku Engineering, Inc., Tokyo, Japan and Waseda University, Tokyo Japan. These financial supports are gratefully acknowledged.

The first author wishes to express special thanks to Professor Satsuya Soda at Waseda University for his invaluable advice, and acknowledge the engineers at Kozo Keikaku Engineering, Inc., particularly Mr. Akihiro Sawaii, Mr. Osamu Takahashi, and Ms. Yuko Murachi, who provided information used in the case study and valuable advice from a practical point of view.

Associate Professor Yoshiaki Hisada at Kogakuin University, Tokyo, Japan provided valuable information on strong motion seismology. Professors Raymond B. Seed and Douglas Dreger at the University of California, Berkeley, admitted the first author to audit their classes and provided knowledge on geotechnical and seismological models, respectively. Mr. Scott McAfee at the California Office of Emergency Services kindly gave the first author an opportunity to study the use of HAZUS99 code for regional loss estimation. Professor Takahiro Ohno at Waseda University provided valuable suggestions from the stand point of engineering economics. Professor Igor A. Beresnev at Iowa State University provided the FORTRAN program FINSIM, and Professor Howard H. M. Hwang at the University of Memphis kindly answered questions on his probabilistic models for surface soils via email. Professor Kenneth H. Stokoe II at the University of Texas, Austin, and Dr. Keisuke Hibiya at Kajima Advanced Technology Research Institute, Tokyo, Japan mailed to us two master's theses (Isenhower, 1979; Lodde, 1982) and a doctoral dissertation (Hara, 1980), respectively. Dr. Kiyoshi Kishida, who was a visiting scholar at the Lawrence Berkeley National Laboratory from Kyoto University, Kyoto, Japan, encouraged the first author to advance this study with his constructive suggestions. They are all gratefully acknowledged.

TABLE OF CONTENTS

LIST OF FIGURES

CHAPTER 2

CHAPTER 3

LIST OF TABLES

CHAPTER 3

APPENDIX C

CHAPTER 1

INTRODUCTION

1.1 Background and objective

As a society advances, peoples' demands grow and become more specific. Seismic performance required of a building is not an exception. In an advanced society, a building is expected to remain safe and provide its intended function throughout its planned life time, with only acceptably small probabilities of performance interruption or damage due to earthquakes. Risk may be defined as the integration of the probability of an undesirable event, e.g., the occurrence of casualties (injuries and fatalities), damage, and loss of function due to earthquakes, times the cost associated with the event, i.e., the cost of casualties, repair or replacement of the damaged building, and loss of profit due to business interruption. Risk due to earthquakes can be reduced by providing more strength and ductility to the building, or using various anti-seismic devices. However, these measures come at a premium. Therefore, seismic design of buildings entails an important risk-management decision problem as an optimal balance between the initial costs and the future risks must be achieved. Depending on the performance demands specified by the client (e.g., the owner of a building or a company, government agency, residents, tenants, users, investors, insurance or real estate companies, and so on), project-specific solutions to the above decision problem are required in addition to design based on uniform codes. Because of this need, the management of seismic risk has become an increasingly important engineering task in recent years.

As an ultimate goal of seismic design and risk management, it could be imagined that the seismic performance of a building would be displayed as a specification attached to the building similar to the manner in which specifications are attached to electronic equipment, machinery, automobiles, etc. Furthermore, the engineer and the client would discuss the desired specifications and decide how to manage the risks just like informed discussions between a doctor and a patient in a hospital. Such risk management consulting is needed not only in design of new buildings, but also in decisions on how to protect one's existing property, e.g., replace,

upgrade, retrofit, relocate, or purchase earthquake insurance. This type of risk management may also be extended to decisions in business, e.g., renting an office, buying or selling real estate, or investing in real estate securities. Therefore, the technologies of seismic risk assessment, methods for communication of the risk to clients, and decision analysis to determine the best solution and how to manage the risks are becoming increasingly more important. While numerous studies on risk analysis of a single building can be found (Ang and De Leon, 1996; Ferritto, 1984; Harris and Harmon, 1986; Hwang and Huo, 1994; Inoue and Kanda, 1998; Lee, 1996; Liu and Neghabat, 1972; Rosenblueth, 1986; Takahashi *et al.*, 2000; Whitman *et al.*, 1979), these studies are yet to be developed into comprehensive decision methodologies in seismic risk management in the specific senses described below.

The seismic performance of a building cannot be determined by only considering the building itself. This is because seismic hazards are different from site to site. For example, two similar buildings, one located in the vicinity of active seismic sources and the other located far from them, will have different performances because their potential risks are different. Furthermore, even the same building at a given site will have different risks depending on the time window of its life span because, in general, activities of seismic sources are time-dependent. Thus, it is clear that the seismic profile of the site during the lifetime of the building should be considered in estimating the performance, and reflected in the final decisions on the management of the risk. It is generally agreed that the occurrence of earthquakes in a seismic source should be described using stochastic models (e.g., Anagnos and Kiremidjian, 1988), and recently several groups of seismologists have announced earthquake forecasts based on such models, i.e., probabilities of earthquake occurrence estimated using stochastic models based on historical, geodetic and trench investigation data (HERP, 2001a; WGCEP, 1990; 1999). These advanced stochastic models and forecasts unfortunately have not been incorporated into the above mentioned studies on the seismic risk management of buildings.

In the estimation of risk due to earthquakes in a wide region or for an institution with a lot of facilities, such as a university or industrial campus, it is appropriate to relate the physical damages of buildings to ground motion intensities, e.g., PGA (Peak Ground Acceleration), MMI (Modified Mercalli Intensity) and response spectral ordinates (ATC, 1985; Comerio, 2000; EERI, 1997; FEMA, 1999). Such simple intensity measures have also been used for the conventional risk analyses of specific buildings. Ang and De Leon (1996), Hwang and Huo (1994), Inoue and

Kanda (1998), Lee (1996), Pires *et al.* (1996), and Takahashi *et al.* (2000) performed dynamic response analyses of building models to estimate risks by applying time histories of recorded or classical stochastic ground motions with specified intensities. A similar approach is advocated by the PEER (Pacific Earthquake Engineering Research) framing formula (Cornell and Krawinkler, 2000). In reality, seismic risk is generated as a result of a sequence of related processes: fault rupture in a seismic source, elastic wave propagation in rock, surface soil amplification, dynamic response of the building, and generation of losses. Simulation models for each of these processes are continually being refined in the respective fields of seismology, geotechnical engineering, structural engineering, and social economics. However, refined techniques developed in these fields, particularly site-specific seismological or geotechnical models, are not and cannot be effectively utilized in risk analyses of buildings that are based on simple measures of ground motion intensity.

The background described above motivated us to set the objective of our study as developing a decision methodology in seismic risk management, which can directly incorporate newly obtained information as well as existing data on activities of surrounding seismic sources, and systematically utilize up-to-date simulation models for the relevant processes, aiming to provide clients with final decisions of better quality. In the proposed approach, conditioning is done on the earthquake magnitude and source, rather than on the ground motion intensity as in the above mentioned studies. This preliminary study begins with only one fundamental risk, i.e., costs imposed on the decision maker. Other risks such as generation of casualties are beyond the scope of this study, and would be taken into account as a multi-attribute decision problem (Ang and Tang, 1984) in the near future. The risk is expressed as the expected life-cycle cost, which is the expected amount of payments during the lifetime of the building. These include the initial cots of the design and its construction, and the expected cost of damages generated due to earthquakes during the life of the building. As an example, the proposed methodology is applied to an actual office building newly constructed in Tokyo. In this case study, we examine the cost effectiveness of oil dampers installed in the building in reducing the life-cycle cost.

1.2 Organization

Chapter 2 presents the overall proposed decision methodology. We begin with the basic concept of decision theory that is widely used in civil engineering, and describe how to apply it to our problem of seismic risk management. Decisions are made based on the expected life-cycle cost, where the occurrence of earthquakes is formulated by utilizing renewal theory. The expected losses are obtained by conditioning on the earthquake magnitude and source, as opposed to the ground motion intensity. A formulation for computing the expected damage cost due to an earthquake of given magnitude, which is necessary to estimate the life-cycle cost, is then described.

Chapter 3 applies the proposed decision methodology to an actual office building in Tokyo. The first part outlines the building under consideration, and a simple decision problem between two alternatives is set: one is the bare steel frame, and the other is the steel frame equipped with oil dampers at an additional cost. The activity of an influential seismic source, the Sagami trough, is investigated using typical earthquake catalogs, and is described using both a Poisson and a non-Poisson renewal model. Monte Carlo simulations are performed to estimate expected damage costs due to given magnitudes, using up-to-date analytical models developed in seismology, geotechnical engineering, structural engineering and economics. The life-cycle costs of the two alternatives are then compared.

Chapter 4 summarizes this study.

CHAPTER 2

BASIC CONCEPT AND FORMULATION

2.1 Introduction

In this chapter, a decision framework for the management of seismic risk of buildings is described. The next section introduces the basic concepts of decision theory that is widely used in civil engineering, and describes how to apply it to problem of reducing seismic risk. As described in Section 2.3, decisions are made based on the expected life-cycle cost of the building. Section 2.4 describes the method for obtaining the expected damage costs due to earthquakes of given magnitudes, which are required for computation of the expected life-cycle cost.

2.2 Decision criterion

Decision theory is frequently used in civil engineering as well as in engineering economics. Various decision problems in civil engineering are dealt with in textbooks; e.g., written by Ang and Tang (1984) and Benjamin and Cornell (1970). Figure 2.1 illustrates a simple decision tree involving several alternatives (= choices), where a_i represents the ith alternative.

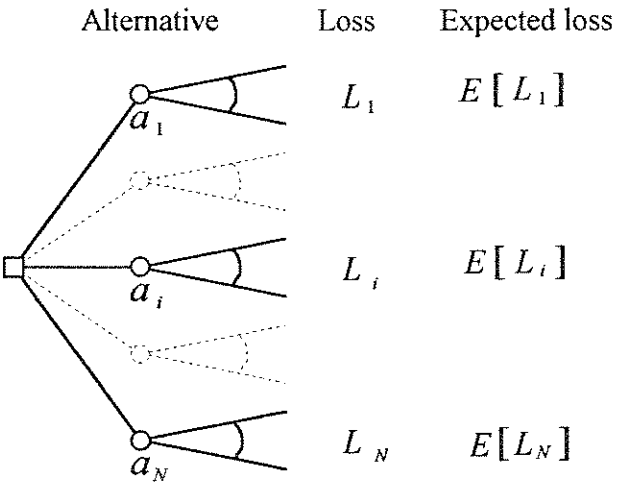

Figure 2.1 Decision tree

In theory, infinite alternatives may exist for a problem, but in practice engineers usually can consider a finite set of viable alternatives. Although engineers may be able to analyze the consequent loss of each alternative, this loss cannot be predicted deterministically since nature inevitably involves uncertainties. Hence, the loss of each alternative, L_i, is considered as a random variable and it is described by its probability density function (PDF), $f_{L_i}(l)$, as illustrated in Figure 2.2.

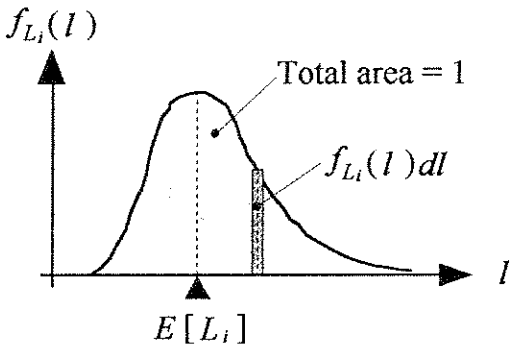

Figure 2.2 PDF (Probability Density Function) of loss of each alternative

According to the minimum expected loss criterion in decision theory, among a given set of alternatives, the alternative with the minimum expected loss is the optimal choice (Ang and Tang, 1984; Benjamin and Cornell, 1970). This expectation is also displayed in Figure 2.2, where the notation $E[L_i]$ represents the mean of L_i defined by

$$E[L_i] = \int_{-\infty}^{\infty} l f_{L_i}(l) dl \tag{2.1}$$

It is clear that the expected loss criterion accounts for the occurrence probabilities of the consequent loss in an average sense. In order to reflect preferences of decision makers in a broader framework, the maximum expected utility criterion, where loss is transformed into utility, is also used (Ang and Tang, 1984; Benjamin and Cornell, 1970).

This study focuses on decisions in seismic risk management of a building during its lifetime. The total amount of payments during the lifetime, so-called life-cycle cost (LCC), can be

regarded as one of the concerned losses for decision makers (Ang and De Leon, 1996, Lee, 1996; Liu and Neghabat, 1972; Pires *et al.*, 1996; Takahashi *et al.*, 2000). The life-cycle cost of a building is expressed as

$$C_L = C_I + C_D^C \tag{2.2}$$

where C_L is the life-cycle cost, C_I is the initial cost, and C_D^C is the cumulative damage cost, which is the sum of damage costs caused by all earthquakes that occur during the lifetime of the building under consideration. The life-cycle cost C_L is a random quantity since it is virtually impossible to estimate C_D^C deterministically because of uncertainties in such events as the occurrence of earthquakes, their magnitudes and locations, properties of ground motions, surface soil conditions, buildings properties, and so on. Therefore, C_L and C_D^C are treated as random variables while C_I is considered as a deterministic value. Taking expectation of both sides of Eq. (2.2), one has

$$E[C_L] = C_I + E[C_D^C] \tag{2.3}$$

In seismic design of new buildings or upgrading existing ones, engineers have been using "hard" (structural) technologies in order to mitigate damages, e.g., strong and ductile frames, bracing, lateral bearing walls, energy dissipating devices and base isolation systems. Recent "soft" technologies, e.g., earthquake insurances or post-earthquake prompt response could also be effective. Engineers can propose some of them or, more in general, combinations of them as alternatives. Investments in these technologies can be effective to reduce damage costs caused by earthquakes in seismic regions. In general, initial and cumulative damage costs are traded off since the higher initial cost can yield less cumulative damage cost. Figure 2.3 illustrates the simplest example, a decision between two alternatives. The first alternative, a_1, is a moderately designed building, and the second alternative, a_2, is a building of better quality with additional initial cost. The lower bounds of the PDFs are equal to their initial costs. In a seismic region, $E[C_L]$ of a_2 can be less than that of a_1 if the additional cost is invested in appropriate elements

even though its initial cost is higher. In this case, the better-quality building, a_2, can be chosen.

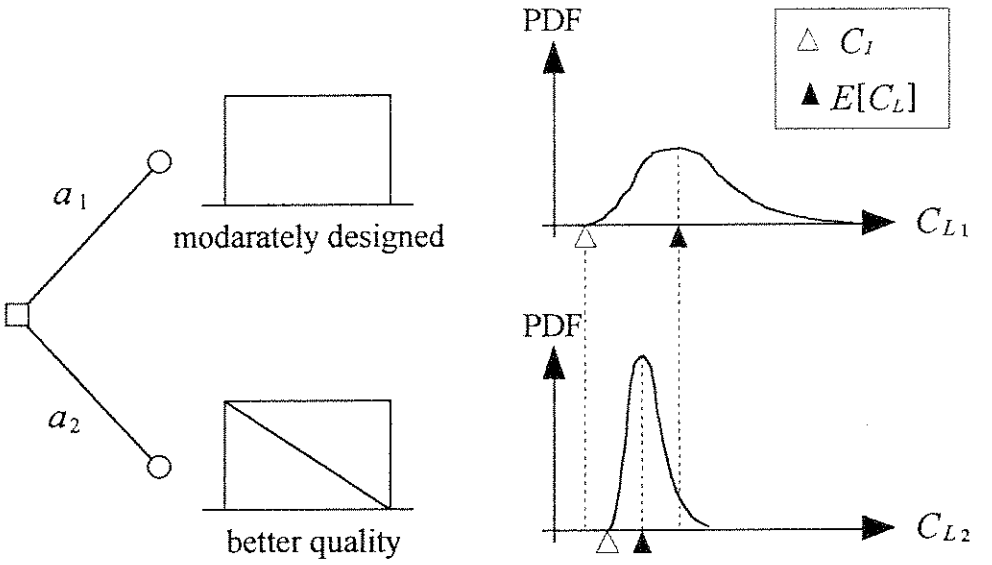

Figure 2.3 Simple example: decision between two alternatives

It is clear that determining $E[C_L]$ of each alternative is the critical step in decision making. Formulation of this term is described in the next section.

2.3 Formulation of expected life-cycle cost

In conventional probabilistic seismic hazard analyses (Cornell, 1968; Kramer, 1995), the relationship between magnitude m and annual exceedance rate $N(m)$ of earthquakes in a seismic source is described using the Gutengerg-Richter or the bounded Gutengerg-Richter model (Gutenberg and Richter, 1944; Kramer, 1995; Wesnousky, 1994; 1999), or the characteristic model (Young and Coppersmith, 1985; Wesnousky, 1994). Figure 2.4(a) illustrates this relationship, where m_{min} and m_{max} are the lower and upper bounds of magnitude to be considered in the analysis, respectively. Figure 2.4(b) shows the relationship between the annual exceedance rate $N(m)$ and the mean annual occurrence rate η (m), which is given by

$$N(m) = \int_{m}^{m_{max}} \eta(m)dm \tag{2.4}$$

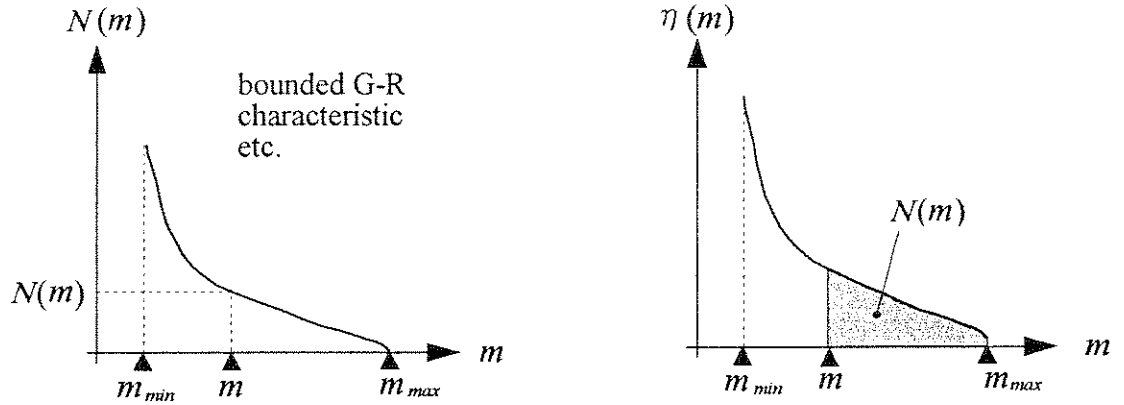

(a) Exceedance rate **(b) Mean occurrence rate**

Figure 2.4 Magnitude vs. annual rate

Solving Eq. (2.4), $\eta(m)$ is obtained as the negative derivative of $N(m)$ with respect to m,

$$\eta(m) = -\frac{d}{dm} N(m) \tag{2.5}$$

In this study, the relationship between m and $\eta(m)$ is discretized by use of a magnitude increment, as shown in Figure 2.5(a). In essence, earthquakes are grouped into several categories based on their magnitudes. Let the centers of the magnitude groups be $m_1, \cdots, m_j, \cdots, m_K$. Then, the mean annual occurrence rate of earthquakes of each group is represented by the area of each segment $\nu(m_j)$. Alternatively, this can be expressed as the bar graph as shown in Figure 2.5(b), where the height of each bar $\nu(m_j)$ represents the mean annual occurrence rate of earthquakes of each group.

Occurrence of earthquakes of each group (m_j) is regarded as a renewal process, where an integer number of events occur during finite time, as reviewed by Anagnos and Kiremidjian (1988). For a renewal process, the PDF of the interarrival time between two successive events, T, is defined as $f_T(t,m_j)$. Let W_n be the waiting time to the nth event from the last event ($t = 0$), i.e., $W_n = T_1 + T_2 + \cdots + T_i + \cdots + T_n$, where T_i for all i are identically distributed. Since it is obvious that $W_1 = T$, the PDF of the time to the first event, $f_{W_1}(t,m_j)$, is identical to $f_T(t,m_j)$ as shown in Figure 2.6. The PDFs of the times to the subsequent events, $f_{W_n}(t,m_j)$, are also illustrated in Figure 2.6. Note that the origin of the time axis is the time of the last event.

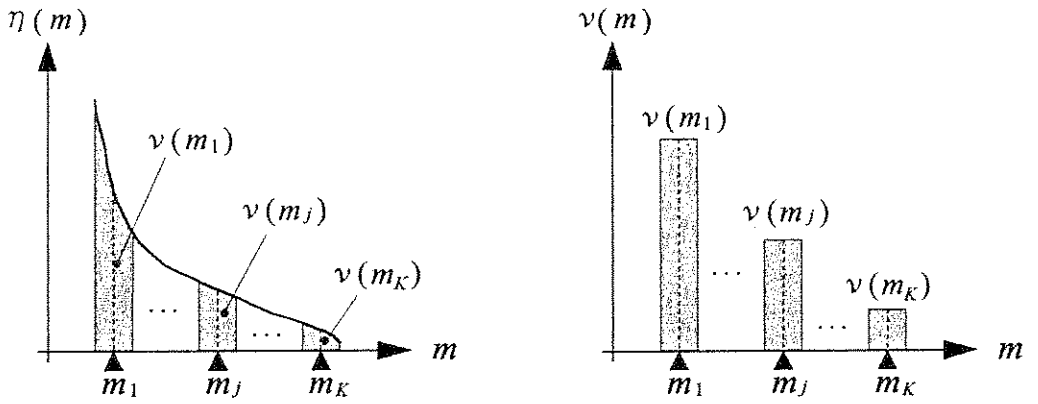

(a) Area of segment **(b) Height of bar**

Figure 2.5 Mean annual occurrence rate for each group

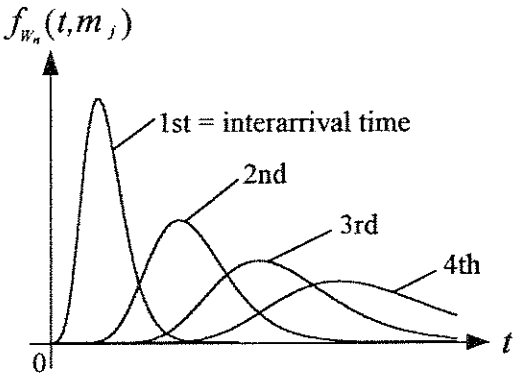

Figure 2.6 Original PDF of waiting time to the *n*th event

The "last event" suggests that no earthquake has occurred since $t = 0$ before the opening time of the building, $t = t_0$. However, the original PDFs, $f_{W_n}(t,m_j)$, in Figure 2.6 include the possibility that earthquakes occur during $0 < t < t_0$. In general, time has elapsed when the building starts to operate since the last earthquake. Therefore, each PDF should be updated on the condition that there is no earthquake during the period $0 < t < t_0$, i.e., $W_1 > t_0$. The updated (conditional) PDF of the waiting time to the first event is (WGCEP, 1990)

$$f_{W_1}(t,m_j|W_1 > t_0) = \frac{f_{W_1}(t,m_j)}{1-\int_0^{t_0} f_{W_1}(t,m_j)dt} \tag{2.6}$$

The denominator of Eq. (2.6) indicates that the event space shrinks because the occurrence of earthquakes is restricted $t > t_0$ rather than $t > 0$. As Figure 2.7 illustrates, the updated PDF, $f_{W_1}(t, m_j | W_1 > t_0)$, is greater than the unconditional PDF , $f_{W_1}(t, m_j)$, when $t_0 > 0$. The updated PDF of the waiting time to the nth event is written as $f_{W_n}(t, m_j | W_1 > t_0)$.

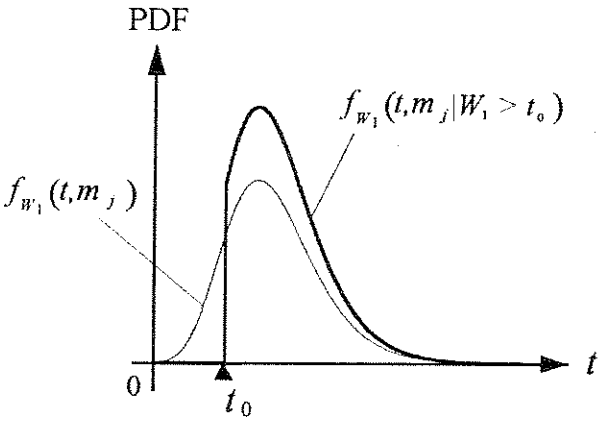

Figure 2.7 Original and updated PDFs of time to the first event

A hypothetical realization of the cumulative damage cost of a building due to earthquakes of magnitude m_j during the lifetime (between t_0 and $t_0 + t_{life}$) is illustrated in Figure 2.8(a). The cumulative damage cost can be expressed as

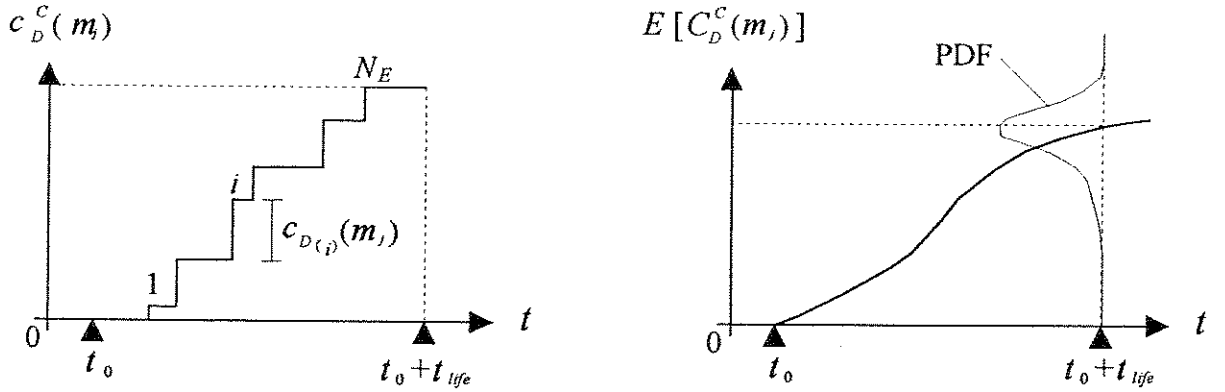

(a) One sample **(b) Expectation**

Figure 2.8 Time vs. cumulative damage cost

$$C_D^C(m_j) = \sum_{i=1}^{N_E(m_j)} C_{D(i)}(m_j) \tag{2.7}$$

where $C_D^C(m_j)$ denotes the cumulative damage cost from earthquakes of a magnitude m_j, $N_E(m_j)$ is the number of events between t_0 and $t_0 + t_{life}$ and $C_{D(i)}(m_j)$ is the damage cost due to the ith event. Under the assumption that $C_{D(1)}(m_j)$, ···, $C_{D(i)}(m_j)$, ···, and $C_{D(N)}(m_j)$ are identically distributed random variables that are statistically independent of $N_E(m_j)$, the expectations of the two sides of Eq. (2.7) are given by (Ross, 1995)

$$E\left[C_D^C(m_j)\right] = E\left[C_D(m_j)\right]E\left[N_E(m_j)\right] \tag{2.8}$$

The assumption described above is equivalent to a stationary assumption, i.e., the statistical properties of all processes related to the generation of damage costs remain invariant of time. This condition is achieved by, in reality, assuming that the building is restored to its original condition immediately after each earthquake, and by ignoring the degradation of the building due to aging and wear and tear (Ang and De Leon, 1996; Lee, 1996; Pires *et al.*, 1996). As shown in Appendix A, the expectation of $N_E(m_j)$ is obtained as the integration of the summation of Eq. (2.6) for all n from t_0 to $t_0 + t_{life}$, i.e.,

$$E\left[N_E(m_j)\right] = \int_{t_0}^{t_0+t_{life}} \sum_{n=1}^{\infty} f_{W_n}(t, m_j | W_1 > t_0)dt \tag{2.9}$$

Equation (2.9) suggests that not only the first but also the second, third, fourth, ···, nth, ··· earthquake could occur between t and $t + t_{life}$, and their probabilities are summed up. The term $\sum_{n=1}^{\infty} f_{W_n}(t, m_j | W_1 > t_0)$ represents the occurrence rate of an earthquake at t. Substituting Eq. (2.9) into Eq. (2.8), we obtain

$$E\left[C_D^C(m_j)\right] = E\left[C_D(m_j)\right]\int_{t_0}^{t_0+t_{life}} \sum_{n=1}^{\infty} f_{W_n}(t, m_j | W_1 > t_0)dt \tag{2.10}$$

The effective worth of a cost varies depending on when it occurs. This is because, in engineering economics, cash flow is always compared with a deposit in a bank, that is, we can obtain an interest in the future if the money is deposited in a bank (Grant *et al.*, 1990; Senju and Fushimi, 2001). For example, if a cost occurs right now, we can get nothing. However, if the money is deposited in a bank until the same cost occurs after one year, we can obtain some interest from the bank. We prefer the latter even though their nominal values are the same. This indicates that the effective worth of a future cost is less relative to the one at present. Therefore, the future cost should be deflated (transformed into an equivalent present worth) using a discount factor $Q = 1/(1+d)$, where d is the discount rate (Ang and De Leon, 1996; Lee, 1996; Pires *et al.*, 1996). The cumulative damage cost in terms of present worth becomes as follows.

$$E\left[C_D^C(m_j)\right] = E\left[C_D(m_j)\right] \int_{t_0}^{t_0+t_{life}} Q^{t-t_0} \sum_{n=1}^{\infty} f_{W_n}(t, m_j | W_1 > t_0) dt \tag{2.11}$$

For the expected damage cost from one seismic source, $E\left[C_D^C(m_j)\right]$ from all magnitudes is obtained as

$$E\left[C_D^C\right] = \sum_{j=1}^{K} E\left[C_D(m_j)\right] \int_{t_0}^{t_0+t_{life}} Q^{t-t_0} \sum_{n=1}^{\infty} f_{W_n}(t, m_j | W_1 > t_0) dt \tag{2.12}$$

In the above equation, $E\left[C_D^C\right]$ is the expected damage cost from one seismic source and K is the number of discretized magnitudes defined in Figure 2.5. Here, a simple but general principle is used: the expectation of the sum of several random variables is equal to the sum of their expectations regardless of their probability distributions or statistical dependence (Ang and Tang, 1975). Eq. (2.12) is the expected cumulative damage cost from only one seismic source. In general, a building is surrounded by several seismic sources as illustrated in Figure 2.9, and the cumulative damage cost from all sources is given by

$$E\left[C_D^C\right] = \sum_{all\ sources} \sum_{j=1}^{K} E\left[C_D(m_j)\right] \int_{t_0}^{t_0+t_{life}} Q^{t-t_0} \sum_{n=1}^{\infty} f_{W_n}(t, m_j | W_1 > t_0) dt \tag{2.13}$$

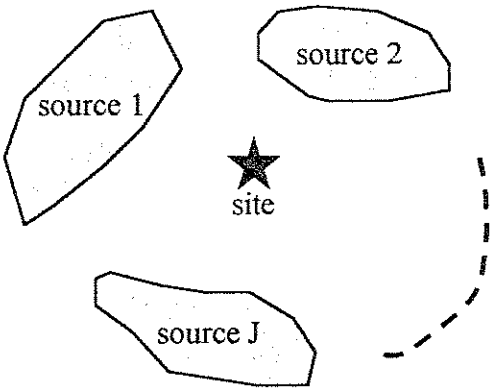

Figure 2.9 Building site and surrounding seismic sources

Substituting Eq. (2.13) into Eq. (2.3), the expected life-cycle cost is obtained as

$$E\left[C_L\right] = C_I + \sum_{all\ sources} \sum_{j=1}^{K} E\left[C_D(m_j)\right] \int_{t_0}^{t_0+t_{life}} Q^{t-t_0} \sum_{n=1}^{\infty} f_{W_n}(t, m_j | W_1 > t_0) dt \tag{2.14}$$

This is the expected life-cycle cost of the building from all seismic sources during its lifetime. Figure 2.10 illustrates one sample realization and the expectation of the life-cycle cost.

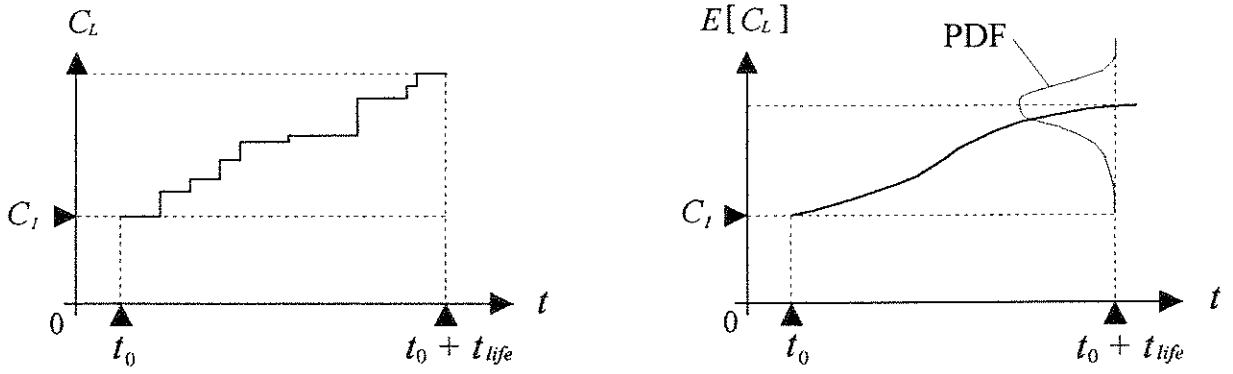

(a) One sample **(b) Expectation**

Figure 2.10 Time vs. life-cycle cost

Now a special form of Eq. (2.14) is compared. Many past studies assumed the Poisson process for the occurrence of earthquakes (Cornell, 1968; Ang and De Leon, 1996; Lee, 1996; Liu and Neghabat, 1972; Pires *et al.*, 1996). The Poisson process is equivalent to a renewal process whose PDF of the interarrival time is the exponential distribution with constant mean rate $\nu(m_j)$. For this process, the waiting time to the nth event is gamma distributed as shown in Figure 2.11(a) and described in the following equation:

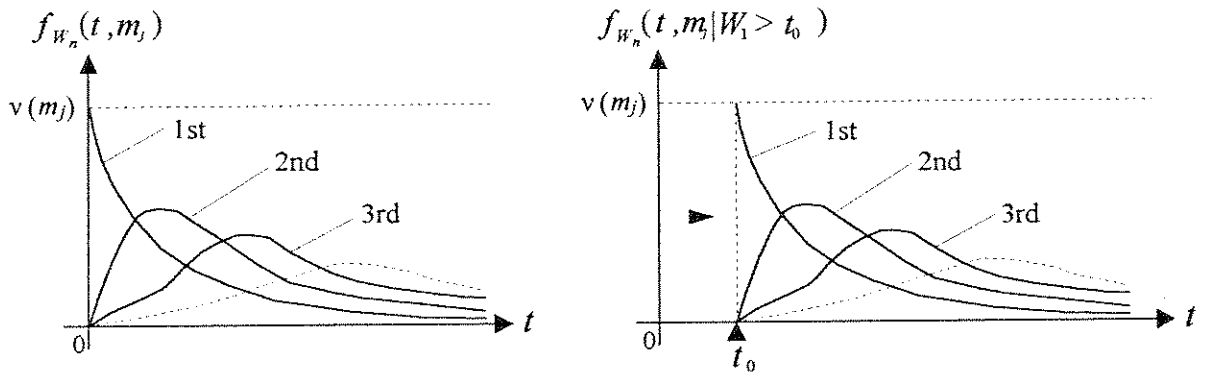

(a) Original **(b) Updated**

Figure 2.11 Gamma distribution

$$f_{W_n}(t, m_j) = \frac{\nu(m_j)\{\nu(m_j)t\}^{n-1}}{(n-1)!} e^{-\nu(m_j)t} \tag{2.15}$$

Because of the "memoryless" property of the Poisson process (Benjamin and Cornell, 1970), the updated PDF of the waiting time to the nth event is also the gamma distribution, except that the origin is now shifted to t_0, as illustrated in Figure 2.11(b). That is,

$$f_{W_n}(t, m_j | W_1 > t_0) = \frac{\nu(m_j)\{\nu(m_j)(t-t_0)\}^{n-1}}{(n-1)!} e^{-\nu(m_j)(t-t_0)} \tag{2.16}$$

In this case, using a Maclaurin expansion, one can show that

$$\sum_{n=1}^{\infty} f_{W_n}(t, m_j | W_1 > t_0) = \sum_{n=1}^{\infty} \frac{\nu(m_j)\{\nu(m_j)(t-t_0)\}^{n-1}}{(n-1)!} e^{-\nu(m_j)(t-t_0)} = \nu(m_j) \qquad (2.17)$$

This equation shows that, for the Poisson process, the occurrence rate of events is equal to the constant $\nu(m_j)$ and is independent of time. Substituting Eq. (2.17) into Eq. (2.14), the expected life-cycle cost for the Poisson model is obtained as

$$E[C_L] = C_I + \frac{Q^{t_{life}} - 1}{\ln Q} \times \sum_{all\ sources} \sum_{j=1}^{K} \nu(m_j) \cdot E[C_D(m_j)] \quad \text{for} \quad Q \neq 1 \qquad (2.18a)$$

and

$$E[C_L] = C_I + t_{life} \times \sum_{all\ sources} \sum_{j=1}^{K} \nu(m_j) \cdot E[C_D(m_j)] \quad \text{for} \quad Q = 1 \qquad (2.18b)$$

The above equations show that the relationship between the lifetime, t_{life}, and the expected life-cycle cost, $E[C_L]$, becomes linear only if $Q = 1$. In that case, the intercept and the gradient are equivalent to C_I and $\sum_{all\ sources} \sum_{j=1}^{K} \nu(m_j) \cdot E[C_D(m_j)]$, respectively, as indicated in Eq. (2.18b). This relationship is illustrated in Figure 2.12 compared with the case of $Q < 1$ since the discount rate d is positive.

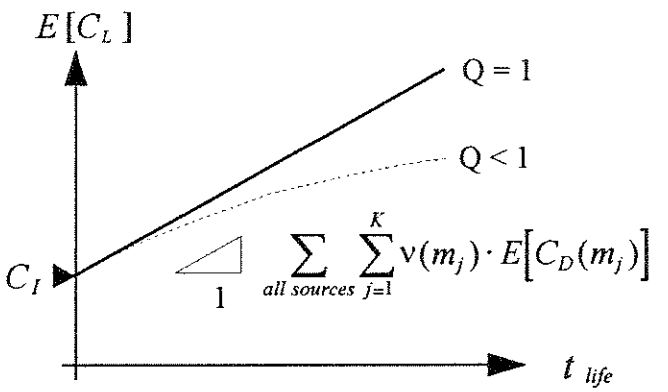

Figure 2.12 Lifetime vs. expected life-cycle cost for Poisson model

It is useful to compare Eq. (2.14) with the following equation formulated in previous studies (Ang and De Leon, 1996; Lee, 1996; Pires *et al.*, 1996):

$$E[C_L] = C_I + \frac{Q^{t_{life}} - 1}{\ln Q} \sum_{j=1}^{K} \nu(y_j) E[C_D(y_j)] \tag{2.19}$$

Similar formulations have been proposed by others such as Cornell and Krawinkler (2000) for seismic performance assessment. In their expression, y_j is the ground motion intensity, normally PGA (Peak Ground Acceleration). The biggest difference between Eq. (2.14) and Eq. (2.19) is that magnitude m_j is used in the former equation (source-focused) instead of PGA y_j in the latter one (site-focused). Thus, the former can directly introduce the activities of surrounding seismic sources using arbitrary renewal models such as Anagnos and Kiremidjian (1988), HERP (2001a) and WGCEP (1990; 1999), while the latter utilizes the relationship between PGA y and its mean annual occurrence rate $\nu(y)$ at the site. (This relationship can be obtained from a conventional probabilistic hazard analysis) Furthermore, different renewal processes can be assumed for different magnitude earthquakes in Eq. (2.14). For example, a non-Poisson renewal process is assumed for large and rare earthquakes, while the Poisson process is assumed for small ones that frequently occur during the lifetime of the building. Further advantage of using Eq. (2.14) is that, when estimating $E[C_D(m_j)]$, site-specific and more sophisticated seismological and geotechnical models can be applied to generate stochastic ground motions, whereas recorded ground motions or classical stochastic ones with specified PGA y_j should be used in Eq. (2.19).

In order to compute $E[C_L]$ of each alternative, the initial cost C_I is estimated first. Then seismic sources to be considered are identified, and their activity rates are quantified, i.e., $\sum_{n=1}^{\infty} f_{W_n}(t, m_j | W_1 > t_0)$ or $\nu(m_j)$ is obtained by utilizing the newest information announced by seismological groups, e.g., WGCEP (1999) and HERP (2001a) as well as existing data such as earthquake catalogs. Finally, the expected damage cost $E[C(m_j)]$ corresponding to each magnitude m_j is evaluated. Figure 2.13 represents the computation system for the expected life-cycle cost of each alternative. In order to estimate $E[C(m_j)]$, relevant processes should be simulated, i.e., fault rupture in seismic sources and elastic wave propagation in rock, surface soil amplification, dynamic response of the building, and generation of damage costs. How to

calculate it is described in the next section, and the simulation models used to compute $E[C_D(m_j)]$ will be introduced in Chapter 3 in connection with a case study.

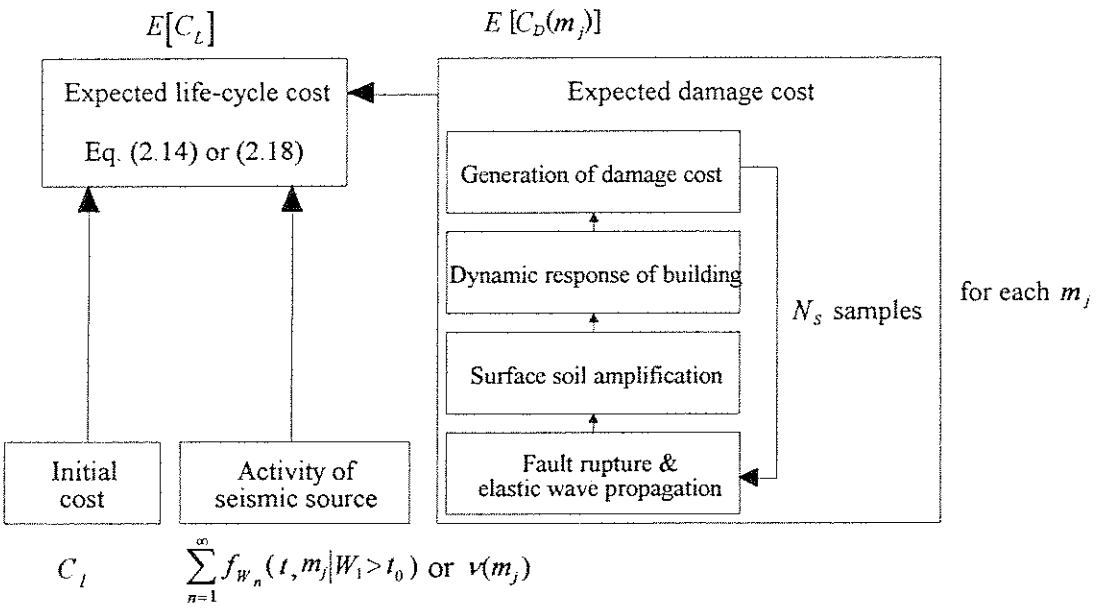

Figure 2.13 Computation system for expected LCC of each alternative

2.4 Expected damage cost

In Eq. (2.14) or (2.18), the expected damage cost $E[C_D(m_j)]$ caused by earthquakes of a specific magnitude m_j should be computed. Relevant processes are shown in Figure 2.14: fault rupture in a seismic source, elastic wave propagation, surface soil amplification, dynamic response of the building and generation of damage costs.

Monte Carlo simulations are performed in this study to simulate a sequence of these processes since they inevitably involve uncertainties, nonlinearity and nonstationarity. In such simulations, each sample is a set of probabilistic models of those processes considering their uncertainties. An adequate number of samples is generated for each given magnitude m_j, and the damage cost of each sample is computed. Then the expected damage cost is estimated as the sample mean.

$$E[C_D(m_j)] = \frac{1}{N_S}\sum_{i=1}^{N_S} c_{D(i)}(m_j) \tag{2.20}$$

where N_S is the number of samples and $c_{D(i)}(m_j)$ denotes the damage cost of the ith sample.

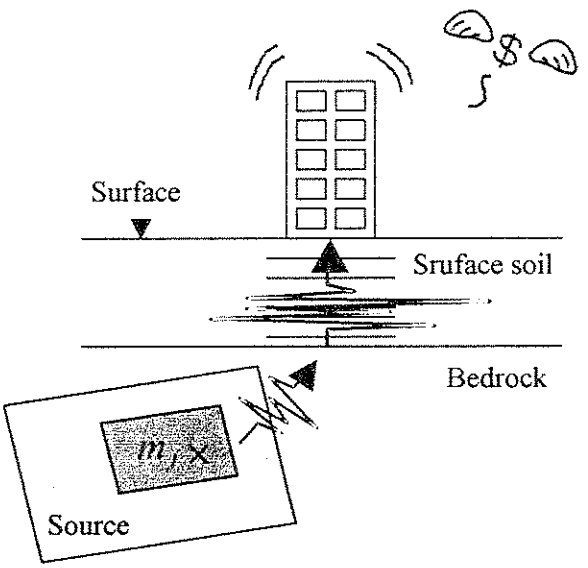

Figure 2.14 Processes from fault rupture to generation of damage costs

To simulate these processes, numerous models have been developed in relevant fields, e.g., seismology, geotechnical engineering, structural engineering and social economics. As a case study, Chapter 3 introduces recent simulation models. It is emphasized that the models employed here are just examples that are widely used at present and can be regarded as appropriate for the application. More sophisticated models may exist in other cases or will be developed in the future in each field. Then they will be able to replace the models used in this study. For example, more technical issues such as liquefaction or soil-structure interaction may also be taken into account if simulation models are available. In this sense, the term $E[C_D(m_j)]$ in Eq. (2.14) or (2.18) can be computed based on the most up-to-date knowledge in each field.

CHAPTER 3

A CASE STUDY IN TOKYO

3.1 Introduction

This chapter applies the decision framework proposed in Chapter 2 to an actual building in Tokyo. Section 3.2 describes the building under consideration, where a simple decision problem between two alternatives is formulated. The activity of the main seismic source affecting the selected building is described in Section 3.3. In Section 3.4, Monte Carlo simulations are performed for the expected damage costs due to given magnitudes using analytical models developed in seismology, geotechnical engineering and structural engineering. Subsequently, the life-cycle costs of the two alternatives are compared.

3.2 Objective building

The building considered here is the newest of several buildings owned by Kozo Keikaku Engineering, Inc. (KKE), which is an architectural/structural engineering firm (KKE, 2001a). The building has a total area of about 7,000 m^2 and was completed and started to operate in 1999 in Nakano, Tokyo. It has nine stories above the ground, and consists of steel moment resistant frames with box-shaped columns and H-shaped beams. It has two underground floors that consist of steel reinforced concrete frames. The plan and cross section of the building are shown in Figures 3.1 and 3.2, respectively. The bare frame was designed to satisfy the current Japanese building code. To reduce seismic response, a set of 8 oil dampers were installed in each above-ground floor of the building, for a total of 72 dampers throughout the building. Figure 3.3 shows the exterior view of the building, and Figure 3.4 shows the interior. Diagonal braces are seen in the latter figure. Oil dampers are built-in directly in the diagonal braces. The company has developed the ODB (Oil Damper Bracing) system and is commercializing it. More details about the building are given by Takahashi *et al.* (2001) and on the website of KKE (2001b).

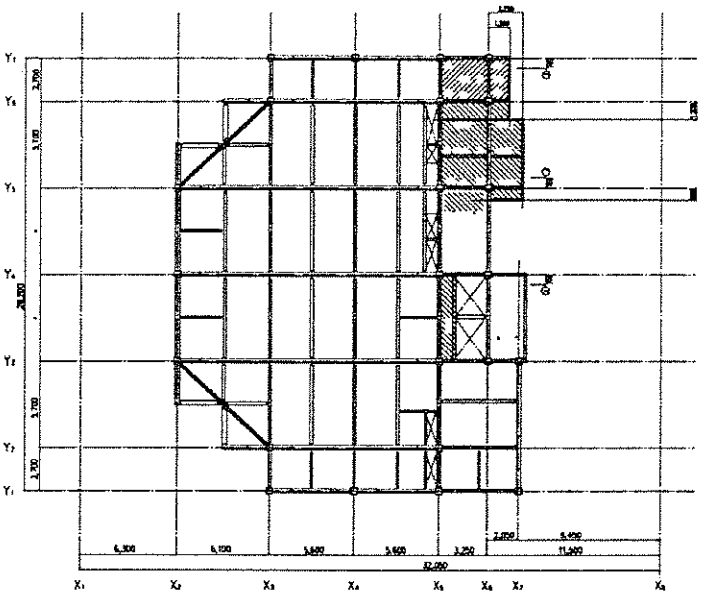

Figure 3.1 4F - 6F plan of model building (courtesy of KKE)

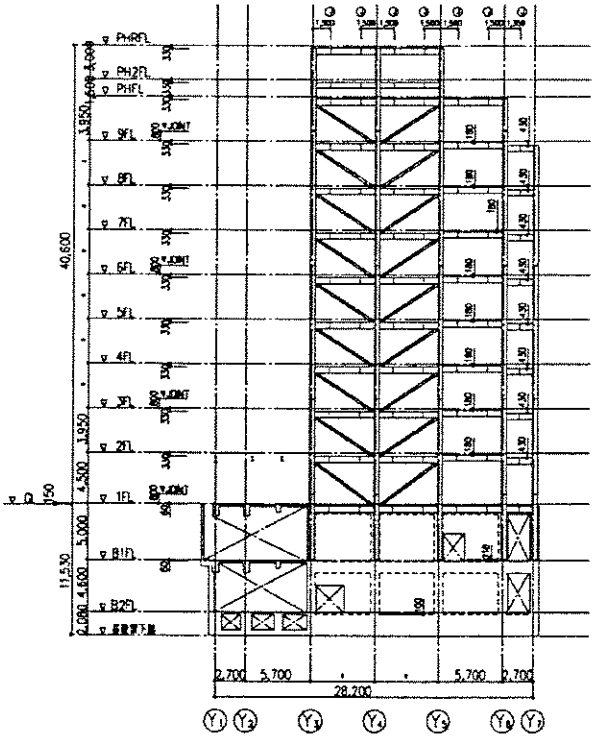

Figure 3.2 X_6 and X_8 cross sections of model building (courtesy of KKE)

Figure 3.3 Exterior view of the KKE building (courtesy of KKE)

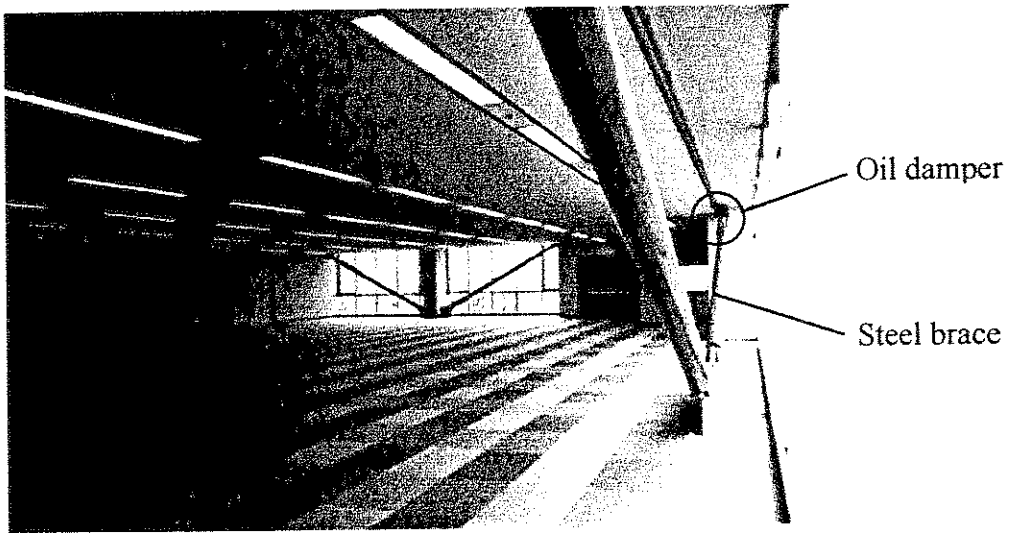

Figure 3.4 Interior view of the KKE building (courtesy of KKE)

In this case study, the life-cycle costs of two alternatives will be compared:

a_1: the bare steel frame (assuming the dampers are removed)
a_2: the actual building equipped with the dampers

As described in a latter section, the initial costs of the two alternatives are \$15.12 million and \$15.48 million, respectively. The life-cycle cost of a_2 is expected to be less, while its initial cost is more because of the added cost of the dampers. The purpose of this study is to determine the cost effectiveness of the damper. In this problem, the decision maker is assumed to be the president of the company who is also an owner of the building. Then he is responsible for not only the costs for repair or replacement of the building and contents but also loss of profit whenever the building is damaged. The lifetime of the building is assumed to be 50 years, that is, t_{life} = 50 years in Eq. (2.14) or (2.18).

3.3 Activity of seismic source

In this case study, the Sagami trough, a boundary between the Philippine Sea plate and the Eurasia plate, is considered as a seismic source. The Philippine Sea plate is subsiding below the Eurasian plate at about 15° on average as shown in Figure 3.5, and there have been numerous earthquakes in the vicinity of the Sagami trough because of relative movements of the two plates. A star in the figure represents the building site, the longitude and latitude of which are 139.67°E and 35.69°N, respectively.

A simple rectangular plane is assumed for the seismic source. The size and the location are determined by referring to Noguchi (1985), and its projection is shaded in Figure 3.6. The origin is represented as ○ in the figure (140.50°E and 34.50°N), and the dip (from the horizon) and the strike (from the north) are specified to be 15° and 290°, respectively. The upper edge of the plane is represented as a bold line, and its depth is specified to be 2.6 km below the ground level (see 3.4.1). The depth to the plane is about 35 km at the site of the building.

To investigate the activity of the seismic source, earthquake catalogs by Usami (1996), Utsu (1982) and Japan Meteorological Agency (1996) are used for up to A.D.1884, A.D.1885 - A.D.1925 and A.D.1926 - A.D.1995, respectively, referring to past seismic hazard

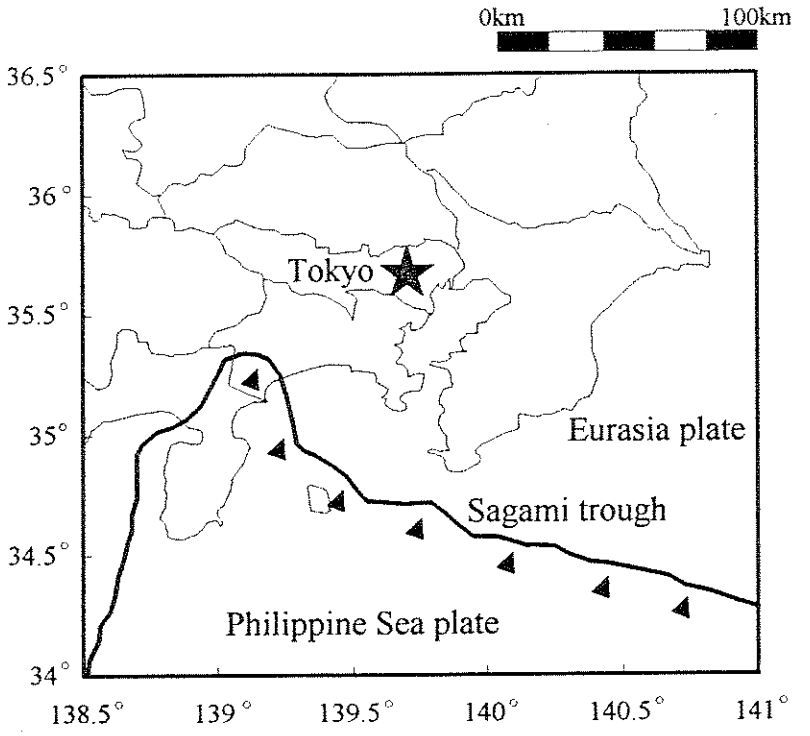

Figure 3.5 Sagami trough and building site

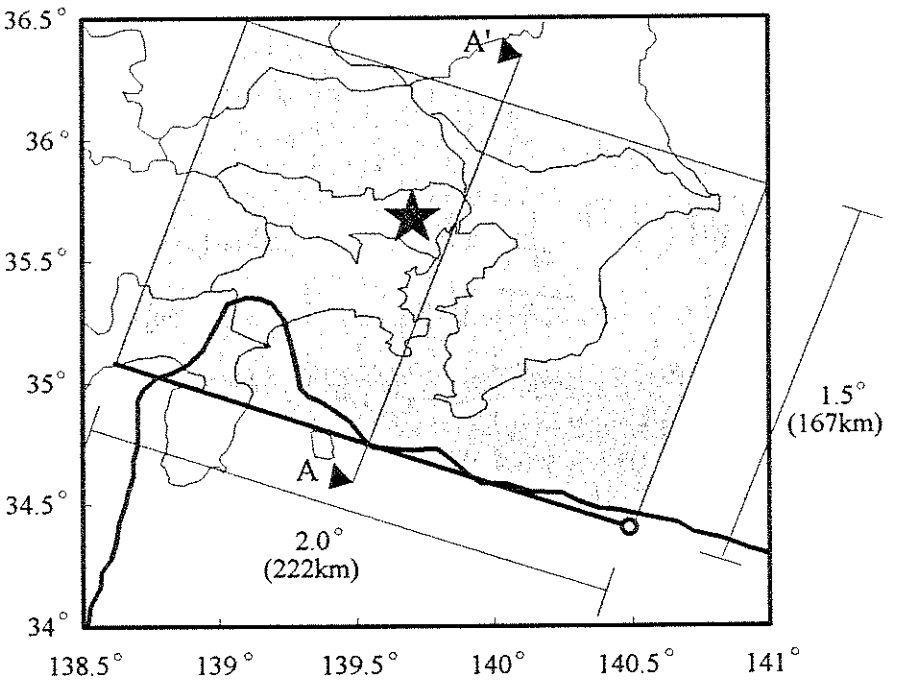

Figure 3.6 Projection of seismic source

analyses in Japan (Campbell *et al.*, 2000; Inoue and Kanda, 1993; Itoh *et al.*, 1987; Nagahashi and Shibano, 1999, Wesnousky *et al.*, 1984). Earthquakes recorded within a solid, the A - A' cross section of which is shown in Figure 3.7, are regarded as the ones that occurred near the Sagami trough.

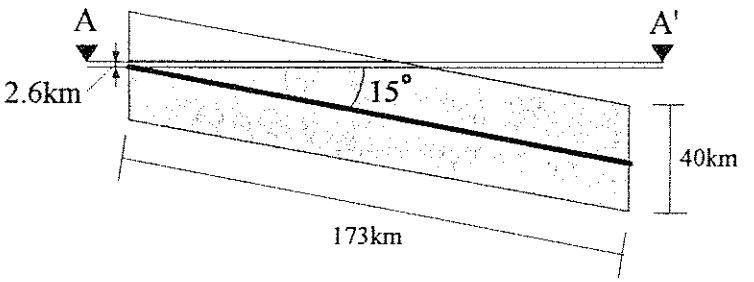

Figure 3.7 A - A' cross section of solid to be considered

The epicenter locations and times of occurrence of the selected earthquakes are plotted in Figures 3.8 and 3.9, respectively. The earthquakes are classified into three groups according to their magnitudes, $5.5 \leq m < 6.5$, $6.5 \leq m < 7.5$ and $7.5 \leq m < 8.5$, and their representative values are m_j = 6.0, 7.0 and 8.0, respectively. They are called m_j = 6.0, 7.0 and 8.0 earthquakes hereafter.

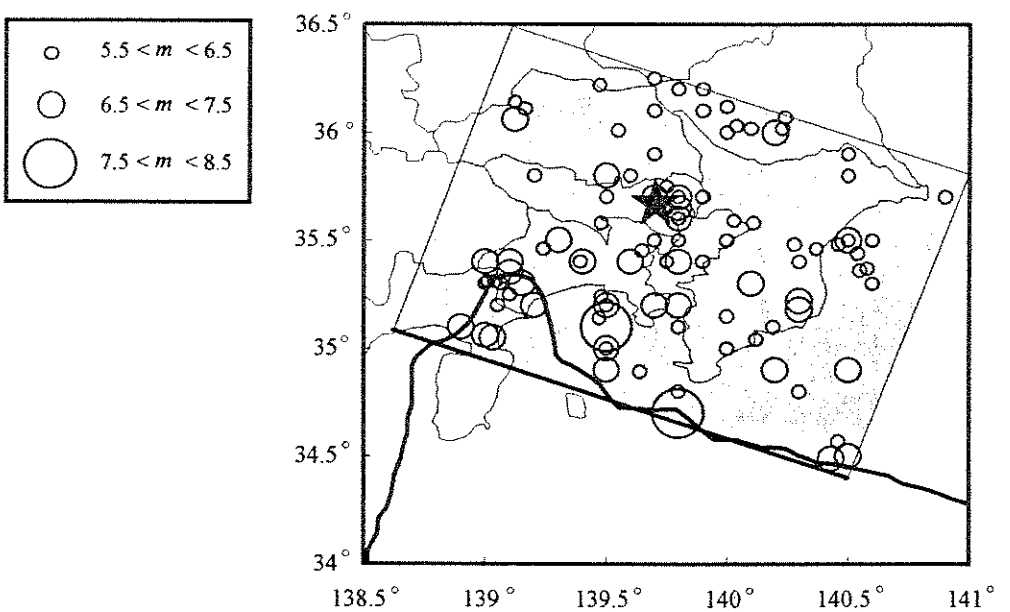

Figure 3.8 Recorded earthquakes around Sagami trough

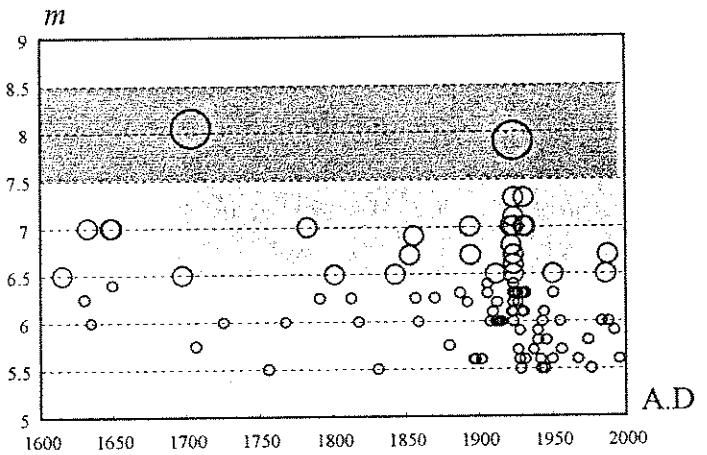

Figure 3.9 Time vs. magnitude of earthquakes around Sagami trough

As the number of groups, K, in Eq. (2.14) or (2.18) increases, the solution would become more accurate. However, it conflicts with computational efficiency because a Monte Carlo simulation with a large sample size should be performed for each m_j. For this reason, we have considered only three categories in this case study. The m_j = 6.0, 7.0 and 8.0 respectively correspond to occasional, rare and very rare events in the conventional seismic design.

Based on the above historical data, we model activities of the seismic source using both the Poisson model and a non-Poisson renewal model.

Poisson model

In order to compute the mean annual occurrence rate for the Poisson model, only earthquakes during A.D.1896 – A.D.1995 (100 years) and A.D.1696 – A.D.1995 (300 years) are taken into account for $5.5 \leq m < 6.5$ and $6.5 \leq m < 7.5$, respectively (shown as shaded segments in Figure 3.9). In the case of $7.5 \leq m < 8.5$, it is impossible to calculate the mean annual occurrence rate because only two events, the 1703 Genroku Earthquake (m = 8.1) and the 1923 Kanto Earthquake (m = 7.9), were recorded. The return period of these events is estimated to be about 200 years based on their interarrival time (Inoue and Kanda, 1993; Wesnousky *et al.*, 1984). On this basis, $\nu(8.0)$ = 1/200 is assumed. Figure 3.10 shows the mean annual occurrence rates for the three magnitude categories in arithmetic and logarithm scales. This figure demonstrates that the relationship between the magnitude and the logarithm of the annual rate is almost linear, and it approximately satisfies the Gutenberg-Richter relationship.

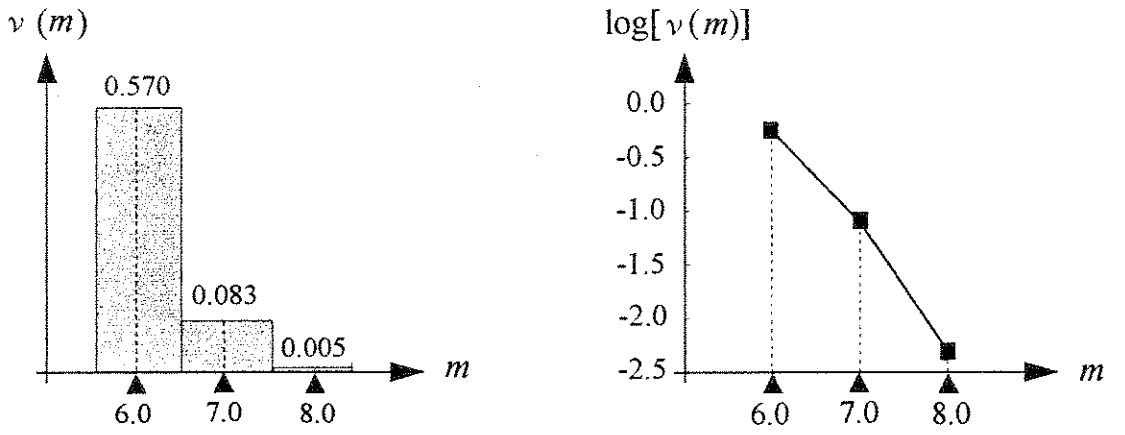

(a) Normal axis **(b) Log axis**

Figure 3.10 Magnitude vs. mean annual occurrence rate for Poisson model

Substituting the values from Figure 3.10 (a) into Eq. (2.18), the following equations are obtained.

$$E[C_L] = C_I + \frac{Q^{t_{life}} - 1}{\ln Q}\{0.570E[C_D(6.0)] + 0.083E[C_D(7.0)] + 0.005E[C_D(8.0)]\}$$

for $Q \neq 1$ (3.1a)

and

$$E[C_L] = C_I + t_{life}\{0.570E[C_D(6.0)] + 0.083E[C_D(7.0)] + 0.005E[C_D(8.0)]\}$$

for $Q = 1$ (3.1b)

Non-Poisson renewal model

The Poisson model is adequate for earthquakes that frequently occur during the lifetime of the building (m_j = 6.0 and 7.0 earthquakes). However, for infrequent earthquakes (m_j = 8.0 earthquakes), non-Poisson renewal models may be more appropriate as described in Section 2.3. In this case, Eq. (2.14) is transformed as follows.

$$E[C_L] = C_I + \frac{Q^{t_{life}} - 1}{\ln Q}\{0.570E[C_D(6.0)] + 0.083E[C_D(7.0)]\}$$

$$+ E[C_D(8.0)]\int_{t_0}^{t_0+t_{life}} Q^{t-t_0}\sum_{n=1}^{\infty} f_{W_n}(t, 8.0 | W_1 > t_0)dt$$

for $Q \neq 1$ (3.2a)

and

$$E[C_L] = C_I + t_{life}\{0.570E[C_D(6.0)] + 0.083E[C_D(7.0)]\} + E[C_D(8.0)]\int_{t_0}^{t_0+t_{life}} \sum_{n=1}^{\infty} f_{W_n}(t, 8.0 | W_1 > t_0)dt$$

for $Q = 1$ (3.2b)

Anagnos and Kiremidjian (1988) reviewed several renewal models used to describe earthquake occurrences. More recently, one renewal model, the Brownian Passage Time (BPT) model, has been applied to long-term estimation of earthquake probabilities (HERP, 2001a; WGCEP, 1999) since it was proposed by Matthews (1998). The Brownian motion with a drift is able to simulate physical phenomena similar to seismic activity, i.e., accumulation of stress or strain of the crust around the rupture plane. The Brownian motion is renewed when it hits a certain limit as illustrated in Figure 3.11, and this corresponds to a relief of the accumulated stress, that is, a fault rupture. The BPT model is the PDF of the interarrival time between successive renewals and is expressed as

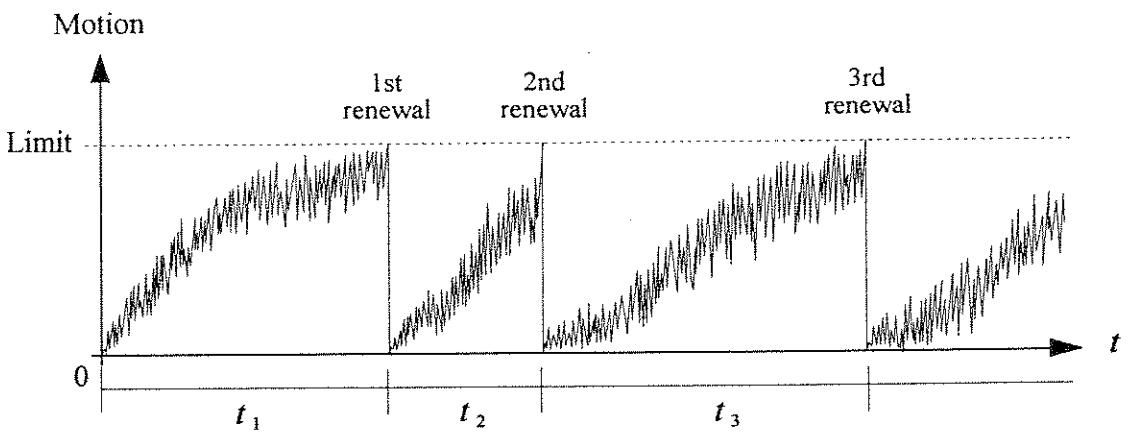

Figure 3.11 Time vs. Brownian motion with drift and renewal

$$f_T(t) = \sqrt{\frac{\mu}{2\pi\alpha^2 t^3}} \exp\left\{-\frac{(t-\mu)^2}{2\mu\alpha^2 t}\right\} \tag{3.3}$$

where T is a random variable standing for the interarrival time, μ is the mean and α is the

aperiodicity (= coefficient of variation). This model is applied only to m_j = 8.0 earthquakes, and the original (unconditional) PDF of the time to the first event from the last one is

$$f_{W_1}(t,8.0) = \sqrt{\frac{\mu}{2\pi\alpha^2 t^3}} \exp\left\{-\frac{(t-\mu)^2}{2\mu\alpha^2 t}\right\} \tag{3.4}$$

The updated PDF, $f_{W_1}(t,8.0|W_1 > t_0)$, can be obtained by using Eq. (2.6). The integration of the denominator in Eq. (2.6) is performed numerically. In general, it is difficult to obtain theoretical solutions of $f_{W_n}(t,8.0|W_1 > t_0)$ or $\sum_{n=1}^{\infty} f_{W_n}(t,8.0|W_1 > t_0)$ for non-Poisson renewal models. (One particular case, where the interarrival times are gamma distributed, leads to manageable expressions. See Appendix B for the case.) Fortunately, for infrequent events, the probability of the first one is dominant and the others are negligible, i.e., we can assume that the earthquake occurs only once at most during the lifetime. This assumption has been explicitly used to estimate earthquake probabilities (HERP, 2001a; WGCEP, 1990; 1999). This approximation is expressed as

$$\sum_{n=1}^{\infty} f_{W_n}(t,8.0|W_1 > t_0) \approx f_{W_1}(t,8.0|W_1 > t_0) \tag{3.5}$$

With the above approximation, Eq. (3.2) becomes

$$E[C_L] = C_I + \frac{Q^{t_{life}} - 1}{\ln Q}\{0.570E[C_D(6.0)] + 0.083E[C_D(7.0)]\} + E[C_D(8.0)]\int_{t_0}^{t_0+t_{life}} Q^{t-t_0} f_{W_1}(t,8.0|W_1 > t_0)dt$$

for $Q \neq 1$ (3.6a)

and

$$E[C_L] = C_I + t_{life}\{0.570E[C_D(6.0)] + 0.083E[C_D(7.0)]\} + E[C_D(8.0)]\int_{t_0}^{t_0+t_{life}} f_{W_1}(t,8.0|W_1 > t_0)dt$$

for $Q = 1$ (3.6b)

Wesnousky *et al.* (1984) modeled the occurrence of large earthquakes on the Sagami trough using the lognormal distribution with μ = 200 years and COV = 0.10. Inoue and Kanda (1993) used the Weibull distribution with μ = 200 years and COV = 0.18. A more recent study by HERP (2001a) assumed a common value α = 0.24 for several troughs around Japan for the BPT model. In this study, μ and α for Eq. (3.4) are specified to be 200 years and 0.24, respectively. The last event is the 1923 Kanto Earthquake. Figure 3.12(a) shows the occurrence rate, $\sum_{n=1}^{\infty} f_{W_n}(t,8.0|W_1 > t_0) \approx f_{W_1}(t,8.0|W_1 > t_0)$, for t_0 = A.D.1999 when the actual building started to operate, i.e., 76 years after the last event. Figure 3.12(b) is for t_0 = A.D.2075, which is another 76 years after t_0 = A.D.1999. The mean annual occurrence rate of the Poisson model, $\nu(8.0)$ = 0.005, is also displayed in the figures. In the case of t_0 = A.D.1999, the original and updated PDFs are almost the same because the probability before t_0 is nearly equal to zero, that is, the denominator of Eq. (2.6) is almost unity. From Figure 3.12(a), we can see that the Poisson model overestimates the occurrence rate during the lifetime (t_{life} = 50 years, shaded segment). On the other hand, Figure 3.12(b) demonstrates that the Poisson model underestimates in the case of t_0 = A.D.2075.

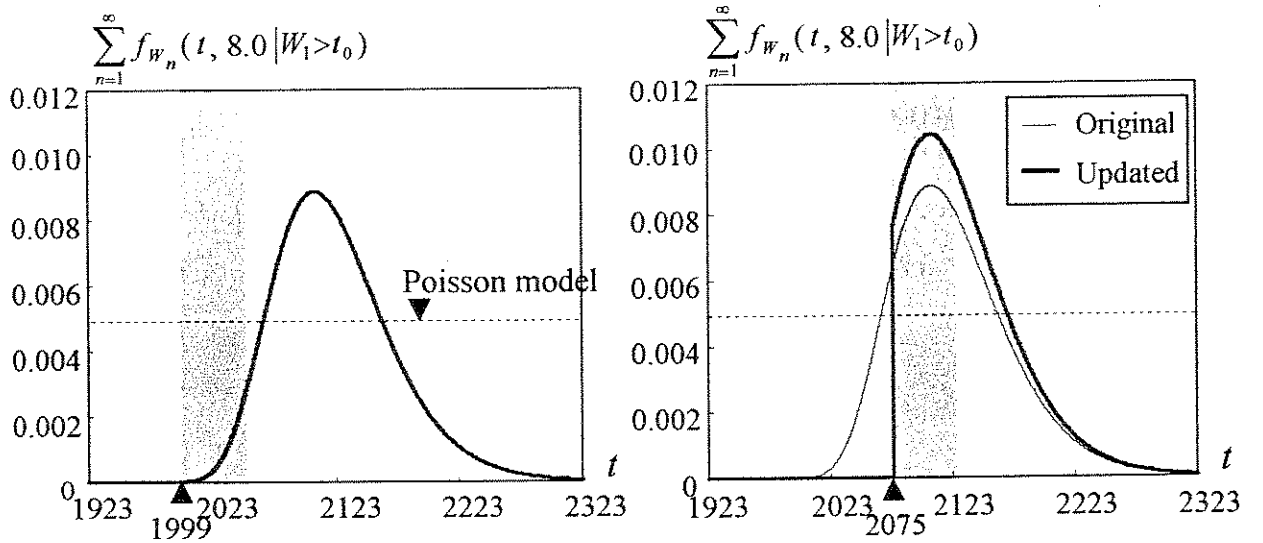

(a) t_0 = A.D.1999 **(b) t_0 = A.D.2075**

Figure 3.12 Occurrence rate for BPT model (μ = 200 years and α = 0.24)

There are many seismic sources around Tokyo besides the Sagami trough. Earthquakes that occur around troughs are called interplate earthquakes. The return periods of interplate earthquakes around Japan are roughly estimated about a few hundred years, and they are considered prominently in risk analyses because of their high probability. On the other hand, several active faults that produce intraplate earthquakes also exist around the Tokyo Area (Research Group for Active Faults in Japan, 1991). Such seismic sources should be taken into account though their return periods are estimated to be several hundred to several thousand years. Their contributions can be added in Eq. (2.14) or (2.18) if historical data or trench investigation data is available (HERP, 2001b; Research Group for Active Faults in Japan, 1991).

In Eqs. (3.1) and (3.6), we have to compute $E[C_D(6.0)]$, $E[C_D(7.0)]$ and $E[C_D(8.0)]$ (the expected damage costs due to earthquakes with magnitudes m_j = 6.0, 7.0 and 8.0, respectively). The following section describes the method for estimating these expected values.

3.4 Simulations

3.4.1 Fault rupture and elastic wave propagation*

In conventional seismic hazard analyses, empirical relationships are utilized to predict the intensity of ground motion at specified sites. Recent empirical models are reviewed by Abrahamson and Shedlock (1997). These relationships are convenient for computing intensities at numerous points for such application as developing of hazard maps, loss estimation of wide regions or institutions (Comerio, 2000; EERI, 1997; FEMA, 1999). However, more physically-based techniques to generate time histories of ground motions have been developed in seismology, and they are more appropriate for risk analyses of a specific building. Among them, the FSGF (Finite-fault Stochastic Green's Function) method is selected for this study. This method was proposed by Kamae *et al.* (1991) so as to generate strong ground motions considering finite fault effects such as directivity and heterogeneous slip. Der Kiureghian and Ang (1977) were the first to point out the importance of these effects in seismic hazard analyses, and that has been well recognized by others (Si and Midorikawa, 2001; Somerville *et al.*, 1997). The FSGF method accounts for mainly shorter period (< 1.0 second) ground motions, and is

* References for the fundamentals: Aki and Richards (1980); Lay and Wallace (1995)

frequently applied in Japan (Dan *et al.*, 2000; Itoh and Kawase, 2001; Si and Midorikawa, 2001). In the United States, Beresnev and Atkinson (1998a) developed a FORTRAN program FINSIM, and have been calibrating parameters comparing with ground motions recorded in Mexico and Western and Eastern United States (1997, 1998a, 1999). The Hybrid Green's function method (Kamae *et al.*, 1998), which is a combination of the FSGF method and the theoretical Green's function method, can account for not only short period but also long period (> 1.0 second) motions. This is expected to be one of the foremost techniques to predict strong ground motions. However, it requires long calculation time to generate sample ground motions until now.

The concept of the FSGF method is that a strong ground motion from a large fault rupture is the sum of several motions from small ruptures, as illustrated in Figure 3.13. A rupture plane is divided into several subfaults, and the rupture initiates from a hypocenter. An elastic wave propagates from the hypocenter to the building site, and simultaneously the rupture propagates radially over the rupture plane. When the rupture reaches other subfaults, elastic waves propagate from them. At the site, ground motions from all subfaults are integrated considering time delays because of wave and rupture propagations as shown in the right side of Figure 3.13. This method is able to generate finite fault effects, such as directivity and heterogeneous slip.

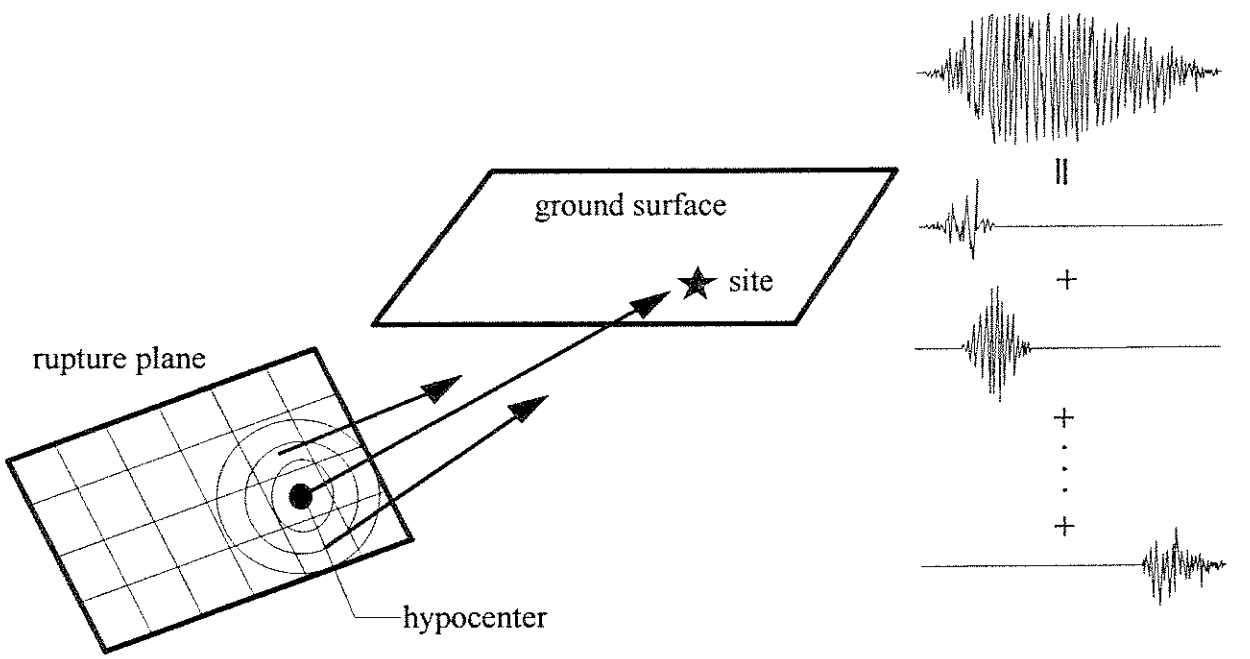

Figure 3.13 FSGF (Finite-fault Stochastic Green's function) method

One example of the directivity effects generated by FINSIM is shown in Figure 3.14. The size of the rupture plane corresponds to that of a strike slip earthquake with m_j = 7.0 (Wells and Coppersmith, 1994). The rupture is assumed to start at the southern end of the rupture plane, and propagate toward the north. In order to compare the pure effect of rupture directivity, homogeneous slips are assumed over the plane. The top and bottom figures are ground motion histories observed at points N and S, respectively. The origins of the horizontal axes represent the time when the rupture initiates. The directivity is like the Doppler effect in physics: a ground motion with a higher frequency content, larger amplitude and shorter duration is observed at point N (in the direction toward which the rupture propagates).

A ground motion from each subfault is expressed as one generated by the PSGF (Point-source Stochastic Green's Function) method that was proposed by Boore (1983) to predict strong ground motions from future earthquakes. Since the PSGF method assumes a point source for a rupture plane, it is appropriate when the rupture can be regarded to be small relative to the distance between the rupture and the observation point. In seismology, it is well known that shorter period (< 1.0 second) accelerations are deterministically unpredictable. Therefore, the PSGF method utilizes a stochastic time history. Following Boore (1983), first a Gaussian white noise $w(t)$ is modulated in the time domain using a shape function (Saragoni and Hart, 1974)

$$w(t) = at^b e^{-ct} H(t) \tag{3.7}$$

where $H(t)$ is the unit step function, and

$$b = -\frac{\varepsilon \ln \eta}{1 + \varepsilon(\ln \varepsilon - 1)} \tag{3.8}$$

$$c = \frac{b}{\varepsilon T_w} \tag{3.9}$$

$$a = \sqrt{\frac{(2c)^{2b+1}}{\Gamma(2b+1)}} \tag{3.10}$$

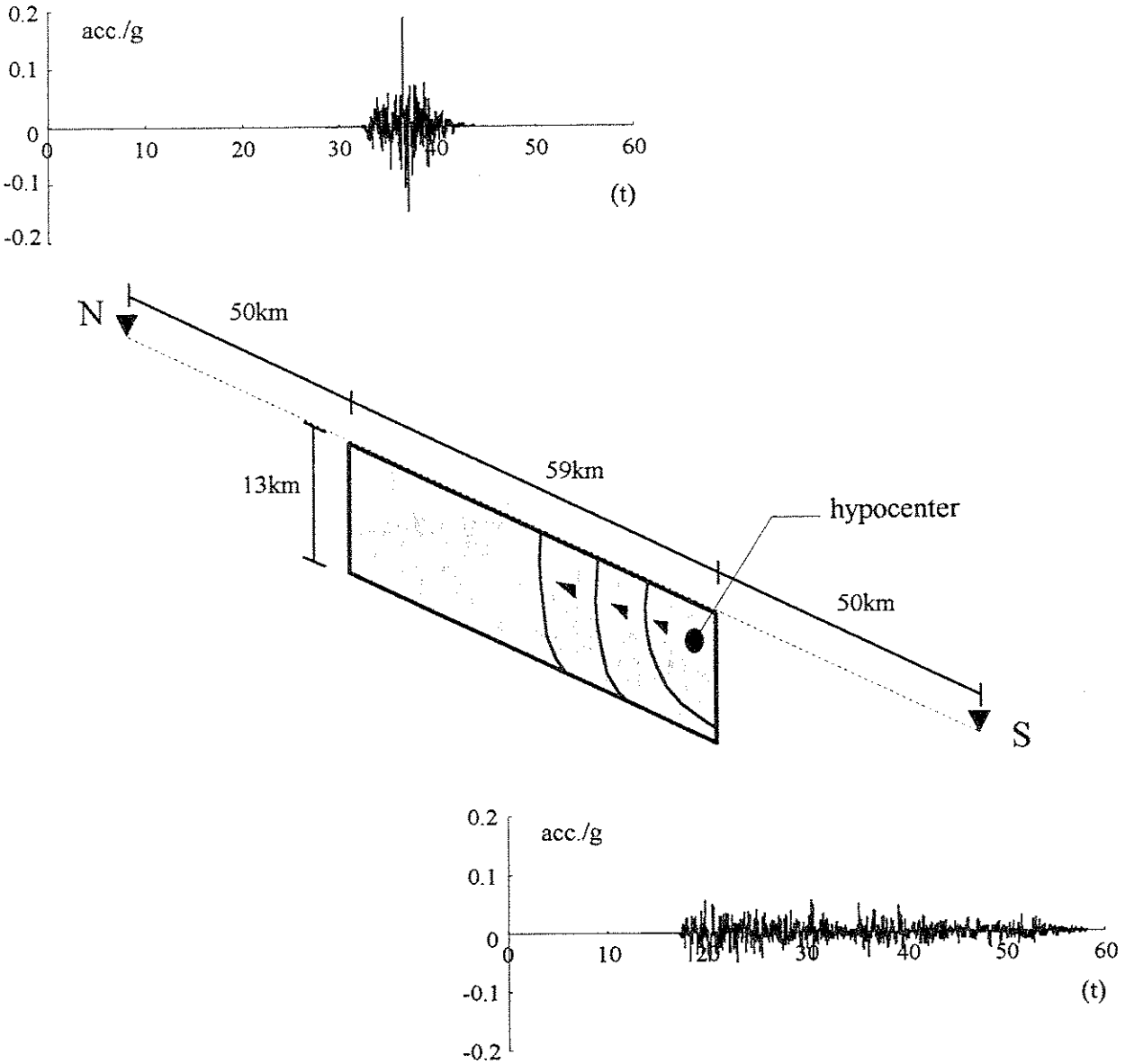

Figure 3.14 Effect of directivity generated by FINSIM

where $T_w = 2T_d$, $\eta = 0.05$ and $\varepsilon = 0.2$. Here, T_d is the source duration

$$T_d = f_c^{-1} \tag{3.11}$$

where f_c is the corner frequency obtained as

$$f_c = 4.9 \times 10^6 V_S (\Delta\sigma / M_0)^{1/3} \tag{3.12}$$

where f_c is in Hertz, V_S is the shear wave velocity in km/s, $\Delta\sigma$ is the stress parameter in bar, and M_0 is the seismic moment in dyne-cm (Brune, 1970; 1971). The windowed Gaussian white noise is transformed into the frequency domain to be multiplied by the acceleration spectrum $A(f)$, and then transformed back to the time domain. The acceleration spectrum $A(f)$ of shear wave at distance R from a fault rupture with seismic moment M_0 is given by

$$A(f) = \frac{R_{\theta\phi} \cdot FS \cdot PRTITN}{4\pi\rho V_S^{\,3}} M_0 S(f, f_c) P(f, F_{\max}) \frac{e^{-\frac{\pi f R}{Q V_S}}}{R} \tag{3.13}$$

where FS is the amplification due to the free surface and $PRTITN$ is the reduction factor for partitioning the energy into two horizontal components; 2.0 and $1/\sqrt{2}$, respectively. $R_{\theta\varphi}$ is the radiation pattern coefficient, which is specified to be 0.55 in the FINSIM based on Boore and Boatwright (1984). ρ is the density of the base rock. Moment magnitude m_j is converted into the seismic moment M_0 (in dyne-cm) according to (Kanamori, 1977)

$$M_0 = 10^{\frac{3}{2}(m_j + 10.73)} \tag{3.14}$$

For the source spectrum, the ω^2 model (Aki, 1967; Brune, 1970; 1971) is used:

$$S(f, f_c) = \frac{(2\pi f)^2}{1 + (f / f_c)^2} \tag{3.15}$$

$P(f, F_{max})$ is a high-cut filter that accounts for a sharp decrease above some frequency F_{max}.

$$P(f, F_{max}) = \frac{1}{\sqrt{1+(f / F_{max})^8}} \tag{3.16}$$

F_{max} is taken as 15.0 Hertz by Boore (1983). In this PSGF method, only the average spectrum of the sample ground motions matches the target spectrum $A(f)$ instead of each sample.

In this study, the program FINSIM by Beresnev and Atkinson (1998b) is used to generate strong ground motions because it is widely used, easy to handle, and is readily available from the authors. To consider uncertainties of fault rupture such as location within a seismic source and slip distribution, several improvements were made to the original FINSIM. In the original FINSIM, the location, strike and dip of the rectangular rupture plane are specified deterministically. However, it is almost impossible to predict those parameters for future earthquakes. Therefore, in the modified FINSIM, only the location, strike and dip of a rectangular seismic source where ruptures are possible to occur are determined. Then a rectangular rupture plane is randomly located within the given source, and a hypocenter is also randomly located within the rupture plane as shown in Figure 3.15. In determining the size of the rupture plane (length L and width W in Figure 3.15), empirical relations between the moment magnitude m_j and the size of the rupture plane can be used according to the type of the earthquake, e.g., intraplate or interplate, normal, reverse, or strike slip (Sato, 1979; Watanabe *et al.*, 1998; Wells and Coppersmith, 1994). Among them, the following two equations obtained by Sato (1979), which are applicable to interplate earthquakes around Japan including those near the Sagami trough, are used in this case study.

$$L = 10^{0.5m_j - 1.88} \tag{3.17}$$

$$W = L / 2 \tag{3.18}$$

The values for L and W corresponding to m_j = 6.0, 7.0 and 8.0 earthquakes are shown in Table 3.1. Modeling errors are ignored since they are not found in the study by Sato (1979).

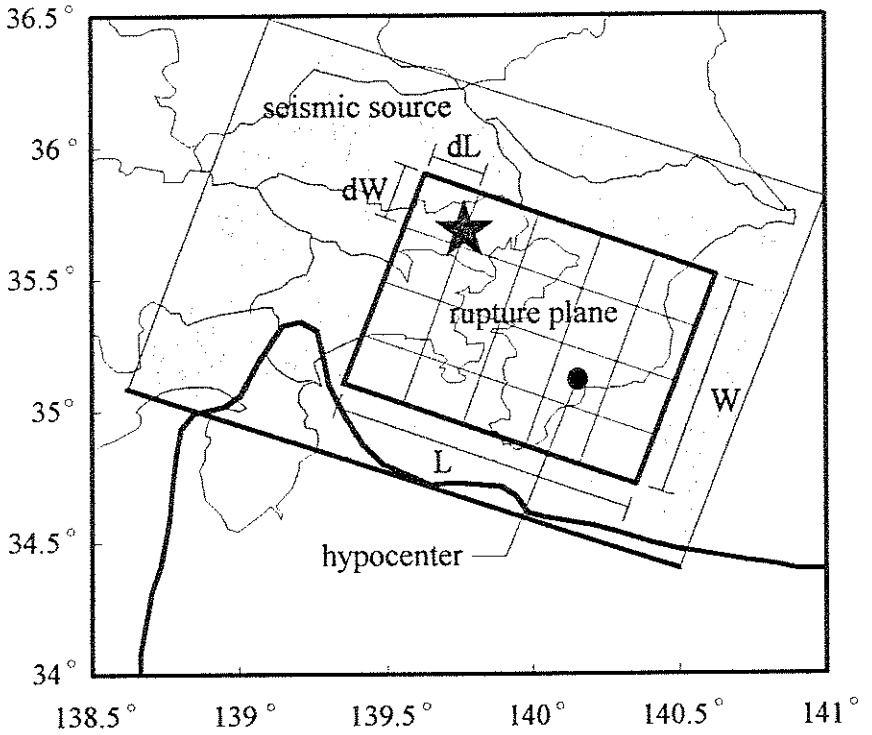

Figure 3.15 Rupture plane on seismic source

Table 3.1 Size of fault and subfault (in km)

m_j	L	W	dL	dW
6.0	13.2	6.6	2.6	2.2
7.0	41.7	20.8	6.0	6.9
8.0	131.8	65.9	16.5	16.5

The finite fault rupture plane is divided into several subfaults with dimensions dL and dW, as listed in Table 3.1. These dimensions are used as approximations in place of the subfault dimensions proposed by Beresnev and Atkinson (1999).

$$dl = 10^{0.4m_j - 2} \tag{3.19}$$

In the original FINSIM, an array of random slips over a rupture plane is specified by the user or generated using normal random variables. The random variable generator is modified to produce

lognormal random variables because a set of normal variables includes negative values. The generated variables represent relative slips, and absolute values are determined so that the average slip $\overline{D}$ satisfies the following equation.

$$M_0 = \mu \overline{D} LW \tag{3.20}$$

where M_0 is the given seismic moment defined in Eq. (3.14), μ is the rigidity of the crust around the rupture, and $\overline{D}$ is the average slip over the rupture plane. Recently, a statistical study concerning slip distribution was conducted (Somerville *et al.*, 1999). Such interesting results will be applied in the future.

After the rupture plane, hypocenter and an array of slips are generated for each sample, the subsequent steps are the same as those of the original FINSIM. The modified FINSIM is able to generate a number of samples (stochastic ground motions) at a specific site. Table 3.2 shows the parameters used in the modified FINSIM to generate ground motions from the Sagami trough.

Table 3.2 Parameters for stochastic ground motions

Source	
$\Delta\sigma$ (bars)	50
V_S (km/s)	3.7
rupture velocity	$0.8 \times V_S$
ρ (g/cm^3)	2.8
fault-slip distribution	heterogeneous (lognormal distribution)
radiation strength factor	1.0
Propagation	
$Q(f)$	1000
geometric spreading	$1/R$
distant-dependent duration time (sec)	0.00
F_{max}(Hz)	15.0
$w(t)$	Saragoni-Hart (1974)

The FINSIM generates ground motions at the surface of a homogeneous medium. Here the base rock (V_S = 3.7 km/s, ρ = 2.8 g/cm^3) the depth of which is about 2.6 km beneath the Kanto region (Sato *et* al., 1999) is taken as a homogeneous medium. Above that, the structure of the crust changes, and the crustal amplification cannot be neglected (Boore and Joyner, 1997). Amplification through the overlaying surface soils (V_S < 600 m/s) is considered in the subsequent section. Boore and Joyner (1997) made approximate amplification factors in Western and Eastern United States using the quarter-wavelength approximation. However, in this study, linear analyses are performed using SHAKE'91 (Idriss and Sun, 1991) so as to utilize the particular underground structure of the Kanto region as shown in Table 3.3 (Sato *et al.*, 1999). H represents the thickness of each layer.

Table 3.3 Underground structure of Kanto region (Sato *et al.*, 1999)

	H (m)	ρ (g/cm^3)	V_S (m/s)	Q value
bedrock ▼	200	1.80	600	100
	800	2.00	1200	150
	800	2.10	1300	150
base rock ▼	800	2.30	1400	150
	∞	2.80	3700	1000

Figure 3.16 shows the acceleration response spectra (5% damping) for m_j = 6.0 earthquakes at the top of the bedrock generated by the modified FINSIM and SHAKE'91. In the figure, statistics of 100 samples are shown. Figures 3.17(a) and 3.17(b) are acceleration time histories with the smallest and largest PGAs of the 100 samples. We can see that there is considerable variation among ground motions resulting from ruptures with the same magnitude. For smaller earthquakes that have small rupture planes, the distance between the rupture plane and the observation point strongly affects the intensity of observed ground motions. It is intuitively understood that a weak ground motion is observed when the rupture occurs far from the point,

and vice versa. Theoretically, the amplitude of a ground motion is inversely proportional to the distance R in Eq. (3.13). Similarly, Figures 3.18 and 3.19 are the results for m_j = 8.0. For larger earthquake, the shortest distances of the 100 samples are not so different regardless of the location of the rupture within the seismic source. In this case, the finite fault effects affect the intensity of the ground motions. Table 3.4 shows the statistics, i.e., the mean, the maximum (max), the minimum (min) and the standard deviation (SD), of PGAs of the 100 time histories for each magnitude.

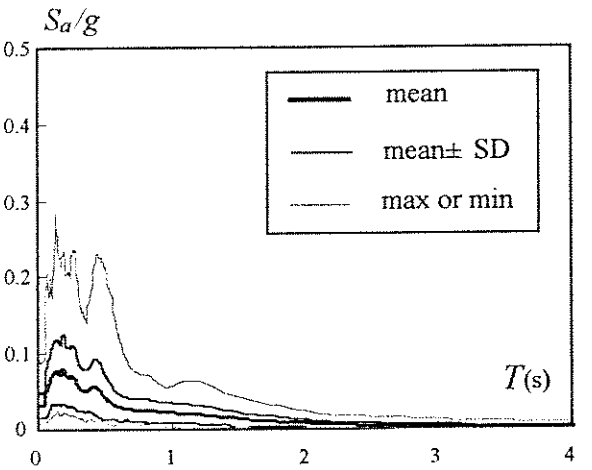

Figure 3.16 Acceleration response spectra at bedrock for m_j = 6.0 earthquakes

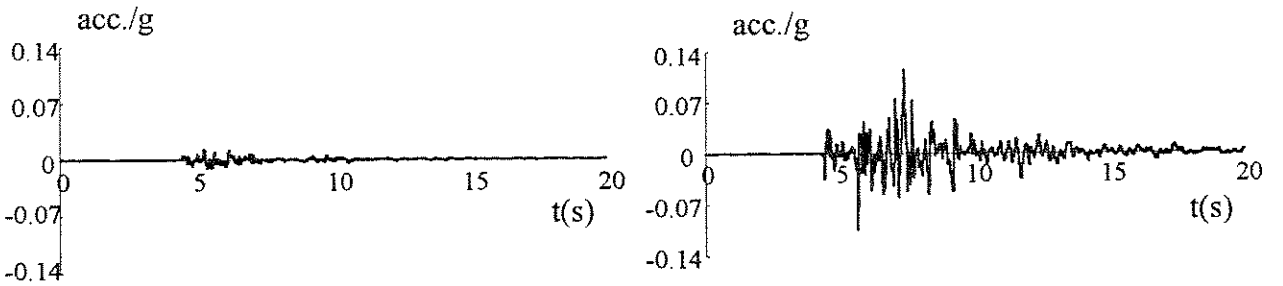

(a) With smallest PGA **(b) With largest PGA**

Figure 3.17 Acceleration time histories at bedrock for m_j = 6.0 earthquakes

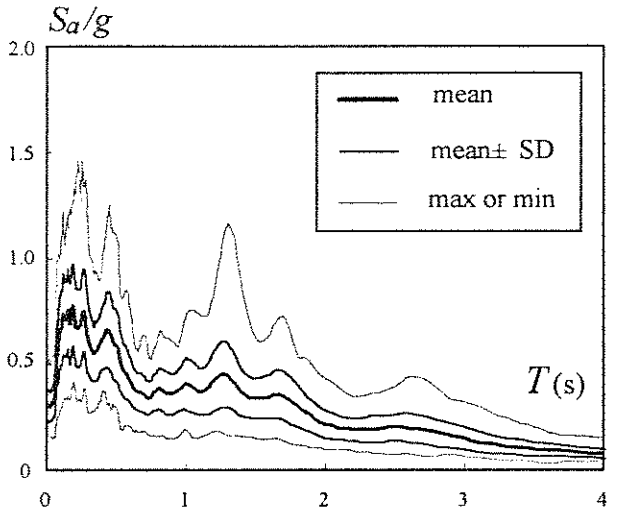

Figure 3.18 Acceleration response spectra at bedrock for m_j = 8.0 earthquakes

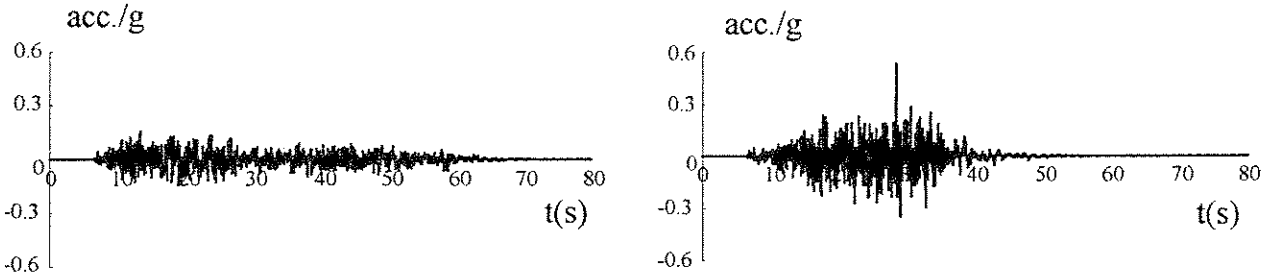

(a) With smallest PGA **(b) With largest PGA**

Figure 3.19 Acceleration time histories at bedrock for m_j = 8.0 earthquakes

Table 3.4 Statistics of PGA at bedrock (in *g*)

m_j	mean	max	min	SD
6.0	0.040	0.115	0.013	0.018
7.0	0.111	0.279	0.037	0.049
8.0	0.308	0.532	0.157	0.073

3.4.2 Surface soil amplification*

Hwang *et al.* (1990) and Hwang and Huo (1994) simulated local site effects using SHAKE (Schnabel *et al.*, 1972) while considering uncertainties of soil properties. In this study, SHAKE'91 (Idriss and Sun, 1991), which is a slightly improved version of the original SHAKE, is used, and similar equivalent linear analyses are performed. Only the crust profile (Table 3.3) was analyzed to show the ground motions at the top of the bedrock ($V_S \geq 600$ m/s) of the previous section. If amplifications by the crust and surface soils ($V_S < 600$ m/s) are simulated separately, the refraction and the reflection between them are ignored. For this reason, the surface soil profile is connected to the top of the crust profile, and base rock accelerations generated by the modified FINSIM are input into the combined profile again in SHAKE'91. The crust and the soil profile beneath the site is shown in Table 3.5 (Sato *et al.*, 1999; KKE, 2001c). As described in Section 3.2, the building under consideration has two underground floors, and the depth to the base from the GL (Ground Level) is 11.0 (m). Thus, the waves at GL – 11.0 (m) are generated to be applied at the base of the building. Values in Table 3.5 are regarded as the mean values of the properties of the surface soils. Uncertainties of representative properties of the surface soils, including shear wave velocity V_S, unit weight ρ and thickness H of each layer, are modeled by lognormal random variables with COV (Coefficient Of Variation) shown in Table 3.6. These values are determined by referring to surveys on the Kanto region by Ahmed *et al.* (1996) and Ohsaki and Sakaguchi (1973). For rock layers (shaded part in Table 3.5), deterministic values are assumed because their variability does not significantly affect the final results.

For clayey and sandy soils, nonlinearity is considered while linear properties are assumed for rock layers. Nonlinearity of soils is expressed as a pair of two relationships: (a) between the shear strain γ and the shear modulus reduction ratio G/G_0, and (b) between γ and the damping ratio ξ. Numerous studies on the nonlinearity are found, e.g., Hara (1980), Isenhower (1979), Lodde (1982), Martin (1976), Seed and Idriss (1970), Seed *et al.* (1984) and Vucetic and Dobry (1991). In particular, Hwang *et al.* (1990) and Hwang and Huo (1994) constructed probabilistic models based on past studies, and we employ them in this study. They set mean, upper- and lower- bounds as illustrated in Figure 3.20. To generate one sample of the nonlinear curve, a normal random variable with the mean = 0.0 and SD (Standard Deviation) = 1.0 is generated,

* Reference for the fundamentals: Kramer (1996)

Table 3.5 Crust and soil profile at the building site (shaded part is same as Table 3.3)

	type	H (m)	ρ (g/cm^3)	V_S (m/s)	Q value
base of building					
GL-11.0m ▼	sandy gravel	2.35	2.10	220	---
	sand	3.45	1.75	210	---
	silty clay	1.45	1.96	180	---
	sandy gravel	4.55	2.10	260	---
	sand	1.90	1.80	230	---
	sand	10.00	1.89	230	---
	silty clay	4.00	1.61	190	---
	silt	3.00	1.70	280	---
bedrock ▼	sand	8.60	1.90	380	---
	rock	200	1.80	600	100
	rock	800	2.00	1200	150
	rock	800	2.10	1300	150
base rock ▼	rock	800	2.30	1400	150
	rock	∞	2.80	3700	1000

Table 3.6 Variability of surface soil properties

(from Ahmed *et al.*, 1996; Ohsaki and Sakaguchi 1973)

	COV
V_S	10%
ρ	20%
H	10%

and multiplied by a given SD and added to the mean at each strain level. The SD of the random variable is determined so that the upper- and lower-bound curves correspond to the mean ± 3SD in this study. If the absolute value of a generated random variable exceeds 3.0 (the sample gets out of either upper- or lower-bound), it is discarded and another one is generated.

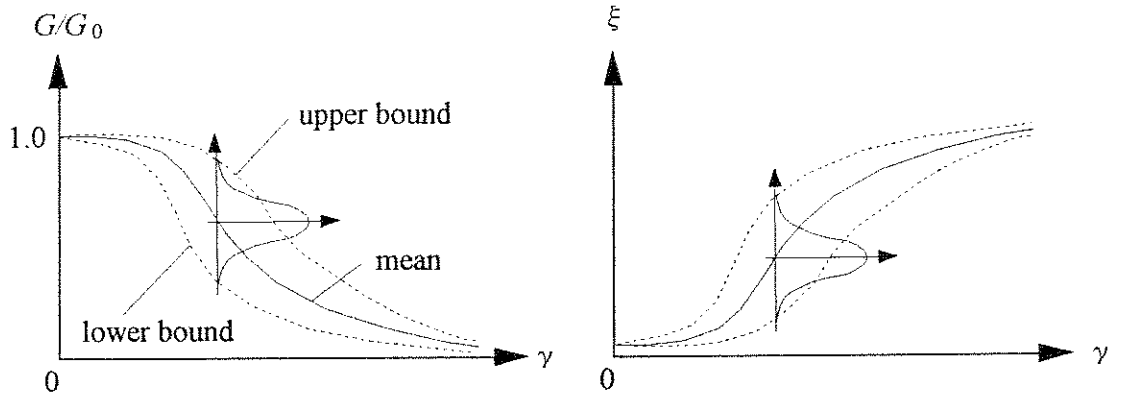

(a) Shear strain – modulus reduction **(b) Shear strain – damping ratio**

Figure 3.20 Probabilistic models for nonlinear curves

Hwang and Huo (1994) generated the mean, upper- and lower-bound curves of clayey soils. For clayey and silty soils, the curves (for Plasticity Index = 50) displayed in Figure 3.21 are used in this study. Tables 3.7 and 3.8 show the values at each strain level.

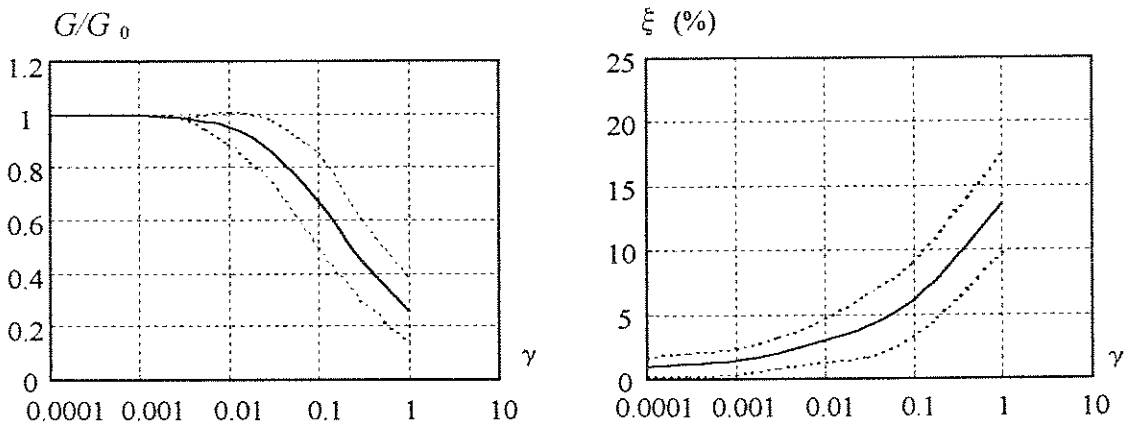

(a) Shear strain – modulus reduction **(b) Shear strain – damping ratio**

Figure 3.21 Nonlinear curves for clayey soils (Hwang and Huo, 1994)

Table 3.7 Modulus reduction ratio for clayey soil (Hwang and Huo, 1994)

strain (%)	mean	SD	COV
1×10^{-4}	1.00	0.00	0.00
3×10^{-4}	1.00	0.00	0.00
1×10^{-3}	1.00	0.00	0.00
3×10^{-3}	0.99	0.00	0.00
1×10^{-2}	0.95	0.02	0.02
3×10^{-2}	0.86	0.04	0.04
1×10^{-1}	0.67	0.06	0.09
3×10^{-1}	0.45	0.05	0.11
1×10^{0}	0.26	0.04	0.15

Table 3.8 Damping ratio for clayey soil (Hwang and Huo, 1994)

strain (%)	mean (%)	SD (%)	COV
1×10^{-4}	1.00	0.25	0.25
3×10^{-4}	1.20	0.30	0.25
1×10^{-3}	1.42	0.40	0.25
3×10^{-3}	2.01	0.60	0.20
1×10^{-2}	3.00	0.97	0.19
3×10^{-2}	4.13	1.22	0.19
1×10^{-1}	6.14	1.61	0.14
3×10^{-1}	9.47	1.45	0.12
1×10^{0}	13.59	1.28	0.09

For sandy and gravelly soils, we also employ the probabilistic models by Hwang and Huo (1994). They modeled the shear modulus reduction curves for sandy soil using Martin-Davidenkov's model (Martin, 1976)

$$\frac{G}{G_0} = 1 - \left[\frac{(\gamma/\gamma_0)^{2B}}{1+(\gamma/\gamma_0)^{2B}}\right]^{A} \tag{3.21}$$

where A and B are parameters that define a form of the curve, and γ_0 is the reference strain expressed as

$$\gamma_0 = \frac{\tau_{max}}{G_0} \tag{3.22}$$

where τ_{max} is the maximum shear stress of soils under dynamic loading, and is estimated using (Harding and Drnevich, 1972)

$$\tau_{max} = \sqrt{\left[\left(\frac{1+K_0}{2}\right)\sigma_V' \sin\phi + c'\cos\phi\right]^2 - \left[\left(\frac{1-K_0}{2}\right)\sigma_V'\right]^2} \tag{3.23}$$

where c' is the apparent cohesion, ϕ is the effective angle of internal friction, σ_V' is the effective vertical stress, and K_0 is the coefficient of earth pressure. The values are estimated following Bowles (1984), Hunt (1984) and Hwang *et al.* (1990). For sandy soils, $c' = 0$ can be assumed, and Eq. (3.23) is simplified as follows.

$$\tau_{max} = \sigma_V' \sqrt{\left[\left(\frac{1+K_0}{2}\right)\sin\phi\right]^2 - \left(\frac{1-K_0}{2}\right)^2} \tag{3.24}$$

In Eq. (3.22), G_0 is calculated as

$$G_0 = \rho V_S^2 \tag{3.25}$$

Parameters A and B for the mean, upper- and lower-bound curves are shown in Table 3.9 (Hwang and Huo, 1994). The modulus reduction curves are displayed in Figure 3.22(a), and the values are listed in Table 3.10. We also employ the probabilistic model for nonlinear damping curves for sandy soils by Hwang and Huo (1994). Figure 3.22 (b) and Table 3.11 show the curves and the values, respectively.

Table 3.9 Parameter values of A and B (Hwang and Huo, 1994)

	A	B
upper	1.775	0.489
mean	0.941	0.441
lower	0.509	0.480

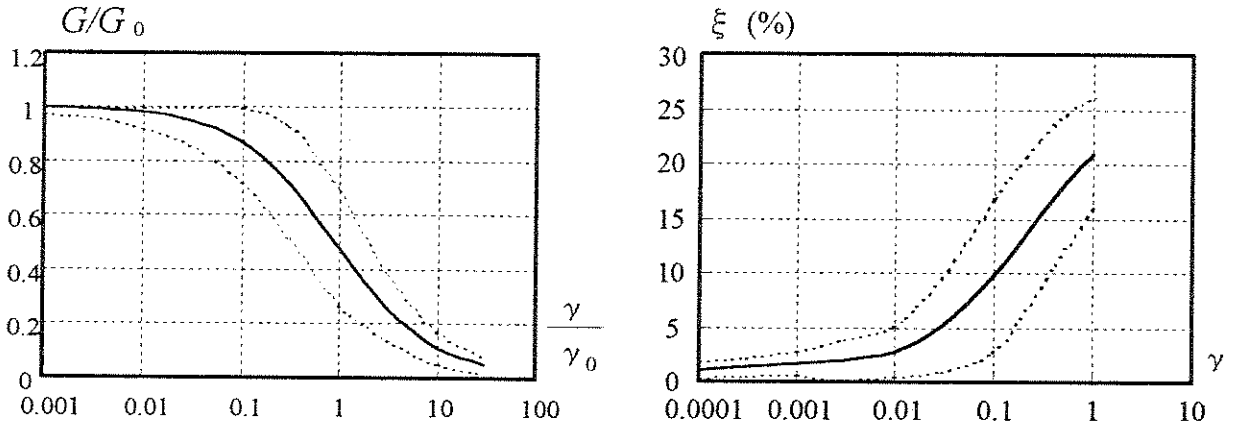

(a) Shear strain ratio – modulus reduction (b) Shear strain – damping ratio

Figure 3.22 Nonlinear curves for sandy soils (Hwang and Huo, 1994)

Table 3.10 Modulus reduction ratio for sandy soil (Hwang and Huo, 1994)

strain ratio γ / γ_0	mean	SD	COV
1×10^{-3}	1.00	0.01	0.01
3×10^{-3}	0.99	0.01	0.01
1×10^{-2}	0.98	0.02	0.02
3×10^{-2}	0.95	0.03	0.03
1×10^{-1}	0.87	0.05	0.06
3×10^{-1}	0.72	0.07	0.09
1×10^{0}	0.48	0.07	0.14
3×10^{0}	0.26	0.04	0.17
1×10^{1}	0.11	0.02	0.17
3×10^{1}	0.05	0.01	0.20

Table 3.11 Damping ratio for sandy soil (Hwang and Huo, 1994)

strain (%)	mean (%)	SD (%)	COV
1×10^{-4}	1.04	0.26	0.25
3×10^{-4}	1.31	0.27	0.21
1×10^{-3}	1.65	0.36	0.22
3×10^{-3}	2.00	0.63	0.32
1×10^{-2}	2.80	0.78	0.28
3×10^{-2}	5.10	1.41	0.28
1×10^{-1}	9.80	2.33	0.23
3×10^{-1}	15.50	2.27	0.15
1×10^{0}	21.00	1.72	0.08

In equivalent linear analyses using SHAKE'91, the equivalent uniform strain ratio is specified to be $(m_j\text{-}1)/10$ (Idriss, 1990), i.e., 0.5, 0.6 and 0.7 for m_j = 6.0, 7.0 and 8.0, respectively.

Figure 3.23 shows the statistics of the acceleration response spectra (5% damping) for m_j = 6.0 earthquakes at the base of the building. Figures 3.24(a) and (b) are acceleration time histories with the smallest and largest PGAs of the 100 samples, respectively. Comparing Figure 3.23 with Figure 3.16, we can see that shorter period contents around 0.3 second are greatly amplified by the surface soil. This is because the fundamental period of the surface soil is about 0.3 second, and weak ground motions from m_j = 6.0 earthquakes do not cause great nonlinearity of the surface soils.

Figures 3.25 and 3.26 are similar results for m_j = 8.0 earthquakes. Comparing Figure 3.25 with Figure 3.18, it is found that longer period contents are amplified by the surface soil, which is also confirmed by comparing the time histories. Nonlinearity of the surface soil layers induced by strong ground motions generates the low frequency amplification.

Table 3.12 shows the statistics of PGAs of the generated ground motions at the base of the building. The Japanese building code is assumed to cover ground motions up to about PGA = 0.4 (g). Thus, moderately designed buildings are expected to work well for m_j = 6.0 and 7.0 earthquakes. However, some ground motions from m_j = 8.0 ruptures exceed the coverage of the code. In addition, as we will describe in the next section, the natural period of the bare building under consideration is 1.19 (s), and the generated ground motions are amplified around that

frequency. When subjected to such ground motions, the bare building may sustain serious damage even if it is designed based on the code. This is investigated in the next section by applying the generated ground motions to the building models.

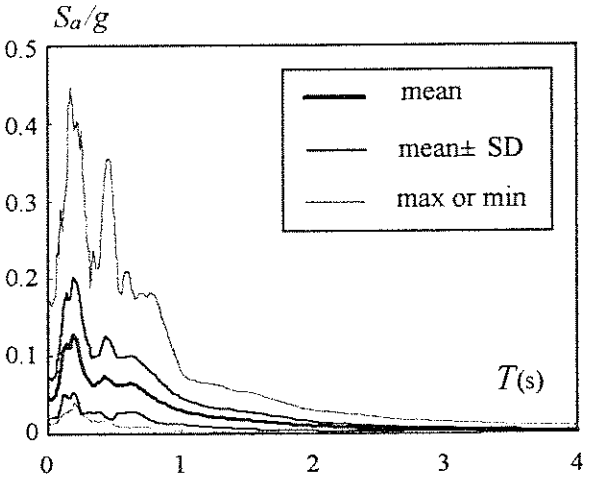

Figure 3.23 Acceleration response spectra at base of building for m_j = 6.0 earthquakes

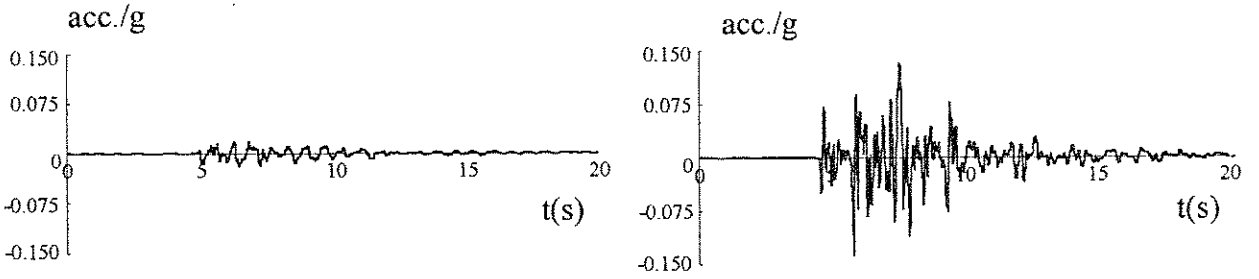

(a) With smallest PGA **(b) With largest PGA**

Figure 3.24 Acceleration time histories at base of building for m_j = 6.0 earthquakes

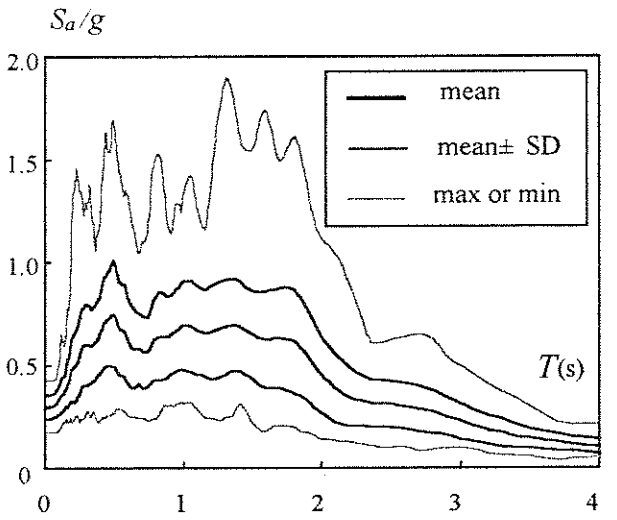

Figure 3.25 Acceleration response spectra at base of building for m_j = 8.0 earthquakes

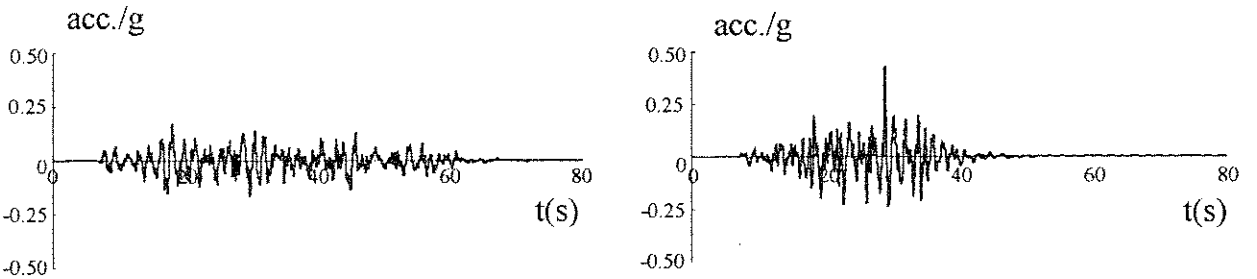

(a) With smallest PGA **(b) With largest PGA**

Figure 3.26 Acceleration time histories at base of building for m_j = 8.0 earthquakes

Table 3.12 Statistics of PGA at base of building (in g)

m_j	mean	max	min	SD
6.0	0.057	0.138	0.019	0.026
7.0	0.156	0.332	0.050	0.066
8.0	0.296	0.425	0.170	0.058

3.4.3 Dynamic response of building*

The building under consideration is modeled as a nine degree of freedom system as shown in Figure 3.27, with which we perform nonlinear dynamic response analyses. The underground stories of the building are so stiff and strong relative to the upper ones that they can be assumed to be rigid. This is equivalent to applying the ground motions generated in the previous section directly as input at the base of the first story of the building model. Monte Carlo simulations are performed, while considering uncertainties in mechanical properties of the building.

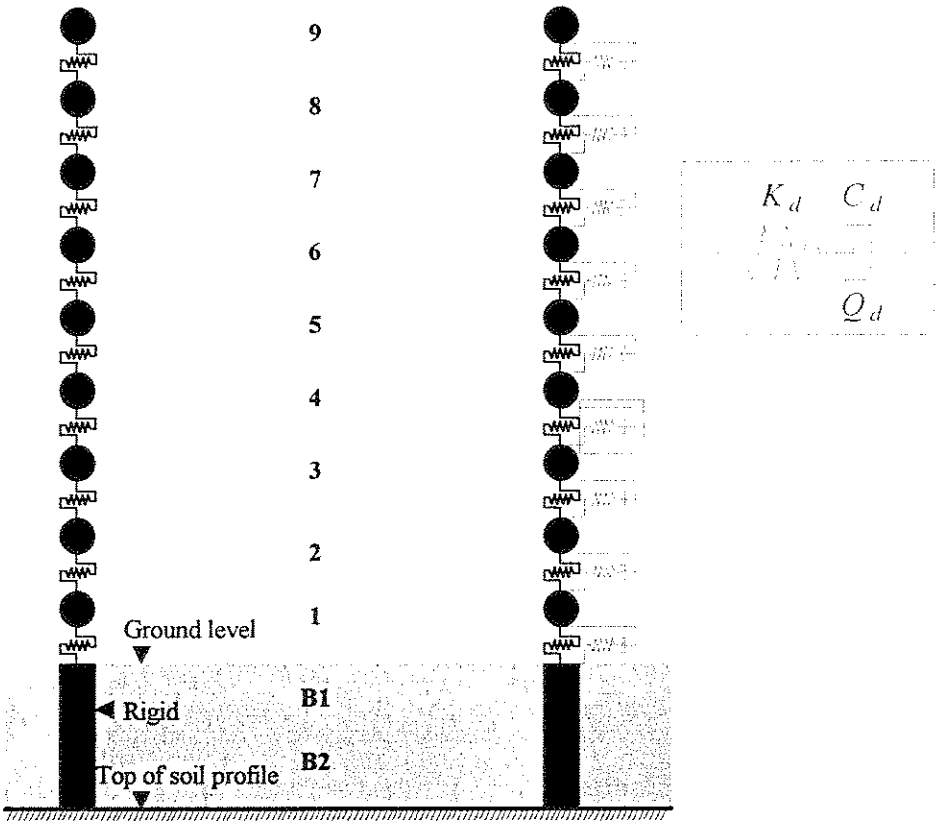

(a) Bare frame **(b) With dampers**

Figure 3.27 Nine degree of freedom system

The relationship between the inter-story drift and shear force of each story is modeled by a tri-linear curve as shown in Figure 3.28. The values of the mass M, stiffnesses K_1 and K_2, and strengths Q_{y1} and Q_{y2}, are listed in Table 3.13. The first, second, and third natural periods of the

* References for the fundamentals: Chopra (1995); Clough and Penzien (1993)

bare frame are 1.19 (s), 0.43 (s), and 0.26 (s), respectively. The base shear coefficient (capacity) is 0.53, which well exceeds 0.2 to 0.3 required for the building by the Japanese design code. The inherent damping is assumed to be 2 % for the first mode proportionally to the instantaneous stiffness.

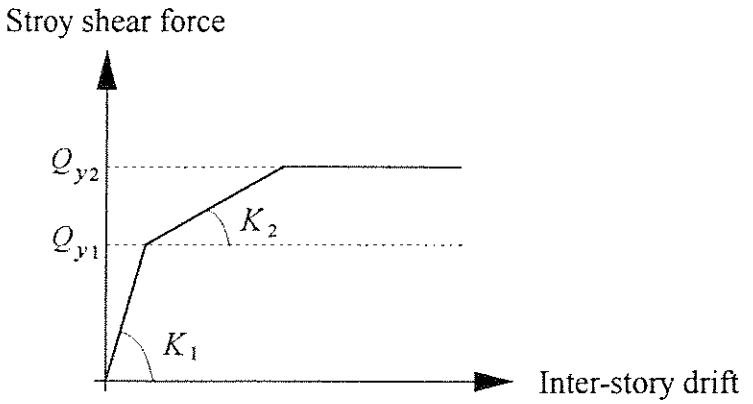

Figure 3.28 Inter-story drift vs. story shear force

Table 3.13 Mechanical properties of building model

Story	M (ton)	K_1 (kN/m)	K_2 (kN/m)	Q_{y1} (kN)	Q_{y2} (kN)
B2	---	---	---	---	---
B1	---	---	---	---	---
1	522.5	718231	492060	15376	23030
2	536.4	546595	440993	13945	20129
3	486.1	499555	412183	13191	18600
4	483.8	471380	396713	12417	17405
5	478.1	460110	397673	11486	16601
6	444.4	408170	343271	11221	15406
7	443.8	383915	351628	9521	13201
8	445.8	356230	334714	8813	10682
9	603.9	314335	313109	5072	7357

Variability of mechanical properties of the steel frame, i.e., story mass, story stiffness, story strength, and inherent damping, is modeled by assuming these variables to be statistically independent lognormal random variables. The COVs for the steel structure are determined from Sues *et al.* (1985), and listed in Table 3.14.

Table 3.14 Variability of mechanical properties of steel building (Sues *et al.*, 1985)

	COV
Stiffness	11%
Strength	10%
Story mass	23%
Inherent damping	65%

The fundamentals for viscous fluid dampers are summarized by Soong and Dargush (1997). Among them, oil dampers have been applied to seismic design of actual buildings in Japan because they have several important practical advantages, e.g., require no inspection or maintenance, little degradation, little sensitivity to ambient temperature and simple analytical models (Niwa *et al.*, 1995; Sano and Suzuki, 1998; Takahashi, *et al.*, 2001). In the KKE building, the oil dampers are installed directly in the diagonal steel braces as shown in Figure 3.4 (Ichihashi *et al.*, 2000; Takahashi, *et al.*, 2001). Figure 3.29 represents the relationship between deformation and load of an actual oil damper under harmonic excitation (1.0 Hz) with various amplitudes. The area of the hysteresis loop is equivalent to the dissipated energy by the damper. The damper exhibits an elliptic histeresis loop under small amplitude, whereas the force is released when it reaches about 450 kN. This is because a stress relief mechanism is incorporated in the damper in order to avoid excessive stress in the structure.

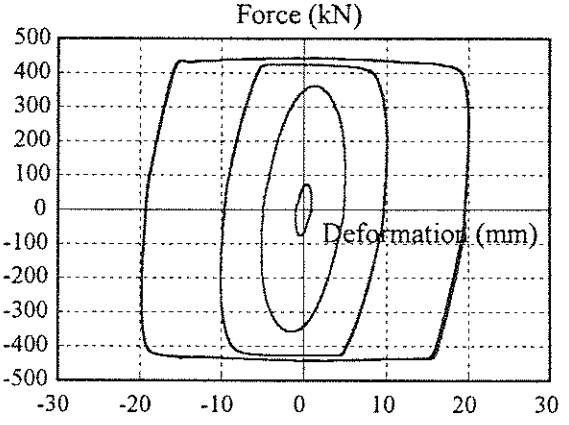

Figure 3.29 Hysiteresis loops of oil damper under harmonic excitation (courtesy of KKE)

The horizontal component of the force in the series of 4 steel braces and oil dampers in the same direction in each story is modeled as a nonlinear Maxwell model as shown in Figure 3.27(b). To simulate the nonlinearity of the oil dampers, the relationship between velocity and restoring force of a dashpot is set to be bi-linear as shown in Figure 3.30 (Ichihashi *et al.*, 2000; Takahashi, *et al.*, 2001). The nonlinear Maxwell models are set between two successive masses as shown in Figure 3.27(b), and their mechanical properties are shown in Table 3.15. Although all 72 dampers are the same in the actual building, different lengths and angles of the braces make slight differences in the horizontal values.

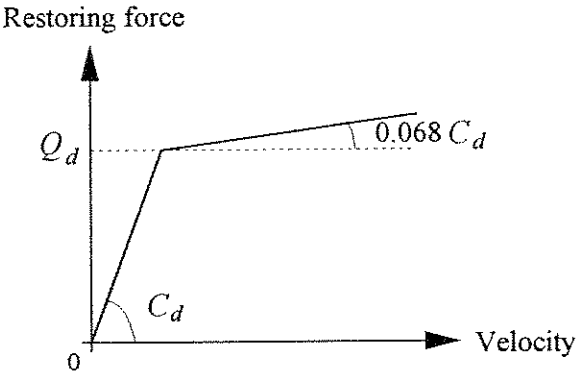

Figure 3.30 Velocity vs. restoring force of dashpot

Table 3.15 Mechanical properties of nonlinear Maxwell model

Story	K_d (kN/m)	C_d (kNs/m)	Q_d (kN)
B2	---	---	---
B1	---	---	---
1	234131.8	26597.2	1047.93
2	244637.4	27773.2	1047.05
3	250840.8	28478.8	1048.02
4	256074.0	29066.8	1046.41
5	258494.6	29341.2	1047.48
6	263100.6	29870.4	1048.45
7	267138.2	30321.2	1046.08
8	271283.6	30791.6	1046.91
9	267902.6	28263.2	952.47

Uncertainty in the mechanical properties of the oil dampers is modeled using statistically independent lognormal random variables. COVs for the nonlinear Maxwell models are judged to be 5 %; no statistical studies are as yet available to provide a more quantitative basis for this assignment.

Table 3.16 Variability of mechanical properties of nonlinear Maxwell model

	COV
K_d	5 %
C_d	5 %
Q_d	5 %

Inter-story drift ratio δ_{max} and peak floor acceleration a_{max} (normalized by the gravitation acceleration g = 9.8 m/s^2) of the 100 building models without (a) and with (b) dampers due to m_j = 6.0 earthquakes are shown in Figures 3.31 and 3.32, respectively. Similarly, Figures 3.33 and 3.34 show the maximum responses caused by m_j = 8.0 earthquakes. We can see the oil dampers reduce the inter-story drifts as well as the peak floor accelerations. In the case of m_j = 6.0 earthquakes, they do not make so much difference because even the bare frame works well against small or moderate ground motions. On the other hand, for m_j = 8.0 earthquakes, the dampers reduce the inter-story drifts greatly while several simulated models without dampers sustain very large inter-story drifts. This suggests that the bare frame may collapse in a few simulated cases despite the fact that it satisfies the Japanese design code, whereas the dampers are able to prevent any collapse. The response is transformed into damage costs in the next section.

3.4.4 Generation of damage costs*

In order to reflect the preferences of a decision maker in seismic risk management, the damage cost is defined as the sum of only those costs for which the decision maker is responsible. This is

* References for the fundamentals: ATC (1985); FEMA (1999)

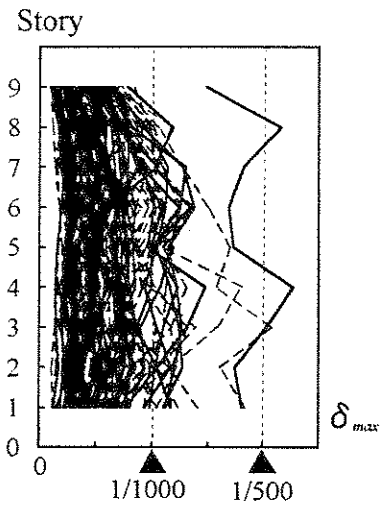

(a) Bare frame

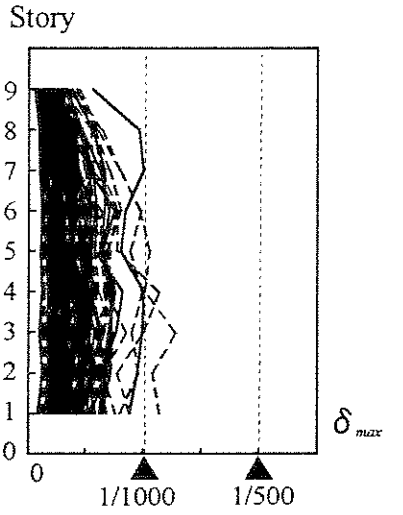

(b) With dampers

Figure 3.31 Inter-story drift ratios for m_j = 6.0 earthquakes

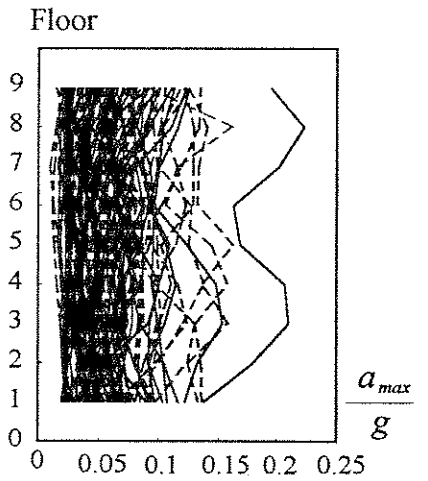

(a) Bare frame

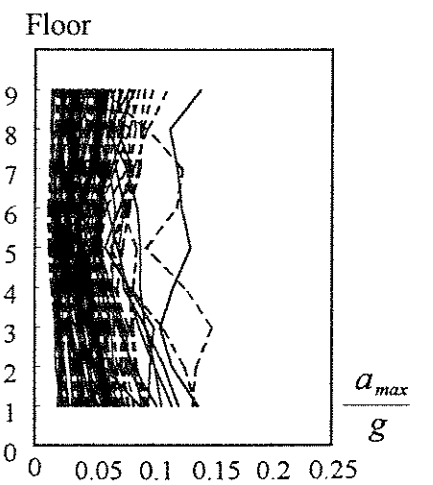

(b) With dampers

Figure 3.32 Peak floor accelerations for m_j = 6.0 earthquakes

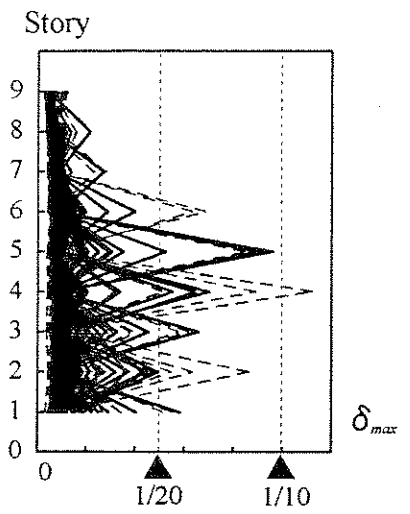

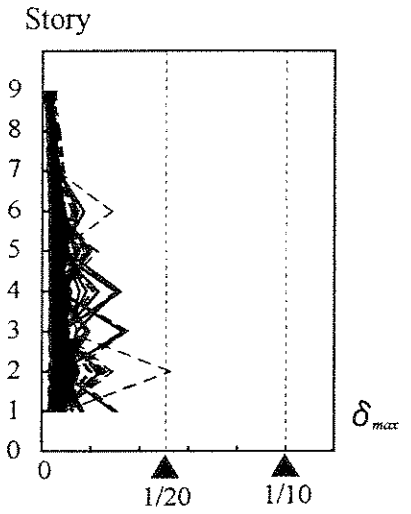

(a) Bare frame **(b) With dampers**

Figure 3.33 Inter-story drift ratios for m_j = 8.0 earthquakes

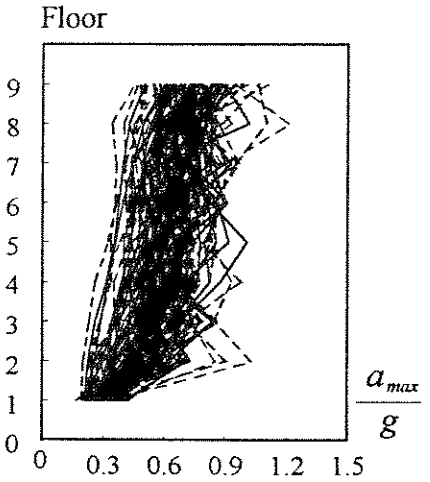

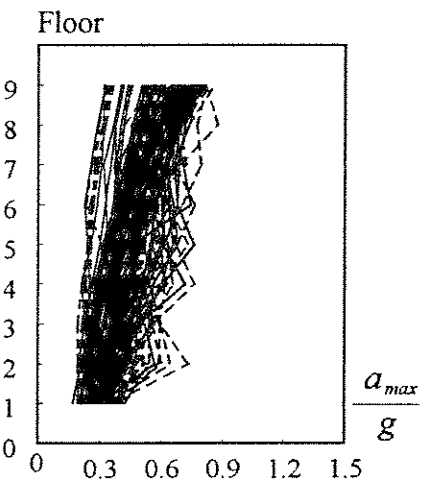

(a) Bare frame **(b) With dampers**

Figure 3.34 Peak floor accelerations for m_j = 8.0 earthquakes

written as

$$C_D = C_B + C_C + \cdots + C_P \tag{3.26}$$

where C_D, C_B, C_C, ···, and C_P are the total damage cost, the repair or replacement cost of the building, the replacement cost of the contents, and the loss of profit due to functional loss of the building, respectively. Any other cost that the decision maker may incur as a result of damage to the building due to earthquakes should be included. However, which term to be added depends on the case under consideration. For example, if the decision maker is the owner of a building that serves or houses his/her company, C_B, C_C and C_P should all be included because the owner must be responsible for them all. On the other hand, for an owner of a residential building, C_C may be excluded because the replacement cost of the contents may be the residents' responsibility, and not the building owner. For insurance companies, costs related to fatalities and injuries must be included. Therefore, engineers should discuss with the decision maker to make a list of the relevant costs to be included in the analysis. Other studies, e.g., Lee (1996), have considered all significant costs affecting the society.

In Section 3.2, the decision maker was assumed to be the owner of the building and the president of the company. For this case, the damage cost is expressed as the sum of fundamental three terms

$$C_D = C_B + C_C + C_P \tag{3.27}$$

Estimation of each term is described below.

The cost for life safety should be included if the relevant cost is the responsibility of the decision maker. However, in this case study, this cost is excluded because money would be paid for any fatality by the insurance companies, and not the decision maker (the building owner). Since even the bare frame satisfies the Japanese building code, both alternatives are regarded to implicitly satisfy social requirements. Of course, life safety should be taken into account quantitatively in decision problems. However, one may choose criteria other than cost, such as the balanced risk concept (Wiggins, 1972). This study focuses on a decision based on life-cycle

costs alone. Other criteria will be discussed in a future study by considering the multi-attribute decision problem formulation (Ang and Tang, 1984).

C_B: Repair/replacement cost of the building

A building is composed of structural and nonstructural components, and nonstructural components are further divided into drift-sensitive and acceleration-sensitive components (FEMA, 1999). The initial cost of the whole building is expressed as

$$C_I = C_{I,Structure} + C_{I,Drift} + C_{I,Acceleration} \tag{3.28}$$

where C_I is the initial cost of the building and $C_{I,Structure}$, $C_{I,Drift}$ and $C_{I,Acceleration}$ are the initial costs of structural, drift-sensitive, and acceleration-sensitive components. Similarly, the repair or replacement cost of the building is expressed as

$$C_B = C_{Structure} + C_{Drift} + C_{Acceleration} \tag{3.29}$$

where $C_{Structure}$, C_{Drift}, and $C_{Acceleration}$ are the repair or replacement costs for structural, drift- and acceleration-sensitive components, respectively.

Structural components are those that support loads, such as beams, columns, floors and bearing walls. The state of a structural component is grouped into one of several damage states, e.g., none (N), slight (S), moderate (M), extensive (E) and complete (C), using fragility curves as illustrated in Figure 3.35 (FEMA, 1999). In the Monte Carlo simulation, one damage state is assigned for each sample by generating a random variable that is defined by the PMF (Probability Mass Function) as illustrated in Figure 3.36(a) or (b). This means that five damage states can occur even if the response is the same. The former figure indicates that a structural component with small response is grouped into the N and S states in most cases, the M state with a small probability, and the E and C states with very small probabilities. On the other hand, Figure 3.36(b) demonstrates that a structural component with large response falls into the N, S or M states with very small probabilities, and in most cases falls into the E or C state.

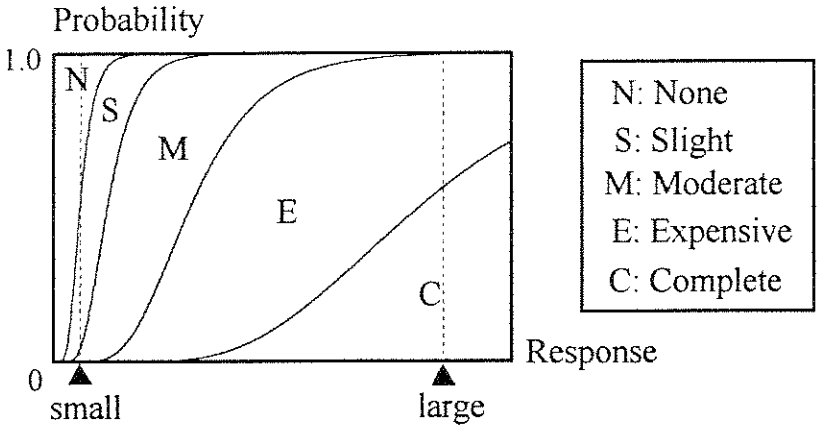

Figure 3.35 Example of fragility curves

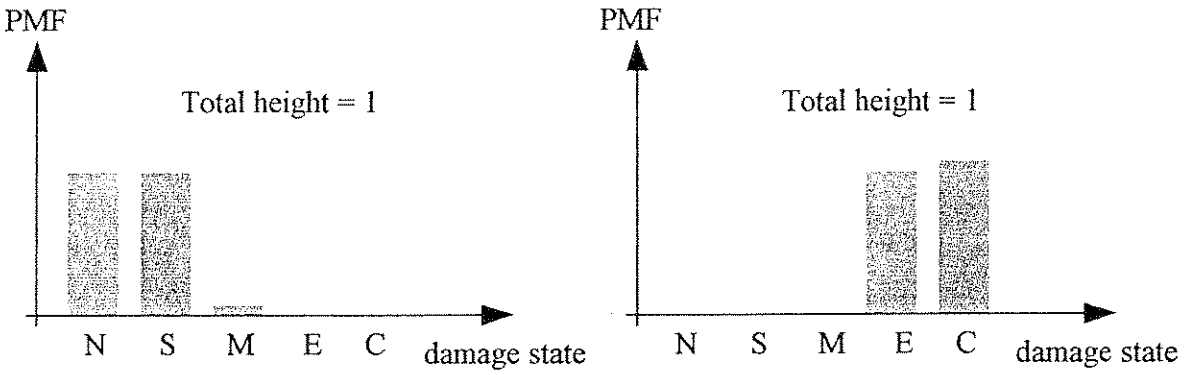

(a) For small response **(b) For large response**

Figure 3.36 PMFs (Probability Mass Functions)

The dynamic response associated with the damage state of steel structural components may be taken as the peak inter-story drift, the dissipated hysteretic energy (Akiyama, 1985) or a combination of them as defined by the Park-Ang index (Chai *et al.*, 1995). Among them, peak inter-story drift ratio is employed for steel structural components as well as FEMA (1999). This means that a damage state is assigned for each story. Figure 3.37 shows the fragility curves for steel moment frames by FEMA (1999). These curves are generated as cumulative distribution functions of lognormal distributions with the parameters listed in the first row of Table 3.17. A *DCR* (= Damage cost ratio: the ratio of the repair/replacement cost of a story to the initial cost of the story) is assigned for each damage state, as shown in the first row of Table 3.18 (FEMA, 1999). The repair or replacement cost of the structural components of the building is estimated as

$$C_{Structure} = \sum_{i=1}^{N} DCR_i \times C_{I,Structure(i)} \tag{3.30}$$

where N, DCR_i and $C_{I,Structure(i)}$ are the number of stories, damage cost ratio and the initial cost of the ith story, respectively.

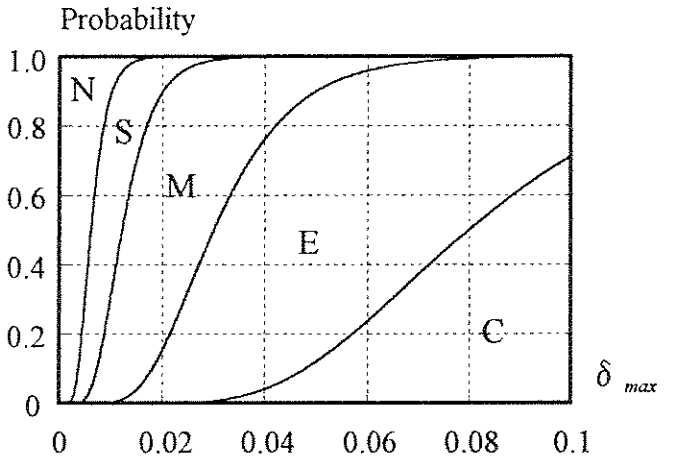

Figure 3.37 Fragility curves for structural components (FEMA, 1999)

Table 3.17 Parameters for fragility curves for building (FEMA, 1999)

	Slight		Moderate		Extensive		Complete	
	Median	COV	Median	COV	Median	COV	Median	COV
Structural (inter-story drift ratio)	0.006	0.4	0.012	0.4	0.030	0.4	0.080	0.4
Drift-sens. (inter-story drift ratio)	0.004	0.5	0.008	0.5	0.025	0.5	0.050	0.5
Acceleration-sens. (peak floor acc. in g)	0.30	0.6	0.60	0.6	1.20	0.6	2.40	0.6

Table 3.18 *DCR* (Damage Cost Ratio) for building (FEMA, 1999)

	None	Slight	Moderate	Extensive	Complete
Structural	0.00	0.02	0.10	0.50	1.00
Drift-sens.	0.00	0.02	0.10	0.50	1.00
Acceleration-sens.	0.00	0.02	0.10	0.50	1.00

Fragility curves for nonstructural drift- and acceleration-sensitive components and the values of their parameters are shown in Figure 3.38, 3.39 and the second and third rows of Table 3.17, respectively. These fragility curves are derived from engineers' judgment based on their experiences. More elaborate damage models such as the ABV model proposed by Porter and Kiremidjian (2001) would be preferred, and should be applied in the future.

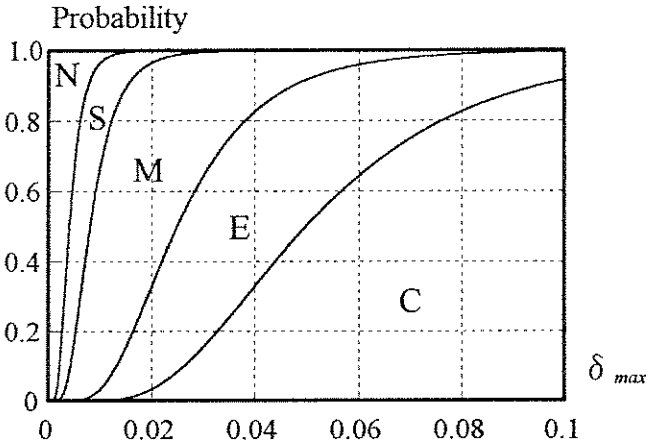

Figure 3.38 Fragility curves for nonstructural drift-sensitive components (FEMA, 1999)

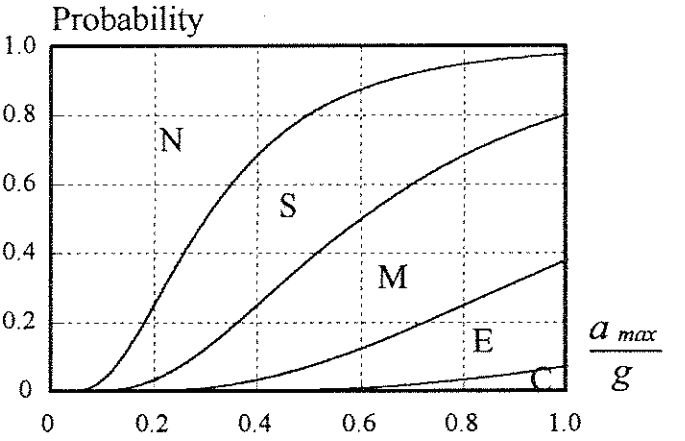

Figure 3.39 Fragility curves
for nonstructural acceleration-sensitive components (FEMA, 1999)

Using *DCR* in Table 3.18, repair or replacement costs for nonstructural drift- and acceleration-sensitive components are also expressed as follows.

$$C_{Drift} = \sum_{i=1}^{N} DCR_i \times C_{I,Drift(i)} \tag{3.31}$$

$$C_{Acceleration} = \sum_{i=1}^{N} DCR_i \times C_{I,Acceleration(i)} \tag{3.32}$$

The initial costs of structural, drift- and acceleration-sensitive components of the building are shown in Table 3.19* (KKE, 2001c), where costs for underground floors are excluded. They are assumed to be distributed uniformly over the height, i.e., they are divided by nine to obtain the costs $C_{I,Structure(i)}$, $C_{I,Drift(i)}$ and $C_{I,Acceleration(i)}$ for each story. Each set of the oil damper and steel brace is sold at ¥500,000 (= $5,000), and 72 sets were installed in the building at a total cost of $0.36 million. This is about 2.4 % of the cost of the bare building; thus the initial cost of the building with the oil dampers is $15.12 million + $0.36million = $15.48 million.

Table 3.19 Initial cost of bare building (in $million or ¥Oku) (KKE, 2001c)

Component	Initial cost
Structural	3.285
Drift-sensitive	7.705
Acc.-sensitive	4.313
Others	+13.57%
Discount	-13.00%
Total	15.120

When constructing a building, other costs (e.g., for the design, removal, and temporary structures) are paid, and the total is conventionally discounted by the contractor. In the case of the KKE building, the additional costs are 13.57% of the total and the discount is 13.00% (KKE, 2001c). We assume these proportions are valid when repairing or replacing the building, i.e.,

* All costs are paid in Japanese yen (¥), whereas they are changed into U.S. dollar ($) in this study using an exchange rate of $1.00 = ¥100.00 for simplicity. Thus, one million dollars is equivalent to one Oku-yen (= one hundred million yen), and both units are displayed in most of the figures and tables.

$$C_B = \left(C_{Structure} + C_{Drift} + C_{Acceleration}\right) \times 1.1357 \times 0.87 \tag{3.33}$$

C_C: Repair/replacement cost of contents

The damage of the building contents is related to the peak floor acceleration (FEMA, 1999). The fragility curves, their parameters and the *DCR* are shown in Figure 3.40 and Tables 3.20 and 3.21, respectively.

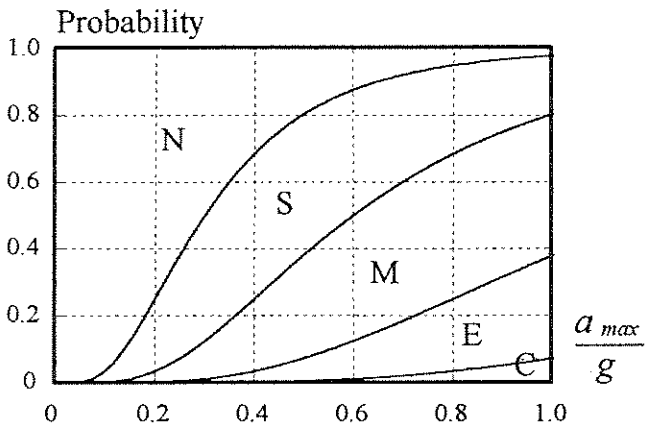

Figure 3.40 Fragility curves for contents (FEMA, 1999)

Table 3.20 Parameters for fragility curves for contents (FEMA, 1999)

	Slight		Moderate		Extensive		Complete	
	Median	COV	Median	COV	Median	COV	Median	COV
Contents (peak floor acc. in g)	0.30	0.6	0.60	0.6	1.20	0.6	2.40	0.6

Table 3.21 *DCR* (Damage Cost Ratio) for contents (FEMA, 1999)

	None	Slight	Moderate	Extensive	Complete
Contents	0.00	0.01	0.05	0.25	0.50

The repair or replacement cost of contents is computed as

$$C_C = \sum_{i=1}^{N} DCR_i \times C_{I,C(i)} \tag{3.34}$$

where $C_{I,C(i)}$ is the initial cost of contents on the ith floor. It is almost impossible to estimate the initial cost of existing contents. Based on FEMA (1999), for the professional, technical and business service buildings, the initial cost of contents is assumed to be 100% of the total initial cost of the building (= \$15.120 million). It is also assumed to be distributed uniformly over the height of the building.

Reparable limit

A heavily damaged building cannot be repaired; it must be demolished and reconstructed. Limits on reparability of reinforced concrete buildings were suggested by Ang and De Leon (1996), Lee (1996), Park *et al.* (1987) and Takahashi *et al.* (2000) based on the Park-Ang index (Park and Ang, 1985; Park *et al.*, 1985; Park *et al.*, 1987), and have been used in their cost analyses. However, in general, a decision between repair and replacement strongly depends on the current repair technology, engineers' subjective judgment, social importance of the building, decision makers' preferences, and other factors. For example, some skillful engineers may try to repair a seriously damaged building whereas others may prefer replacement. On the other hand, an anxious owner may want to replace the building no matter how slight the damage is. Also, whether people die in the damaged building or not may affect the judgment. Therefore, we must conclude that repairable limits cannot be determined solely from engineering considerations. Thus, engineers and decision makers should have discussions on the damage limits for reparability in risk management.

For the KKE building, two common limitations are established: the building is demolished and replaced (a) if any story sustains "complete" structural damage or (b) if DF (Damage Factor) > 60 % (ATC, 1985). These conditions are intended to account for story collapse and total collapse, respectively. DF is defined as

$$DF = \frac{C_B + C_C}{C_{I,B} + C_{I,C}} \tag{3.35}$$

where $C_{I,B}$ ad $C_{I,C}$ are the initial costs of the building and contents, respectively. If the building reaches either of the two limits, both the building and its contents are assumed to be replaced completely, i.e., C_B and C_C will be \$15.12 million, for the present analysis.

C_P: Loss of profit

Based on the value of DF, a damaged building is grouped into one of seven damage states from None to Destroyed as shown in Table 3.22. A function recovery rate curve is defined for each damage state as illustrated in Figure 3.41 (ATC, 1985). Table 3.22 shows the values for professional, technical and business services buildings, i.e., the number of days when 30 %, 60 % and 100 % of the function of the building is recovered.

Table 3.22 Damage state and values for function recovery rate curves (ATC, 1985)

DF (%)	Damage State	d_{30}	d_{60}	d_{100}
0	None	0	0	0
0-1	Slight	1.2	2.4	5.8
1-10	Light	3.4	10.2	20.0
10-30	Moderate	9.8	44.6	71.0
30-60	Heavy	37.0	111.6	202.7
60-100	Major	114.7	213.7	343.1
100	Destroyed	---	---	439.3

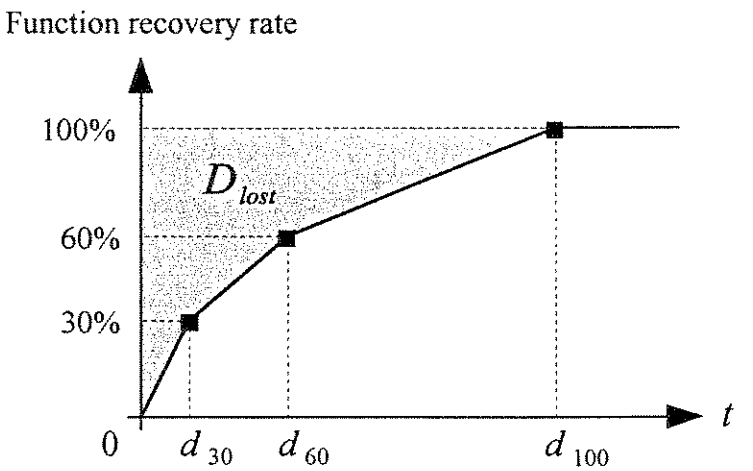

Figure 3.41 Function recovery rate curve (ATC, 1985)

In Japanese convention, pretax profit P_0 without any disaster is expressed as the difference between the usual earnings E_0 and the operating cost C_0, as shown in Figure 3.42(a) (Senju and Fushimi, 2001). After an earthquake, they change into $E(t)$ and $C(t)$, respectively, whereas the profit $P(t)$ is still equivalent to the difference between them, as shown in Figure 3.42(b).

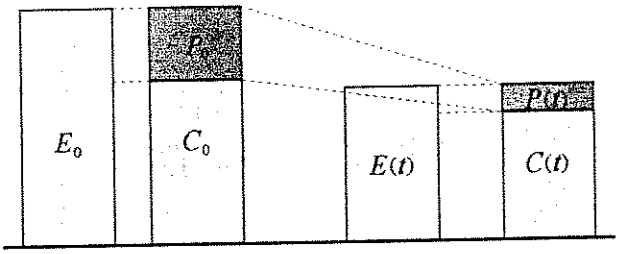

(a) Before earthquake **(b) After earthquake**

Figure 3.42 Earnings, operating cost, and profit

Recovery of the earnings $E(t)$ can be regarded to be identical to the function recovery as illustrated in Figure 3.43(a). However, costs to operate the business cannot be reduced immediately after an earthquake because they include such fixed obligation as contracted labor costs and rental fees. Thus, in general, the total loss of profit before complete recovery is expressed as the integration of changes in profit until the complete recovery day d_{100}, i.e.,

$$C_P = \int_0^{d_{100}} [\{E_0 - C_0\} - \{E(t) - C(t)\}]dt \tag{3.36}$$

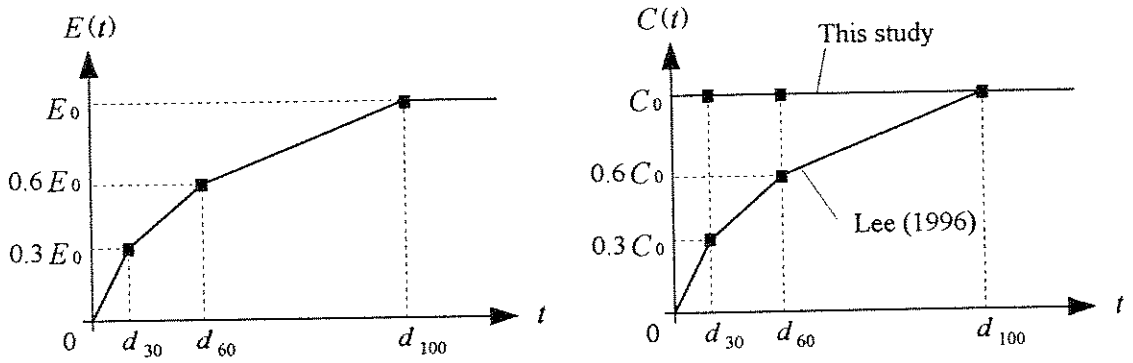

(a) Earnings **(b) Costs**

Figure 3.43 Recovery after earthquake

Equation (3.36) suggests that suppressing operating costs $C(t)$ after an earthquake is one way to reduce loss of profit in seismic risk management. Lee (1996) assumed that the operating cost can always be reduced proportionally to the earnings, as illustrated in Figure 3.43(b). He then obtained the loss of profit as

$$C_P = \int_0^{d_{100}} [\{E_0 - C_0\} - E(t)\{1 - \frac{C_0}{E_0}\}]dt = P_0 \times D_{lost} \tag{3.37}$$

where D_{lost} is the effective lost days due to the earthquake, which is equivalent to the area above the function recovery rate curve demonstrated in Figure 3.41. Eq. (3.37) is the ideal assumption for the decision maker. In reality, reduction of costs after an earthquake depends on the circumstances, and it should be investigated carefully for each case in risk management.

In this case study, the worst case for the decision maker is assumed, i.e., operating costs cannot be reduced as indicated in Figure 3.43(b). Thus, $C(t) = C_0$ and

$$C_P = \int_0^{d_{100}} \{E_0 - E(t)\}dt = E_0 \times D_{lost} \tag{3.38}$$

Kozo Keikaku Engineering, Inc. (2001a) reported the annual earnings and profit of fiscal year 2000 produced by the whole company as ¥101.60 Oku (= $101.60 million) and ¥5.63 Oku (= $5.63 million), respectively (profit/earnings = 5.54 %). The building under consideration accommodates 291 of 547 employees of the whole company. The earnings produced by the building are assumed to be proportional to the number of employees, that is, $54.05 million per year, which is equivalent to $0.148 million per day. Table 3.23 shows D_{lost} and C_P calculated using Eq. (3.38) for each damage state.

If the damage is severe, the decision maker must rent another office in the neighborhood to restart the business just after an earthquake until the building recovers completely, rather than remain in the damaged building. The average rental fee for office buildings in Tokyo is reported to be ¥5,513 (= $55.13)/m^2/month (Ministry of Land, Infrastructure and Transport, 2000). The rental fee until the complete recovery is expressed as $55.13/m^2/month $\times$ 7,000m^2 $\times$ d_{100} (in

month). However, in the case of renting an office, the loss is not only the rental fee since complete business cannot be started immediately because employees have to move, prepare contents, and suffer various inconveniences. The loss due to these factors should be added to the rental fee when renting a office. In order to account for the functional loss, the additional function recovery rate curve for DF = 10 % - 30 % is assumed (C_p = \$4.85 million) when moving to a rented building. It is obvious that the employees should continue to work in the damaged building when $DF \leqq 30$ % because C_p is equal to or less than \$4.85 million as seen in Table 3.23. The last column of Table 3.23 shows the sum of C_p and the rental fee for $DF > 30$ % and for the case that the building is demolished and reconstructed. From the table, we can see that to reduce the total loss, the decision maker should rent another office only when $DF > 30$ % or the building is replaced. The values in the shaded squares in Table2.23 are used for C_p (+ the rental fee when renting a office).

Table 3.23 Lost days and loss of profit

DF (%)	Damage State	D_{lost} (days)	remain	rent office
			C_P (\$million)	C_P + rental fee (\$million)
0	None	0	0	---
0-1	Slight	2.4	0.35	---
1-10	Light	8.6	1.27	---
10-30	Moderate	32.8	4.85	---
30-60	Heavy	90.7	13.43	7.46
60-100 or story collapse	Collapse	439.3	73.05	11.20

The loss of profit described above is caused by functional loss of the building itself, and it is called the first round loss (Lee, 1996) or direct economic loss (FEMA, 1999). In addition to that, functional loss of other facilities in the damaged region may affect the earnings $E(t)$ and operating cost $C(t)$ of the building. These are known as the second round loss (Lee, 1996) or indirect economic loss (FEMA, 1999). It is obvious that to estimate the indirect economic loss,

we should perform a regional economic analysis using the Input-Output model (FEMA, 1999) or loss estimation of facilities of strongly dependent suppliers and customers. For this reason, the second round loss is excluded in this study. Lee (1996) inferred regional economic loss from the first round loss of the building under consideration.

Figure 3.44 demonstrates the event tree representing the damage cost models constructed above.

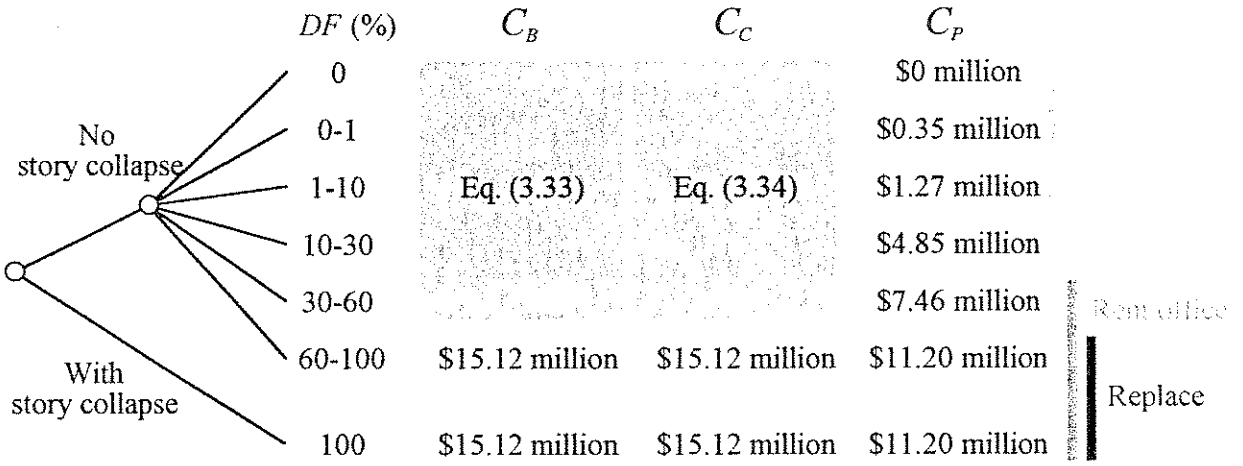

Figure 3.44 Event tree for estimation of costs

Figures 3.45 and 3.46 show the damage costs of 100 samples due to m_j = 6.0 and 8.0 earthquakes, respectively, for the building without (a) and with (b) dampers. In most cases of the m_j = 6.0 earthquakes, the building does not generate damage with or without dampers. This suggests that even the bare frame is sufficient for small or moderate ground motions. For m_j = 8.0 earthquakes, 8 out of 100 samples of the bare frame exceed the reparable limits and generate a full damage cost ($41.44 million = $15.12 million + $15.12 million + $11.20 million). All of them suffer story collapse, and not total collapse. On the other hand, the building with dampers will prevent collapses, and damage costs are reduced overall. Table 3.24 shows the expected damage costs for m_j = 6.0, 7.0 and 8.0 earthquakes computed using Eq. (2.20). These values are substituted into Eq. (3.1) and (3.6) in the next section for life-cycle cost analysis. Here 100 samples are taken, however, we cannot affirm whether it is sufficient or not. Appendix C describes the selection of the required sample size to achieve reliable estimates.

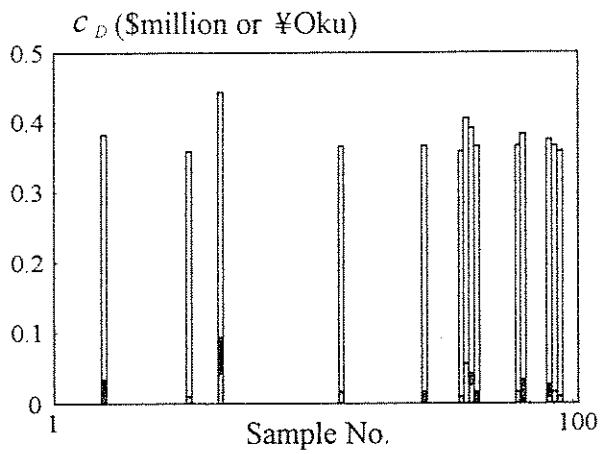

(a) Bare frame

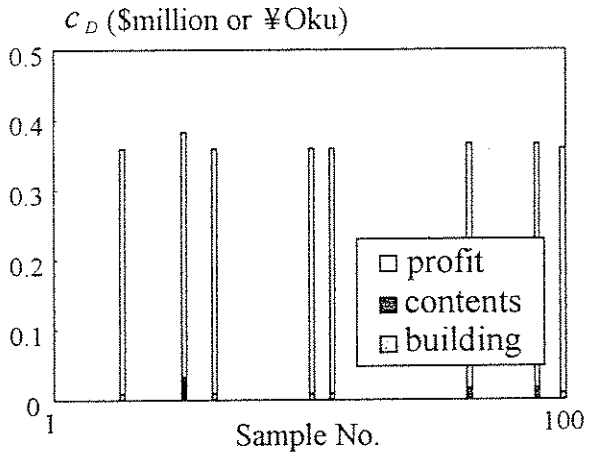

(b) With dampers

Figure 3.45 Damage costs for m_j = 6.0 earthquakes

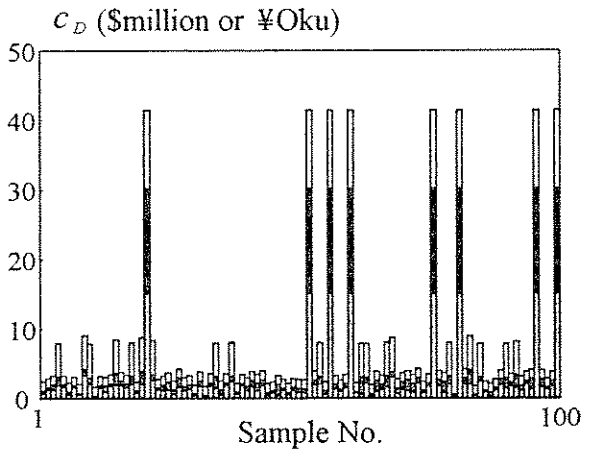

(a) Bare frame

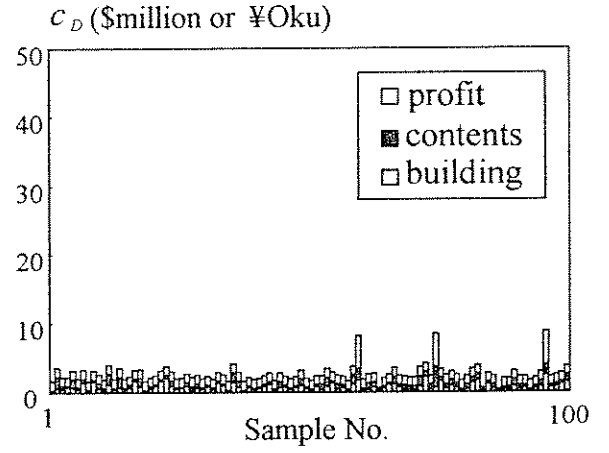

(b) With dampers

Figure 3.46 Damage costs for m_j = 8.0 earthquakes

Table 3.24 Expected damage cost (in $million or ¥Oku)

m_j	$E[C_D(m_j)]$	
	Bare frame	With dampers
6.0	0.0529	0.0291
7.0	0.8440	0.4537
8.0	7.1332	2.6742

3.5 Lifetime vs. expected life-cycle cost

To compute the life-cycle costs of the two alternatives, the values in Table 3.24 are substituted into Eq. (3.1) assuming Poisson process for earthquake occurrences. The computed values of the expected annual damage costs $\sum_{m_j=6}^{8} \nu(m_j) \cdot E\left[C_D(m_j)\right]$ are shown in Figure 3.47, which are equivalent to the gradient of Eq. (3.1b).

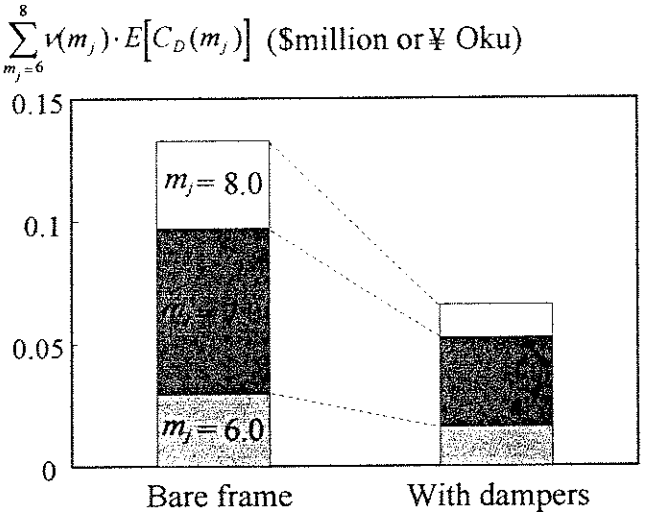

Figure 3.47 Expected annual damage cost for Poisson model (Q = 1)

Initial costs of the two alternatives ($15.12 million for a_1 and $15.48 million for a_2) are also substituted into Eq. (3.1b) assuming Q = 1, and Figure 3.48 shows their expected life-cycle costs. They intersect at 5.3 years after the starting time. This indicates that dampers are effective from the aspect of life-cycle cost if the lifetime of the building is longer than 5.3 years. The difference at the end of the lifetime (t_{life} = 50 years) is $3.05 million. This is an expected profit to the decision maker gained by adopting dampers in this risk management. On the other hand, someone may ask "Is the better alternative free from risks?". The answer is "No". Even the best alternative would generate damage costs, and its expectation is expressed as the difference between the life-cycle cost and the initial cost, $3.38 million in this case as shown in Figure 3.48. This is the expected risk the decision maker is exposed to. In risk management, such residual risks should be reduced into the levels the decision maker can accept.

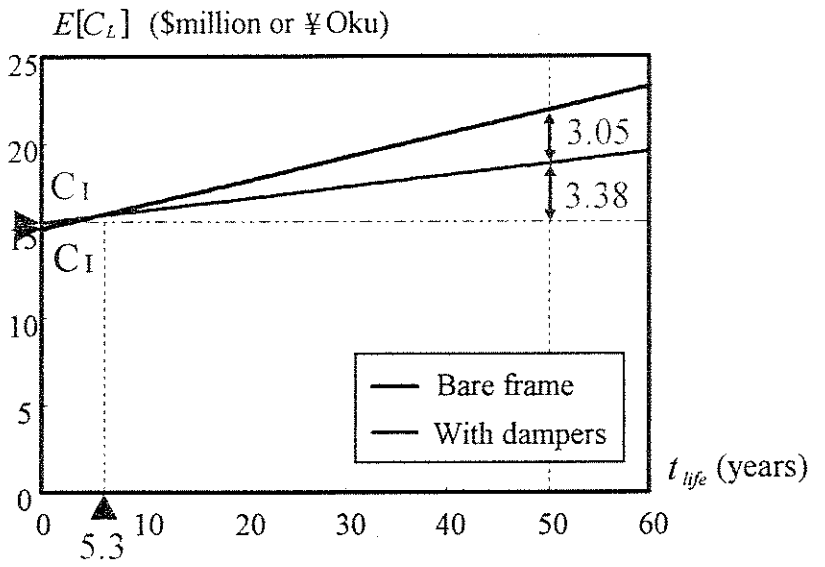

Figure 3.48 Lifetime vs. expected life-cycle cost for Poisson model (Q = 1)

The life-cycle costs assuming the BPT model are computed using Eq. (3.6b), and Figures 3.49 and 3.50 illustrate the results for t_0 = A.D.1999 and t_0 = A.D.2075, respectively. The integration in Eq. (3.6b) is performed numerically. The results for the Poisson model in Figure 3.48 are also displayed using dotted lines for comparison. In the case of t_0 = A.D.1999, the slopes becomes less steep than the dotted lines because the Poisson model overestimates occurrence rate of m_j = 8.0 earthquakes as shown in Figure 3.12. Consequently, the cross point becomes later and the gain and residual risk at the end of the lifetime are reduced. Opposite results are observed in the case of t_0 = A.D.2075 because the Poisson model underestimates the seismic activity. The effectiveness of the initial investment varies according to activities of the seismic source, i.e., the initial investment becomes more valuable as the seismic source becomes more active. By utilizing the non-Poisson renewal model, time-dependence of risk can be quantified. Although the numbers are different in each case, the optimal alternative remains the same for all models.

We now examine the effect of the discount rate d in Eqs. (3.1) and (3.6). Although one cannot predict future values of the discount rate, they may be inferred from recent official discount rates (Senju and Fushimi, 2001). Recent official discount rates reported by the Bank of Japan (2001) are listed in Table 3.25. The average value, i.e., 0.3 %, is used for d. This yields Q = 0.997. The recent discount rates are so small because Japanese economy has been in depression for several years.

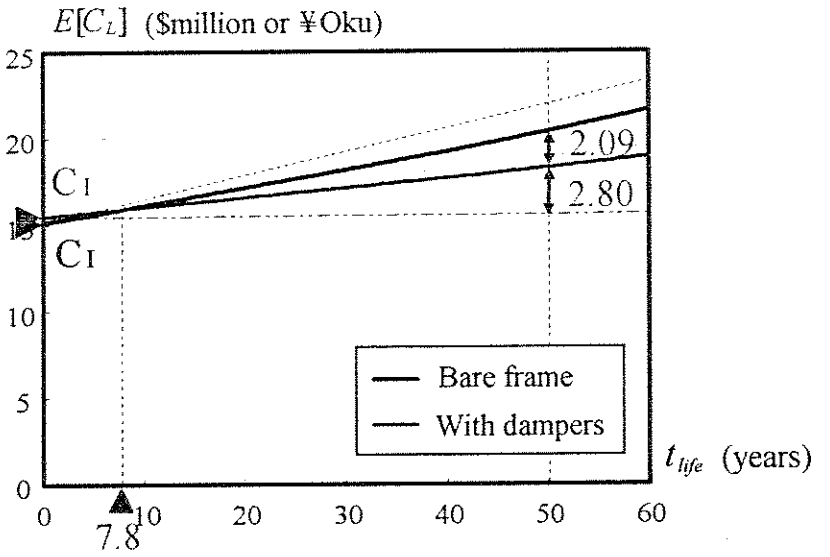

Figure 3.49 Lifetime vs. expected life-cycle cost for BPT model (t_0 = A.D.1999, Q = 1)

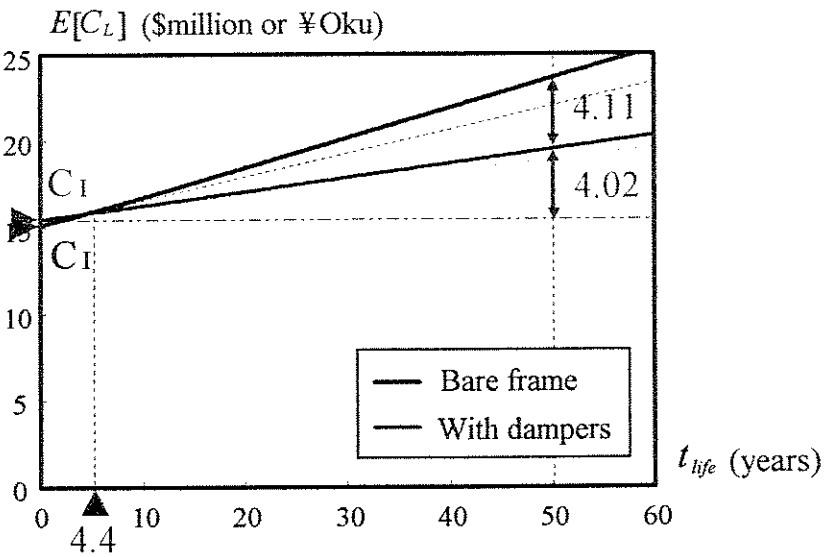

Figure 3.50 Lifetime vs. expected life-cycle cost for BPT model (t_0 = A.D.2075, Q = 1)

Table 3.25 Official discount rate

(Bank of Japan, 2001)

Month/Year	Annual rate (%)
January/2001	0.50
February/2001	0.35
March/2001	0.25
September/2001	0.10
Average	0.30

Figure 3.51 shows the relationship between the elapsed time (t - t_0) and the discount factor. After 50 years, the worth of a cost becomes about 85% of the initial worth. Figures 3.52, 3.53 and 3.54 show the same results as those of Figures 3.48, 3.49 and 3.50, respectively, except that $Q = 0.997$ rather than $Q = 1.0$ is used. The slopes in the graphs become less steep because the worth of future costs is discounted by the factor shown in Figure 3.51. However, installation of dampers is still a better alternative. These results also indicate that, under such a low discount rate, the investment in the oil damper is more effective than making a deposit of the same amount of money in a bank for the reason described when formulating Eq. (2.11)

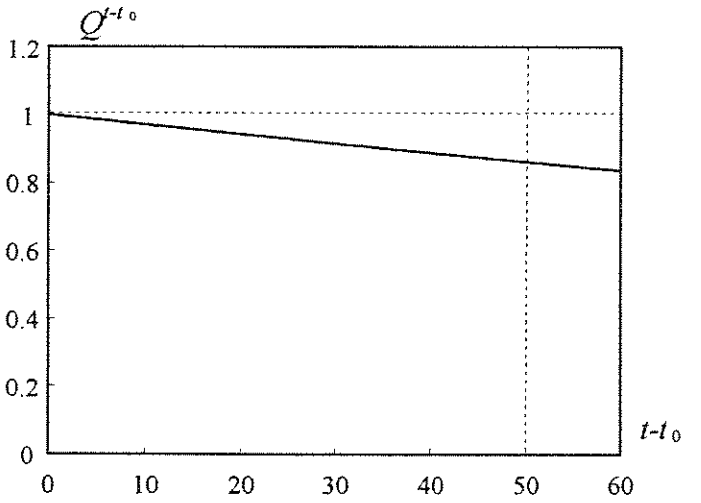

Figure 3.51 Elapsed time vs. discount factor ($Q = 0.997$)

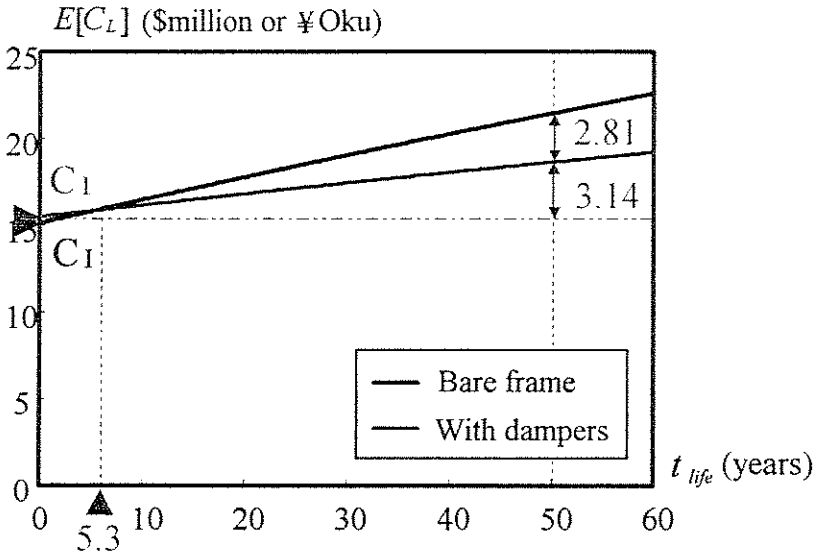

Figure 3.52 Lifetime vs. expected life-cycle cost for Poisson model (Q = 0.997)

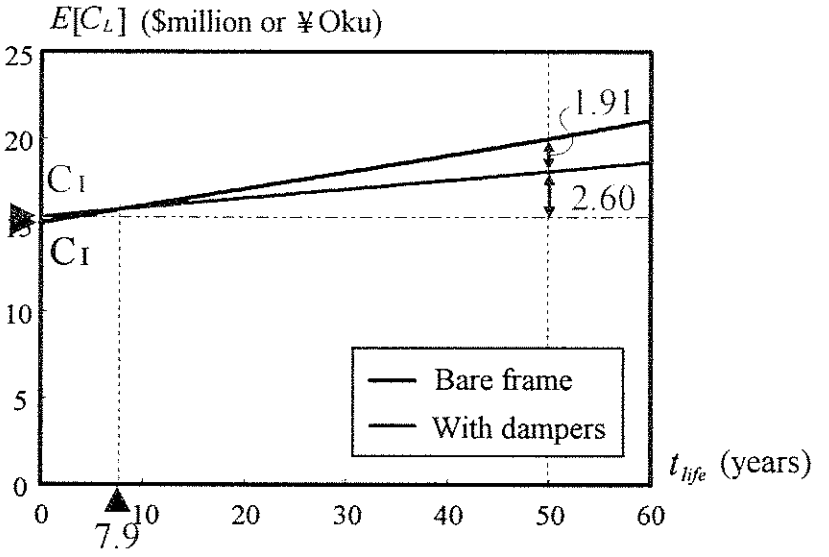

Figure 3.53 Lifetime vs. expected life-cycle cost for BPT model (t_0 = A.D.1999, Q = 0.997)

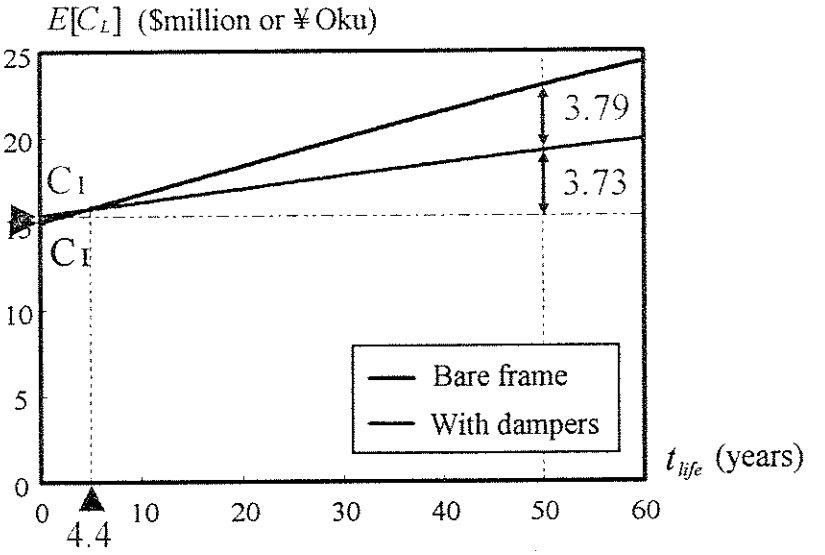

Figure 3.54 Lifetime vs. expected life-cycle cost for BPT model (t_0 = A.D.2075, Q = 0.997)

CHAPTER 4

SUMMARY

A decision methodology in seismic risk management of a building is presented in Chapter 2. This methodology is able to reflect up-to-date knowledge on activities of surrounding seismic sources and simulation techniques for relevant processes in the final decisions. In Chapter 3, the methodology is applied to an actual building in Tokyo as an example. It turns out to be effective to install oil dampers in the building in order to reduce the fundamental seismic risk, life-cycle cost. The main results of the study are summarized as follows.

Based on decision theory, an alternative that minimizes the expected life-cycle cost is chosen as an optimum. The expected life-cycle cost of each alternative is formulated utilizing renewal theory. In the equation, the occurrences of earthquakes in a seismic source are assumed to follow a renewal process. Different renewal models can be applied to different magnitude earthquakes, e.g., the Poisson model for small but frequent earthquakes and a non-Poisson renewal model for large magnitude, rare earthquakes. In the equation, the expected damage costs due to earthquakes with specified magnitudes need to be computed, i.e., we need to simulate the relevant processes including fault rupture, elastic wave propagation, surface soil amplification, dynamic response of a building and generation of damage costs. This is achieved by performing Monte Carlo simulations using appropriate analytical models developed in seismology, geotechnical engineering, structural engineering and social economics. In this sense, the equation proposed in this study can systematically utilize up-to-date knowledge obtained in relevant fields, and help make decisions for better quality.

The building taken as an example is one owned by Kozo Keikaku Engineering, Inc. (KKE), which is located in Tokyo. This building has nine stories and consists of steel moment frames. The feature is that oil dampers are installed in each story to mitigate damages against earthquakes. Here a simple decision problem between two alternatives is set: a_1 is the bare frame (assumed that the oil dampers were not installed) and a_2 is the building with oil dampers. The decision maker is the owner of the building and the president of the company, and the lifetime of the

building is specified to be 50 years.

The Sagami trough, which is a boundary between the Eurasia plate and the Philippine Sea plate, is regarded as a seismic source that may generate earthquakes causing damages to the building. Using typical earthquake catalogs, recorded earthquakes are investigated, and classified into three groups: earthquakes with magnitude 6.0 (occasional), 7.0 (rare), and 8.0 (very rare). The occurrences of the occasional and rare earthquakes are described by the Poisson model. For the very rare earthquake, both the Poisson and a non-Poisson renewal models are considered, and the results are compared. Among non-Poisson renewal models, the Brownian Passage Time (BPT) model is applied. The Poisson model overestimates the occurrence rate just after the last earthquake, and underestimates it after a long time.

In order to compute the expected damage costs caused by earthquakes with magnitudes 6.0, 7.0 and 8.0, Monte Carlo simulations are performed considering uncertainties of the related processes. The size of the fault rupture plane corresponds to a given magnitude is determined based on empirical relations, and the rupture is randomly placed in the Sagami trough. From a rupture plane, stochastic ground motions are generated using the finite-fault stochastic Green's function method. The amplification by surface soil deposits is simulated using a one-dimensional wave propagation theory. Generated ground motions are applied to the building models, and nonlinear dynamic response analyses are performed. Dynamic response measures such as the inter-story drift ratio and the peak floor acceleration are transformed into damage costs using fragility curves, damage cost ratios and function recovery rate curves. In this study, damage costs are defined as the sum of only costs of interest to the decision maker so as to reflect his preferences in the solution. Repair or replacement costs of the building, its contents and loss of profit are included.

The computed expectations of damage costs due to earthquakes of magnitudes 6.0, 7.0 and 8.0 are substituted into the basic formulation, and the expected life-cycle costs of the two alternatives are obtained. In the case of assuming the Poisson process for all magnitudes, the relationship between the lifetime and the expected damage cost becomes linear. In this case, the expected life-cycle costs for the two alternatives cross at 5.3 years after the start time of the building, and the life-cycle cost of alternative a_2 (building with dampers) is less than that of a_1 at the end of the building lifetime. Comparing the results for the Poisson and the BPT models, the slopes for the former model are steeper than those of the latter one if the building starts just after

the last earthquake. This is because the Poisson model overestimates the occurrence rate in this case as described above. In the case the building operation starts in the year 2075, opposite results are observed. By applying non-Poisson renewal models, we can quantify seismic risk that varies depending on the activity of the seismic source. In addition, we examine the effects of the discount factor. Even though the values are not the same, the life-cycle cost of a_2 is less than that of a_1 in all cases. Consequently we can conclude that the installation of oil dampers is effective in the KKE building from the stand point of life-cycle cost.

While a newly constructed building is taken as an example, the presented methodology would also be applicable to a variety of decision problems in risk management of existing buildings. Alternatives would be to demolish and reconstruct, only to upgrade, to move, to purchase earthquake insurance, combinations of them, and so forth.

APPENDIX A

EXPECTED NUBER OF EVENTS

IN A RENEWAL PROCESS

Following Ross (1995), the number of events in a renewal process occurring during an interval $t_0 < t < t_0 + t_{life}$ can be written as

$$N_E(m_j) = \sum_{n=1}^{\infty} I_n \tag{A.1}$$

where

$$I_n = \begin{cases} 1 & \text{if the } n\text{th event occurs between } t_0 \text{ and } t_0 + t_{life} \text{ conditioned on } W_1 > t_0 \\ 0 & \text{otherwise.} \end{cases} \tag{A.2}$$

For our application, $N_E(m_j)$ denotes the number of earthquakes of magnitude m_j. Taking expectations of both sides of Eq. (A.1), one obtains

$$E\left[N_E(m_j)\right] = E\left[\sum_{n=1}^{\infty} I_n\right]$$

$$= \sum_{n=1}^{\infty} E\left[I_n\right]$$

$$= \sum_{n=1}^{\infty} P\left(I_n = 1\right) \tag{A.3}$$

where $P(E)$ denotes the probability that an event E occurs. The probability that the nth event occurs between t_0 and $t_0 + t_{life}$ on the condition that $W_1 > t_0$ is equal to the integration of the updated PDF, $f_{W_n}(t, m_j | W_1 > t_0)$, from t_0 to $t_0 + t_{life}$, that is, the area of the shaded part in Figure A.1. This is expressed as

$$P(I_n = 1) = \int_{t_0}^{t_0 + t_{life}} f_{W_n}(t, m_j | W_1 > t_0) dt \tag{A.4}$$

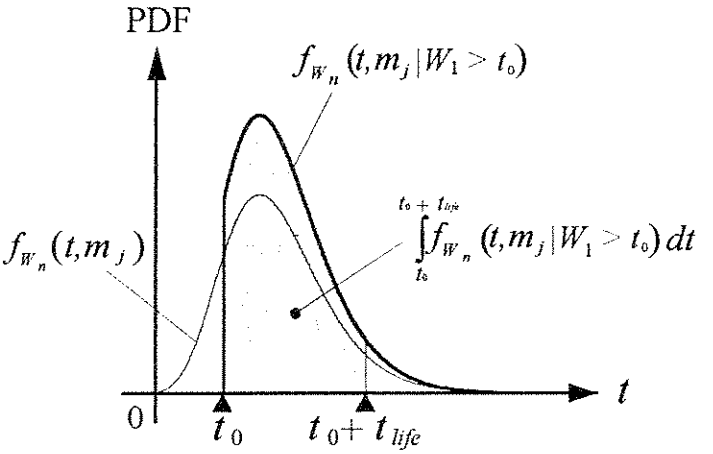

Figure A.1 Probability that the *n*th event occurs between t_0 and $t_0 + t_{life}$ on $W_1 > t_0$

Substituting this result into Eq. (A.3),

$$E\left[N_E(m_j)\right] = \sum_{n=1}^{\infty} \int_{t_0}^{t_0 + t_{life}} f_{W_n}(t, m_j | W_1 > t_0) dt \tag{A.5}$$

Equation (2.9) is obtained by exchanging the orders of the summation and integration operations.

APPENDIX B

PDF OF WAITING TIME TO EVENTS

WITH GAMMA DISTRIBUTED INTERARRIVAL TIME

Let T_i denotes the interarrival time between occurrence of earthquakes of a given magnitude, and assume that T_i's are statistically independent and identically distributed with a gamma PDF (Probability Density Function)

$$f_T(t) = \frac{\lambda(\lambda t)^{k-1} e^{-\lambda t}}{\Gamma(k)} = gamma(k, \lambda) \tag{B.1}$$

where λ and k are the parameters defining the form of the distribution. Note that the mean of the distribution is k/λ and its coefficient of variation is $1/\sqrt{k}$. The time to the nth occurrence can be written as

$$W_n = T_1 + T_2 + \cdots + T_i + \cdots + T_n \tag{B.2}$$

where $W_1 = T_1$. It is well known that the sum of independently and identically distributed gamma random variables is also gamma distributed. The PDF of W_n is

$$f_{W_n}(t) = \frac{\lambda(\lambda t)^{nk-1} e^{-\lambda t}}{\Gamma(nk)} = gamma(nk, \lambda) \tag{B.3}$$

We wish to define the conditional PDF of W_n given that $W_1 > t_0$. Noting that $X = T_2 + \cdots + T_n$ is gamma($(n - 1)k, \lambda$) distributed, for $n > 1$, we can write

$$P(W_n < t|W_1 > t_0) = \int_{t_0}^{t} P(W_n < t|W_1 = \tau) f_{W_1}(\tau|W_1 > t_0) d\tau$$

$$= \int_{t_0}^{t} P(\tau + X < t) f_{W_1}(\tau|W_1 > t_0) d\tau$$

$$= \int_{t_0}^{t} P(X < t - \tau) f_{W_1}(\tau|W_1 > t_0) d\tau \qquad \text{for } t_0 < t \qquad \text{(B.4)}$$

where $f_{W_1}(t|W_1 > t_0)$ is the conditional PDF of W_1 given by

$$f_{W_1}(\tau|W_1 > t_0) = \frac{\lambda(\lambda\tau)^{k-1} e^{-\lambda\tau}}{\Gamma(k) - \Gamma(k, \lambda t_0)} \qquad \text{(B.5)}$$

Taking derivation of Eq. (B.4) with respect to t, we obtain the conditional PDF of W_n,

$$f_{W_n}(t|W_1 > t_0) = \frac{d}{dt} P(W_n < t|W_1 > t_0)$$

$$= \int_{t_0}^{t} f_X(t - \tau) f_{W_1}(\tau|W_1 > t_0) d\tau \qquad \text{for } t_0 < t \qquad \text{(B.6)}$$

Substituting for the PDF of X and the conditional PDF of W_1, we finally obtain

$$f_{W_n}(t|W_1 > t_0) = \int_{t_0}^{t} \frac{\lambda[\lambda(t-\tau)]^{(n-1)k-1} e^{-\lambda(t-\tau)}}{\Gamma[(n-1)k]} \frac{\lambda(\lambda\tau)^{k-1} e^{-\lambda\tau}}{\Gamma(k) - \Gamma(k, \lambda t_0)} d\tau$$

$$= \frac{\lambda^{nk} e^{-\lambda t}}{\Gamma[(n-1)k][\Gamma(k) - \Gamma(k, \lambda t_0)]} \int_{t_0}^{t} (t-\tau)^{(n-1)k-1} \tau^{k-1} d\tau \qquad \text{for } t_0 < t \qquad \text{(B.7)}$$

Using Eq. (B.7), we can numerically compute the updated (conditional) PDF of the waiting time to the nth event (for $n > 1$), when the gamma distributed interarrival times are assumed. Note that if k is an integer, then closed form solution can also be derived.

Figure B.1 shows the unconditional PDFs of the interarrival times for the gamma model and BPT (Brownian Passage Time) model. The mean and COV are specified to be 200 years and 0.24, respectively. The figure demonstrates a close agreement between the two models. Figure B.2 represents the conditional PDFs of the waiting time to the nth (n = 1, 2, 3 and 4) events of the gamma model for t_0 = 76 and 152 years.

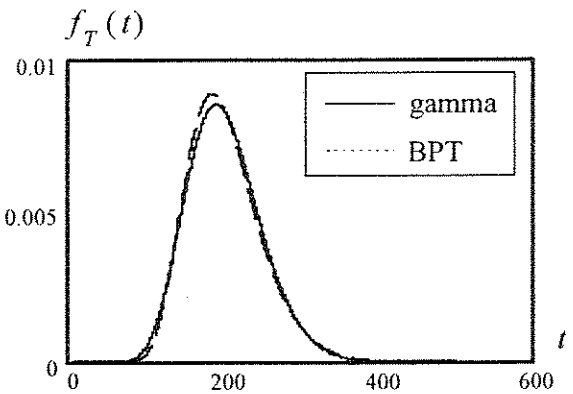

Figure B.1 Original PDF of interarrival time

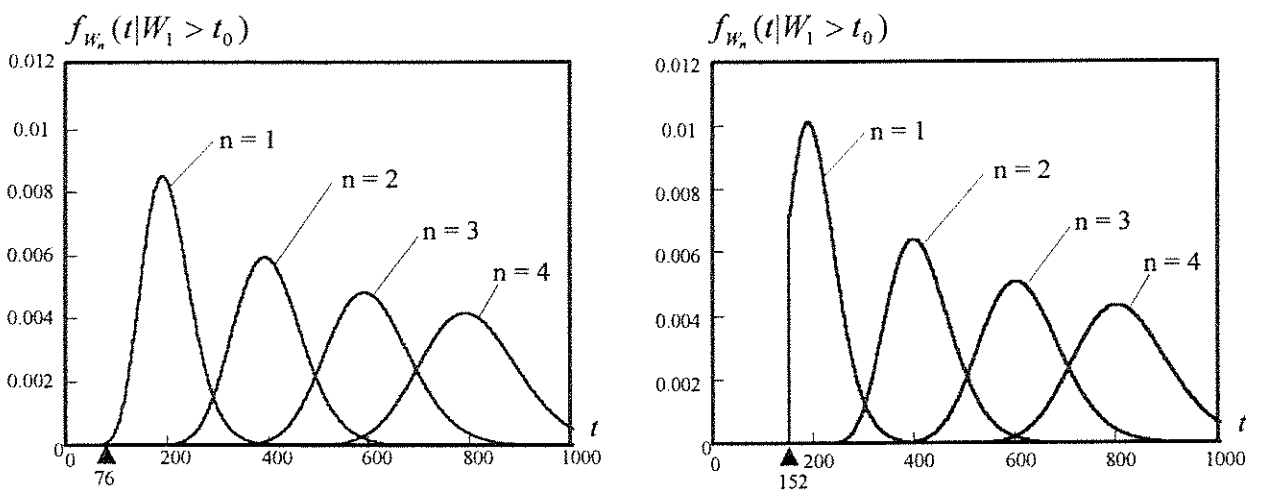

(a) t_0 = 76 years **(b) t_0 = 152 years**

Figure B.2 Conditional PDF of waiting time to the nth event

APPENDIX C

RQUIRED SAMPLE SIZE

The sample size (number of samples) affects the accuracy of estimation of the expected damage costs shown in Table 3.24, which also have an influence on the final solution. We discuss how to determine sample sizes required for Monte Carlo simulations.

As sketched in Figure C.1, the population (real event space) includes an infinite number of samples, and we can never know the actual values of the parameters (the mean μ and the variance σ^2) of the population. What we can do is to infer the values of the unknown parameters by considering a finite number of samples from the population, as shown in Figure C.1. This is called statistical inference (Ang and Tang, 1975), and it is applicable to Monte Carlo simulations (Ang and Tang, 1984).

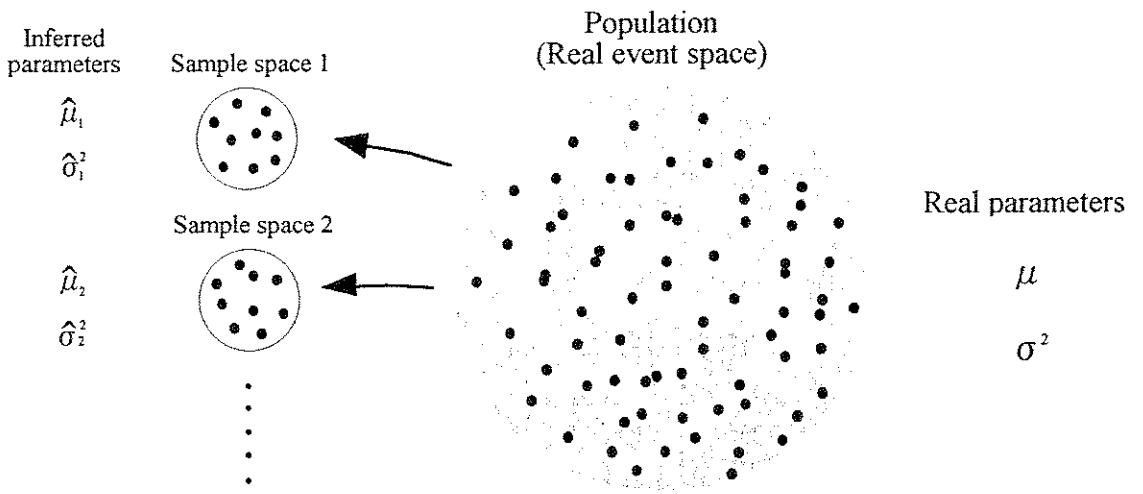

Figure C.1 Statistical inference by sampling

The estimators (inferred parameters) are computed as (Ang and Tang, 1975)

$$\hat{\mu} = \frac{1}{N_S}\sum_{i=1}^{N_S} X_i \tag{C.1}$$

$$\hat{\sigma}^2 = \frac{1}{N_S - 1}\sum_{i=1}^{N_S} (X_i - \hat{\mu})^2 \tag{C.2}$$

where $\hat{\mu}$ and $\hat{\sigma}^2$ are the unbiased estimators of the mean and the variance (the hat represents an inferred value rather than a real value), N_S is the sample size, and X_i is the ith sample in a sample space. As illustrated in Figure C.1, infinite sets of samples (infinite sample spaces) exist, and different values come from different sample spaces. Hence $\hat{\mu}$ can be regarded as a random variable. Figure C.2 illustrates the PDFs of the population and the estimated mean. Under random sampling, the variance of $\hat{\mu}$ is expressed as (Ang and Tang, 1975)

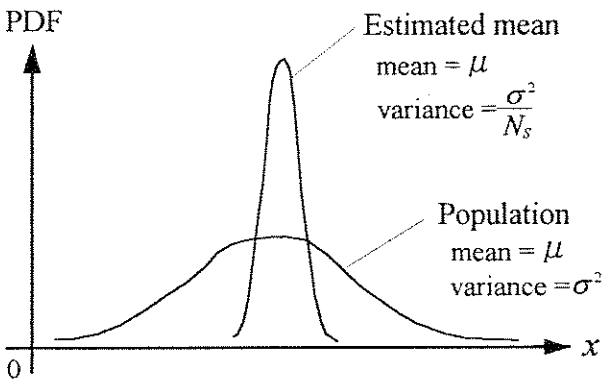

Figure C.2 PDFs of population and estimated mean

$$\sigma_{\hat{\mu}}^2 = \frac{\sigma^2}{N_S} \tag{C.3}$$

where $\sigma_{\hat{\mu}}^2$ is the variance of $\hat{\mu}$ and σ^2 is the variance of the population. Assuming that the unknown variance of the population is identical to that of the sample space ($\sigma^2 \approx \hat{\sigma}^2$), which is the case when the sample size is sufficiently large, $\sigma_{\hat{\mu}}^2$ can be approximated by (Ang and Tang,

1975)

$$\sigma_{\hat{\mu}}^2 \approx \frac{\hat{\sigma}^2}{N_S} \tag{C.4}$$

The COV of $\hat{\mu}$ is then given by

$$\delta_{\hat{\mu}} = \frac{1}{\sqrt{N_S}} \frac{\hat{\sigma}}{\hat{\mu}} \tag{C.5}$$

where $\delta_{\hat{\mu}}$ is the COV of $\hat{\mu}$. It is seen that the COV of the estimator becomes smaller as N_S becomes larger. This corresponds to the simple fact that more accurate estimators can be obtained by increasing the sample size in Monte Carlo simulations. The estimator $\hat{\mu}$ comes from a random variable with the mean = μ and the COV = $\delta_{\hat{\mu}}$. Because the real value of μ is still unknown, what we can say is that the probability that the estimator $\hat{\mu}$ approaches the real parameter μ becomes larger as the sample size N_S increases. From Eq. (C.5), we obtain the required sample size as

$$N_{Sreq} = \left(\frac{\hat{\sigma}}{\hat{\mu}\delta_{target}} \right)^2 \tag{C.6}$$

where N_{Sreq} and δ_{target} denote the required sample size and the target COV, respectively. When using this equation, the target COV should be determined first to obtain a required sample size.

By substituting the expected damage costs shown in Table 3.24 ($\hat{\mu}$) and the computed standard deviations of the damage costs ($\hat{\sigma}$) into Eq. (C.5), COVs of the estimators form 100 samples are obtained. They are shown in Table C.1. For m_j = 6.0, the COVs are particularly large since the damage costs for this magnitude vary greatly ($\hat{\sigma}$ is large in Eq. (C.5)) as seen in Figure 3.45. In such cases, we may have to increase the sample size to obtain more accurate expectations.

For example, if the target COV is specified to be around 10 %, Eq. (C.6) tells us that, for $m_j = 6.0$ with the case with dampers, the sample size should be increased to about 1000.

Table C.1 COV of expected damage cost (%)

m_j	COV of $E[C_D(m_j)]$	
	Bare frame	With dampers
6.0	24.96	34.09
7.0	9.35	10.72
8.0	14.56	4.73

REFERENCES

Abrahamson, N.A. and Shedlock, K.M. (1997). Overview, *Seismological Research Letters*, Vol. 68, No. 1, pp. 9-23.

Ahmed, K.A., Kanda, J, and Iwasaki, R. (1996). Estimation of uncertainties in the dynamic response of urban soils in Japan, *Proceedings of 11th World Conference on Earthquake Engineering*, Paper No. 736, Acapulco, Mexico.

Aki, K. (1967). Scaling law of seismic spectrum, *Journal of Geophysical Research*, Vol. 72, No. 4, pp. 1217-1231.

Aki, K. and Richards, P.G. (1980). *Quantitative Seismology, Vol. 1*, Freeman, San Francisco, California.

Akiyama, H. (1985). *Earthquake-Resistant Limit-State Design for Buildings*, University of Tokyo Press, Tokyo, Japan. (in Japanese)

Anagnos, T. and Kiremidjian, A.S. (1988). A review of earthquake occurrence models for seismic hazard analysis, *Probabilistic Engineering Mechanics*, Vol. 3, No. 1, pp. 3-11.

Ang, A.H-S. and Tang, W.H. (1975). *Probabilistic Concepts in Engineering Planning and Design, Vol. 1: Basic Principles*, John Wiley & Sons.

Ang, A.H-S. and Tang, W.H. (1984). *Probabilistic Concepts in Engineering Planning and Design, Vol. 2: Decision, Risk, and Reliability*, John Wiley & Sons.

Ang, A.H-S. and De Leon, D. (1996). Determination of optimal target reliabilities for design and upgrading of structures, *Proceedings of 11th World Conference on Earthquake Engineering*, Paper No. 1054, Acapulco, Mexico.

Applied Technology Council (1985). *Earthquake Damage Evaluation Data for California, ATC-13*, Redwood City, California.

Bank of Japan (2001). *Official Discount Rate*, http://www.boj.or.jp/en/siryo/stat/discount.html.

Benjamin, J.R. and Cornell, C.A. (1970). *Probability, Statistics, and Decision for Civil Engineering*, McGraw Hill.

Beresnev, I.A. and Atkinson, G.M. (1997). Modeling finite-fault radiation from the ω^n spectrum, *Bulletin of the Seismological Society of America*, Vol. 87, No. 1, pp. 67-84.

Beresnev, I.A. and Atkinson, G.M. (1998a). Stochastic finite-fault modeling of ground motions from the 1994 Northridge, California, Earthquake - I . Validation on rock sites, *Bulletin of the Seismological Society of America*, Vol. 88, No. 6, pp. 1392-1401.

Beresnev, I.A. and Atkinson, G.M. (1998b). FINSIM – a FORTRAN program for simulating stochastic acceleration time histories from finite faults, *Seismological Research Letters*, Vol. 69, No. 1, pp. 27-32.

Beresnev, I.A. and Atkinson, G.M. (1999). Generic finite-fault model for ground-motion prediction in eastern north America, *Bulletin of the Seismological Society of America*, Vol. 89, No. 3, pp. 608-625.

Boore, D.M. (1983). Stochastic simulation of high-frequency ground motions based on seismological models of the radiated spectra, *Bulletin of the Seismological Society of America*, Vol. 73, No. 6, pp. 1865-1894.

Boore, D.M. and Boatwright, J. (1984). Average body-wave radiation coefficients, *Bulletin of the Seismological Society of America*, Vol. 74, No. 5, pp. 1615-1621.

Boore, D.M. and Joyner, W.B. (1997). Site amplification for generic rock site, *Bulletin of the Seismological Society of America*, Vol. 87, No. 2, pp. 327-341.

Bowles, J.E. (1984). *Physical and Geotechnical Properties of Soils: 2nd Edition*, McGraw Hill.

Brune, J.N. (1970). Tectonic stress and the spectra of seismic shear waves from earthquakes, *Journal of Geophysical Research*, Vol. 75, pp. 4997-5009.

Brune, J.N. (1971). Correction, *Journal of Geophysical Research*, Vol. 76, pp. 5002.

Campbell, K.W., Thenhaus, P.C., Barnhard, T.P., and Hampson, D.B. (2000). Seismic hazard model for loss estimation and risk management in Japan, *Proceedings of 6th International Conference on Seismic Zonation: Managing Earthquake Risk in the 21st Century*, Oakland, California.

Chai, Y.H., Romstad, K.M., and Bird, S.M. (1995). Energy-based linear damage model for high-intensity seismic loading, *Journal of Structural Engineering*, ASCE, Vol. 121, No. 5, pp. 857-864.

Chopra, A.K. (1995). *Dynamics of Structures: Theory and Applications to Earthquake Engineering*, Prentice Hall.

Clough, R.W. and Penzien, J. (1993). *Dynamics of Structures: 2nd edition*, McGraw Hill.

Comerio, M.C. (2000). The economic benefits of a disaster resistant university, *Proceedings of 12th World Conference on Earthquake Engineering*, Paper No. 388, Auckland, New Zealand.

Cornell, C.A. (1968). Engineering seismic risk analysis, *Bulletin of the Seismological Society of America*, Vol. 58, No. 5, pp. 1583-1606.

Cornell, C.A. and Krawinkler, H. (2000). Progress and challenges in seismic performance assessment, *PEER Center News*, Vo3., No. 2, pp. 1-3.

Dan, K., Watanabe, M., Sato, T., Miyakoshi, J., and Sato, T. (2000). Isoseismal map of strong motions for the 1923 Kanto earthquake (M_{JMA} 7.9) by stochastic Green's function, *Journal of Structural and Construction Engineering*, Architectural Institute of Japan, No. 530, pp. 53-62. (in Japanese)

Der Kiureghian, A. and Ang, A.H-S. (1977). A fault rupture model for seismic risk analysis, *Bulletin of the Seismological Society of America*, Vol. 67, No. 4, pp. 1173-1194.

Earthquake Engineering Research Institute (1997). *Earthquake Spectra: Theme Issue on Loss Estimation*, Vol. 13, No. 4.

Federal Emergency Management Agency (1999). *HAZUS99 technical manual*, Washington, D.C.

Ferritto, J.M. (1984). Economics of seismic design for new buildings, *Journal of Structural Engineering*, ASCE, Vol. 110, No. 12, pp. 2925-2938.

Grant, E.L., Ireson, W.G., and Leavenworth, R.S. (1990). *Principles of Engineering Economy: 8th Edition*, John Wiley & Sons.

Gutenberg, B. and Richter, C.F. (1944). Frequency of earthquakes in California, *Bulletin of the Seismological Society of America*, Vol. 34, No. 4, pp. 185-188.

Hara, A. (1980). Dynamic characteristics of soils and response analysis of soil deposits, *Doctoral Dissertation*, University of Tokyo, Tokyo, Japan. (in Japanese)

Hardin, B.O. and Drnevich, V.P. (1972). Shear modulus and damping in soils: Design equation and curves, *Journal of the Soil Mechanics and Foundations Division*, ASCE, Vol. 98, No. SM7, Paper No. 9006, pp. 667-692.

Harris, J.L. and Harmon, T.G. (1986). A procedure for applying economic analysis to seismic design decisions, *Engineering Structure*, Vol. 8, No. 4, pp. 248-254.

Headquarters for Earthquake Research Promotion (2001a). *Evaluation Method and its Application for the Probability of Long-Term Earthquake Occurrence*, http://www.jishin.go.jp/main/choukihyoka/01b/index.html. (in Japanese)

Headquarters for Earthquake Research Promotion (2001b). *Information on Trench Investigation*, http://www.jishin.go.jp/main/chousa/hyoka.html. (in Japanese)

Hunt, R.E. (1984). *Geotechnical Engineering Investigation Manual*, McGraw Hill.

Hwang, H.H.M., Lee, C.S., and Ng, K.W. (1990). Soil effects on earthquake ground motions in the Memphis area, *Technical Report NCEER-90-0029*, National Center for Earthquake Engineering Research, State University of New York at Buffalo, Buffalo, New York.

Hwang, H.H.M. and Huo, J-R. (1994). Generation of hazard-consistent fragility curves for seismic loss estimation studies, *Technical Report NCEER-94-0015*, National Center for Earthquake Engineering Research, State University of New York at Buffalo, Buffalo, New York.

Ichihasi, S., Okuzono, T., Takahashi, O., Usami, M., Ninomiya, M., Tsuyuki, Y., and Ishida, Y. (2000). Vibration test of a frame which has an oil-damper brace, *Proceedings of 12th World Conference on Earthquake Engineering*, Paper No. 1503, Auckland, New Zealand.

Idriss, I.M. (1990). Response of soft soil site during earthquakes, *Proceedings of H. Bolton Seed Memorial symposium*, Vol. 2, pp. 273-289, Berkeley, California.

Idriss, I.M. and Sun, J.I. (1992). *User's manual for SHAKE91: A computer program for conducting equivalent linear seismic response analysis of horizontally layered soil deposits*, Center for Geotechnical Modeling, Department of Civil and Environmental Engineering, University of California, Davis, California.

Inoue, T. and Kanda, J. (1993). Seismic hazard analysis using source models for interplate earthquakes, *Journal of Structural and Construction Engineering*, Architectural Institute of Japan, No. 443, pp. 35-41. (in Japanese)

Inoue, T. and Kanda, J. (1998). Seismic risk analysis of non-linear MDOF structures, *Journal of Structural and Construction Engineering*, Architectural Institute of Japan, No. 514, pp. 65-72. (in Japanese)

Isenhower, W.M. (1979). Torsional simple shear/resonant column properties of San Francisco Bay Mud, *Master's Thesis*, University of Texas, Austin, Texas.

Itoh, S. and Kawase, H. (2001). Calibration of strong motion prediction method using statistical Green's function and its application to hypothesized Fukuoka, *Journal of Structural and Construction Engineering*, Architectural Institute of Japan, No. 540, pp. 57-64. (in Japanese)

Itoh, T., Ishii, K., Okumura, T., and Ishikawa, Y. (1987). Development of seismic hazard analysis in Japan, *Transactions of the 9th International Conference on Structural Mechanics in Reactor Technology*, Vol. K1, pp. 69-74.

Japan Meteorological Agency (1996). *The Seismological Bulletin of the J.M.A, 1926-1996*, CD-ROM, Tokyo, Japan. (in Japanese)

Kamae, K., Irikura, K., and Fukuchi, Y. (1991). Prediction of strong ground motion based on scaling law of earthquake by stochastic synthesis method, *Journal of Structural and Construction Engineering*, Architectural Institute of Japan, No. 430, pp. 1-9. (in Japanese)

Kamae, K., Irikura, K., and Pitarka, A. (1998). A technique for simulationg strong ground motion using hybrid Green's function, *Bulletin of the Seismological Society of America*, Vol. 88, No. 2, pp. 357-367.

Kanamori, H. (1977). The energy release in great earthquakes, *Journal of Geophysical Research*, Vol. 82, No. 20, pp. 2981-2987.

Kozo Keikaku Engineering, Inc. (2001a). *2001 Annual Report*, Tokyo, Japan. (in Japanese)

Kozo Keikaku Engineering, Inc. (2001b). *Structural Design Division*, http://www.kke.co.jp/major/kozo/kozohpg.html. (in Japanese)

Kozo Keikaku Engineering, Inc. (2001c). *Personal Communication.*

Kramer, S.L. (1996). *Geotechnical Earthquake Engineering*, Prentice Hall.

Lay, T. and Wallace, T.C. (1995). *Modern Global Seismology*, Academic Press.

Lee, J.C. (1996). Reliability-based cost-effective aseismic design of reinforced concrete frame-wall buildings, *Ph.D. Dissertation*, Department of Civil Engineering, University of California, Irvine, California.

Liu, S.C. and Neghabat, F. (1972). A cost optimization model for seismic design of structures, *The Bell System Technical Journal*, American Telephone and Telegraph Company, Vol. 51, No. 10, pp. 2209-2225.

Lodde, P.F. (1982). Dynamic response of San Francisco Bay Mud, *Master's Thesis*, University of Texas, Austin, Texas.

Martin, P.P. (1976). Nonlinear method for dynamic analysis of ground motion, *Ph.D. Dissertation*, Department of Civil Engineering, University of California, Berkeley, California.

Matthews, M.V. (1998). A stochastic model for recurrent earthquakes, *Unpublished Manuscript.*

Ministry of Land, Infrastructure, and Transport (2000). *Survey on Rental Office Fee: October to December 2000*, http://www.mlit.go.jp/tochimizushigen/tocchi/000214.html. (in Japanese)

Nagahashi, S. and Shibano, K. (1999). Seismic hazard evaluation under consideration of historical earthquakes, active faults and surface geology by digital nation land information, *Journal of Structural and Construction Engineering*, Architectural Institute of Japan, No. 516, pp. 113-120. (in Japanese)

Niwa, N., Kobori, T., Takahashi, M., Hatada, T., Kurino H., and Tagami, J. (1995). Passive seismic response controlled high-rise building with high damping device, *Earthquake Engineering and Structural Dynamics,* Vol. 24, pp. 655-671.

Noguchi, S. (1985). Shape of the Philippine Sea plate and characteristics of activity of Ibaraki earthquakes, *Monthly the Earth,* Vol. 67, No. 2, pp. 97-104. (in Japanese)

Ohsaki, Y. and Sakaguchi, O. (1973). Major types of soil deposits in urban area in Japan, *Soil and Foundations,* Japanese Society of Soil Mechanics and Foundation Engineering, Vol. 13, No. 2, pp.49-65.

Park, Y.J. and Ang, A.H-S. (1985). Mechanistic seismic damage model for reinforced concrete, *Journal of Structural Engineering,* ASCE, Vol. 111, No. 4, pp. 722-739.

Park, Y.J., Ang, A.H-S., and Wen, Y.K. (1985). Seismic damage analysis of reinforced concrete buildings, *Journal of Structural Engineering,* ASCE, Vol. 111, No. 4, pp. 740-757.

Park, Y.J., Ang, A.H-S., and Wen, Y.K. (1987). Damage-limiting aseismic design of buildings, *Earthquake Spectra,* EERI, Vol. 3, No. 1, pp. 1-26.

Pires, J.A., Ang, A.H-S., and Lee, J-C. (1996). Target reliabilities for minimum life-cycle cost design: Application to a class of R.C. frame-wall buildings, *Proceedings of 11th World Conference on Earthquake Engineering*, Paper No. 1062, Acapulco, Mexico.

Porter, K.A and Kiremidjian, A.S. (2001). Assembly-based vulnerability of buildings and its uses in seismic performance evaluation and risk management decision-making, *Report 139*, The John A. Blume Earthquake Engineering Center, Department of Civil & Environmental Engineering, Stanford University, Stanford, California.

Research Group for Active Faults in Japan (1991). *Active Faults in Japan: Revised Edition,* University of Tokyo Press, Tokyo, Japan. (in Japanese)

Rosenblueth, E. (1986). Optimum reliabilities and optimum design, Structural Safety, Vol. 3, pp. 69-83.

Ross, S.M. (1995). *Stochastic Process: Second Edition*, John Wiley & Sons.

Sano, T., Takahashi, Y., and Suzuki, T. (1998). Development of hybrid damping system for seismic vibration control: performance test and vibration control effect study on Y-O damper, *Proceedings of 2nd World Conference on Structural Control*, Vol. 24, Kyoto, Japan, pp. 277-286.

Saragoni, G.R. and Hart, G.C. (1974). Simulation of artificial earthquakes, *Earthquake Engineering and Structural Dynamics*, Vol. 2, pp. 249-267.

Sato, R. (1979). Theoretical basis on relationships between focal parameters and earthquake magnitude, *Journal of Physics of the Earth*, Vol. 27, pp.353-372.

Sato, T., Graves, W., and Somerville, P.G. (1999). Three-dimensional finite-difference simulations of long-period strong motions in the Tokyo metropolitan area during the 1990 Odawara earthquake (M_J 5.1) and the great 1923 Kanto earthquake (M_S 8.2) in Japan, *Bulletin of the Seismological Society of America*, Vol. 89, No. 3, pp. 579-607.

Schnabel, P.B., Lysmer, J., and Seed, H.B. (1972). SHAKE: A computer program for earthquake response analysis of horizontally layered sites, *Report No. UCB/EERC 72/12*, Earthquake Engineering Research Center, University of California, Berkeley, California.

Seed, H.B. and Idriss, I.M. (1970). Soil moduli and damping factors for dynamic response analysis, *Report No. UCB/EERC 70/10*, Earthquake Engineering Research Center, University of California, Berkeley, California.

Seed, H.B., Wong, R.T., Idriss, I.M., and Tokimatsu, K. (1984). Moduli and damping factors for dynamic analysis of cohesionless soils, *Report No. UCB/EERC 84/14*, Earthquake Engineering Research Center, University of California, Berkeley, California.

Senju, S. and Fushimi, T. (2001). *Fundamentals for Profitability Engineering: Profitability Analysis for Decisions: New Edition*, JMA Management Center, Inc., Tokyo, Japan. (in Japanese)

Si, H. and Midorikawa, S. (1999). New attenuation relationships for peak ground acceleration and velocity considering effects of fault type and site condition, *Journal of Structural and Construction Engineering*, Architectural Institute of Japan, No. 523, pp. 63-70. (in Japanese)

Si, H. and Midorikawa, S. (2001). Evaluation of rupture directivity effects on peak ground motion using stochastic Green's function method, *Journal of Structural and Construction Engineering*, Architectural Institute of Japan, No. 546, pp. 47-53. (in Japanese)

Somerville, P.G., Smith, N.F., Graves, R.W., and Abrahamson, N.A. (1997). Modification of empirical strong ground motion attenuation relations to include the amplitude and duration effects of rupture directivity, *Seismological Research Letters,* Vol. 68, No. 1, pp. 199-222.

Somerville, P., Irikura, J., Graves, R., Sawada, S., Wald, D., Abrahamson, N., Iwasaki, Y., Kagawa, T., Smith, N., and Kawada, A. (1999). Characterizing crustal earthquake slip models for the prediction of strong ground motion, *Seismological Research Letters*, Vol. 70, No. 1, pp. 59-80.

Soong, T.T. and Dargush, G.F. (1997). *Passive Energy Dissipation Systems in Structural Engineering*, John Wiley & Sons.

Sues, R.H., Wen, Y.K., and Ang, A.H-S. (1985). Stochastic evaluation of seismic structural performance, *Journal of Structural Engineering,* ASCE, Vol. 111, No. 6, pp. 1204-1218.

Sun, J.I., Golesorkhi, R. and Seed, H.B. (1988). Dynamic moduli and damping ratio for cohesive soils, *Report No. UCB/EERC 88/15*, Earthquake Engineering Research Center, University of California, Berkeley, California.

Takahashi, N., Shiohara, H., and Otani, S. (2000). Reparability of building structures vulnerable to earthquake hazards in terms of life cycle economic loss, *Transactions of the Japan Concrete Institute,* Vol. 22, pp. 189-194.

Takahashi, O., Okuzono, T., and Yanagawa, Y. (2001). Response control structure with oil damper bracing system – Vol. 2 vibration test and long term observation –, *The Eighth East Asia-Pacific Conference on Structural Engineering and Construction*, Paper No. 1061, Singapore.

Usami, T. (1996). *Materials for Comprehensive Lists of Destructive Earthquakes in Japan: 416-1995, Revised and Enlarged Edition*, University of Tokyo Press, Tokyo, Japan (in Japanese)

Utsu, T. (1982). Catalog of large earthquakes in the region of Japan from 1885 through 1980, *Bulletin of the Earthquake Research Institute*, University of Tokyo, Vol. 57, pp.401-463. (in Japanese)

Vucetic, M. and Dobry, R. (1991). Effect of soil plasticity on cyclic response, *Journal of Geotechnical Engineering*, ASCE, Vol. 117, No. 1, Paper No. 25418, pp. 89-107.

Watanabe, M., Sato, T., and Dan, K. (1998). Scaling relations of fault parameters for inland earthquakes, *Proceedings of 10th Japan Earthquake Engineering Symposium*, Vol. C1, Yokohama, Japan, pp.583-588. (in Japanese)

Wells, D.L. and Coppersmith, K.J. (1994). New empirical relationships among magnitude, rupture length, rupture width, rupture area, and surface displacement, *Bulletin of the Seismological Society of America*, Vol. 84, No. 4, pp. 974-1002.

Wesnousky, S.G., Scholz, C.H., Shimazaki, K., and Matsuda, T. (1984). Integration of geological and seismological data for the analysis of seismic hazard: a case study of Japan, *Bulletin of the Seismological Society of America*, Vol. 74, No. 2, pp. 687-708.

Wesnousky, S.G. (1994). The Gutenberg-Richter or characteristic earthquake distribution, which is it? *Bulletin of the Seismological Society of America*, Vol. 84, No. 6, pp. 1940-1959.

Wesnousky, S.G. (1999). Crustal deformation and the stability of the Gutenberg-Richter relationship, *Bulletin of the Seismological Society of America*, Vol. 89, No. 4, pp. 1131-1137.

Whitman, R.V., Biggs, J.M., Brennan, J.E., Cornell, C.A., de Neufville, R.L., and Vanmarcke, E.H. (1975). Seismic design decision analysis, *Journal of Structural Division*, ASCE, Vol. 101, No. ST5, pp. 1067-1084.

Wiggins, J.H. (1972). The balanced risk concept: new approach to earthquake building codes, *Civil Engineering*, ASCE, Vol. 42, No. 8, pp. 55-59.

Working Group on California Earthquake Probabilities (1990). Probabilities of large earthquake in San Francisco Bay Region, California, *U.S. Geological Survey Circular 1053*.

Working Group on California Earthquake Probabilities (1999). Earthquake probabilities in San Francisco Bay region: 2000 to 2030 – A summary of findings, *U.S. Geological Survey Open-File Report 99-517.*

Young, R.R. and Coppersmith, K.J. (1985). Implication of fault slip rates and earthquake recurrence to probabilistic seismic hazard estimates, *Bulletin of the Seismological Society of America*, Vol. 75, No. 4, pp. 939-964.